AD_____

GRANT NO: DAMD17-91-Z-1004

TITLE: Mechanisms of Tumor Necrosis Factor/Cachectin (TNFα)-Induced Pulmonary Vascular Endothelial Injury

PRINCIPAL INVESTIGATOR: Simeon E. Goldblum, M.D.

CONTRACTING ORGANIZATION: University of Maryland at Baltimore
School of Medicine
10 South Pine Street
Baltimore, Maryland 21201

REPORT DATE: September 30, 1994

TYPE OF REPORT: Final Report

PREPARED FOR: Department of the Army
U.S. Army Medical Research
and Materiel Command
Fort Detrick, Frederick, MD 21702-5012

DISTRIBUTION STATEMENT: Approved for public release;
distribution unlimited

The views, opinions and/or findings contained in this report are those of the author(s) and should not be construed as an official Department of the Army position, policy or decision unless so designated by other documentation.

REPORT DOCUMENTATION PAGE

Form Approved
OMB No. 0704-0188

1. AGENCY USE ONLY (Leave blank)	2. REPORT DATE	3. REPORT TYPE AND DATES COVERED
	9/30/94	Final 12/90 - 10/94

4. TITLE AND SUBTITLE
Mechanisms of Tumor Necrosis Factor/Cachectin (TNFα)-Induced Pulmonary Vascular Endothelial Injury

5. FUNDING NUMBERS
DAMD17-91-Z-1004

6. AUTHOR(S)
Simeon E. Goldblum, M.D.

7. PERFORMING ORGANIZATION NAME(S) AND ADDRESS(ES)
University of Maryland at Baltimore
School of Medicine
10 South Pine Street
Baltimore, Maryland 21201

8. PERFORMING ORGANIZATION REPORT NUMBER

9. SPONSORING/MONITORING AGENCY NAME(S) AND ADDRESS(ES)
U.S. Army Medical Research and Materiel Command
Fort Detrick
Frederick, Maryland 21702-5012

10. SPONSORING/MONITORING AGENCY REPORT NUMBER

11. SUPPLEMENTARY NOTES

12a. DISTRIBUTION/AVAILABILITY STATEMENT
Approved for public release; distribution unlimited

12b. DISTRIBUTION CODE

13. ABSTRACT *(Maximum 200 words)*

Diverse forms of severe military injuries can all lead to multiple organ failure (MOF). Prominent components to this life-threatening state include systemic vascular collapse, disseminated intravascular coagulation, and the Adult Respiratory Distress Syndrome (ARDS). One common element to these complications is the presence of endothelial cell (EC) injury or dysfunction. Two candidate mediators of pulmonary vascular EC injury and ARDS include the endogenous mediator tumor necrosis factor-α (TNF-α) and the exogenous factor, bacterial lipopolysaccharide (LPS). In addition, an LPS-induced, EC-derived glycoprotein, SPARC (Secreted Protein Acidic and Rich in Cysteine), regulates EC shape. To better study the mechanisms of TNFα-, LPS-, and SPARC-induced changes in endothelial barrier function, we utilized an *in vitro* experimental system that precludes hydrostatic pressure changes, granulocyte effector cells, or other nonendothelial-derived host factors. We studied the influence of human rTNFα, E.*coli* 0111:B4 LPS, and murine SPARC on the movement of ^{14}C-bovine serum albumin across bovine pulmonary vascular EC monolayers grown to confluence on filter supports mounted in chemotaxis chambers. We also studied whether these three mediators regulated endothelial barrier function through actin reorganization. We found that TNFα, LPS, and SPARC each induced dose-, time- and temperature-dependent increments in transendothelial ^{14}C-BSA flux and that these changes in barrier function were mediated through EC actin depolymerization. The LPS effect was profoundly serum-dependent and this serum requirement could be satisfied by LPS-binding protein as well as soluble CD14.

14. SUBJECT TERMS
Endothelium, Actin, Cytoskeleton, permeability, cytokines, endotoxin, SPARC, Osteonectin, Adult Respiratory Distress Syndrome (ARDS)

15. NUMBER OF PAGES

16. PRICE CODE

17. SECURITY CLASSIFICATION OF REPORT	18. SECURITY CLASSIFICATION OF THIS PAGE	19. SECURITY CLASSIFICATION OF ABSTRACT	20. LIMITATION OF ABSTRACT
Unclassified	Unclassified	Unclassified	Unlimited

FOREWORD

Opinions, interpretations, conclusions and recommendations are those of the author and are not necessarily endorsed by the US Army.

SGG Where copyrighted material is quoted, permission has been obtained to use such material.

____ Where material from documents designated for limited distribution is quoted, permission has been obtained to use the material.

SGG Citations of commercial organizations and trade names in this report do not constitute an official Department of Army endorsement or approval of the products or services of these organizations.

____ In conducting research using animals, the investigator(s) adhered to the "Guide for the Care and Use of Laboratory Animals," prepared by the Committee on Care and Use of Laboratory Animals of the Institute of Laboratory Resources, National Research Council (NIH Publication No. 86-23, Revised 1985).

____ For the protection of human subjects, the investigator(s) adhered to policies of applicable Federal Law 45 CFR 46.

____ In conducting research utilizing recombinant DNA technology, the investigator(s) adhered to current guidelines promulgated by the National Institutes of Health.

____ In the conduct of research utilizing recombinant DNA, the investigator(s) adhered to the NIH Guidelines for Research Involving Recombinant DNA Molecules.

SGG In the conduct of research involving hazardous organisms, the investigator(s) adhered to the CDC-NIH Guide for Biosafety in Microbiological and Biomedical Laboratories.

Simeon E Goldblum 10/5/94

PI - Signature Date

(4) TABLE OF CONTENTS

INTRODUCTION:

STATEMENT OF PROBLEM: Tumor Necrosis Factor α (TNFα) and endotoxin or bacterial lipopolysaccharide (LPS) are both candidate mediators of pulmonary vascular endothelial cell (EC) injury. Although the endogenous mediator TNFα, and the exogenous bacterial product LPS, are structurally unrelated, they share an exceedingly long stimulus-to-response lag time compared to other anaphylatoxins. Further, LPS is a potent stimulus for increased TNFα expression. The mechanism(s) by which TNFα and/or LPS regulate pulmonary vascular endothelial barrier function is unknown.

BACKGROUND OF PREVIOUS WORK:

TNFα-induced Pulmonary Vascular Endothelial Injury In Vivo: Elevated circulating levels of TNFα have been reported in humans following endotoxin infusion as well as in septic patients. Septic shock patients with detectible plasma TNFα have a higher incidence and severity of the Adult Respiratory Distress Syndrome (ARDS). Further, increased TNFα bioactivity has been recovered from alveolar macrophages of endotoxin-challenged dogs and in bronchoalveolar lavage fluid (BALF) of ARDS patients.

In 1987, we demonstrated that human rTNFα augments pulmonary edema formation and pulmonary extravasation of ^{125}I-albumin in rabbits (1,2). Electron microscopy revealed endothelial gap formation, pervascular edema and extravasation of permeability tracer. rTNFα also induces acute lung injury in other experimental animals, as well as tachypnea with fluid retention in cancer patients. It was not clear whether hemodynamic alterations are essential to rTNFα -induced lung injury. rTNFα-induced pulmonary extravasation of ^{125}I-albumin in guinea pigs is not associated with significant increments of mean left atrial and pulmonary pressures. Similarly, rTNFα-induced increments of vascular permeability to ^{125}I-albumin in isolated perfused rat lungs occurs in the absence of changes in pulmonary artery (PA) perfusion pressures. On the other hand, rTNFα infusion into awake sheep produces rapid onset, transient increases in PA pressure and pulmonary vascular resistance coincident with increases of pulmonary lymph flow and transvascular protein clearance. It was also unclear whether TNFα-induced lung injury was, in part, granulocyte-dependent. TNFα induces pulmonary leukostasis in numerous species. TNFα augments granulocyte-to-endothelial interactions, stimulates neutrophil degranulation and granulocyte oxygen-dependent metabolism, and increases granulocyte-mediated cytotoxicity for EC. Granulocyte depletion has been shown to prevent TNFα-induced pulmonary endothelial injury in guinea pigs. In another report, granulocyte depletion failed to block rTNFα-induced lung injury in sheep. We showed that a rTNFα challenge that does not produce pulmonary leukostasis can induce pulmonary vascular endothelial injury in rabbits (2). Therefore, whether hemodynamic alterations and/or granulocyte-dependent mechanisms are essential to or even operative in rTNFα-induced lung injury in vivo is uncertain.

Effects of rTNFα on the Pulmonary Vascular Endothelial Barrier In Vitro: There are reports that rTNFα increases movement of radiolabeled tracers across bovine and ovine PA endothelial monolayers within minutes. Using bovine EC from a nonpulmonary source, other investigators

have found that TNFα augments transendothelial albumin flux first detectable at 12h or 2h with a progressive increase over 3-4h. These *in vitro* studies suggest that rTNFα can reversibly influence endothelial barrier function in the absence of hemodynamic alterations, granulocyte effector cells, or EC injury.

Role for LPS in Gram-Negative, Sepsis-Associated EC Injury: Gram-negative septic processes can be complicated by systemic vascular collapse, disseminated intravascular coagulation, the adult respiratory distress syndrome (ARDS), and brain edema. One common element to these complications is the presence of EC injury and/or dysfunction. This loss of endothelial integrity permits movement of intravascular fluid into tissues which results in an ineffective circulating blood volume and tissue edema formation. Evidence exists that the bacterial component responsible for much of the EC injury associated with Gram-negative bacterial sepsis is the bacterial cell envelope constituent, LPS. First, LPS bioactivity has been detected in the bloodstream of Gram-negative septicemic patients and levels of circulating LPS predict development of multiple organ failure, including ARDS. In patients with gram-negative bacterial meningitis, cerebrospinal fluid concentrations of LPS correlate with brain edema. Thus, LPS has been demonstrated within relevant body compartments temporally coincident with loss of endothelial barrier function. Second, administration of LPS alone to experimental animals induces manifestations of EC injury and dysfunction. Lastly, immunological and pharmacological interventions that specifically target the LPS molecule, reportedly protect against the EC complications associated with gram-negative sepsis or experimental LPS challenge.

Direct LPS-EC Interactions and LPS-Induced EC Responses: Although LPS induces numerous mediators of EC injury, evidence also exists for a direct role for LPS. During endotoxemia, the first host tissue barrier seen by circulating LPS is the endothelium. Not only is blood-borne LPS in close proximity to the EC surface but it actually can be transported across and localized to the endothelium. Although LPS internalization and intracellular trafficking through nonendothelial cells has been reported, EC processing of LPS is unclear. Further, LPS directly induces numerous EC responses, *in vitro*, in the absence of nonendothelial-derived host mediator systems. LPS induces EC arachidonate metabolism, nitric oxide production, and cytotoxicity. It upregulates expression of cytokines and leukocyte adhesion molecules, pushes the endothelial surface into a prothrombotic state, and induces endothelial barrier dysfunction.

PURPOSE OF PRESENT WORK AND METHODS OF APPROACH: We hypothesized that TNFα and/or LPS induce actin reorganization in pulmonary vascular EC which leads to EC shape change, cell-to-cell reorientation, and intercellular gaps which permit paracellular transit of macromolecules. In an in vitro experimental system that obviates hydrostatic pressure changes, granulocyte effector cells and nonendothelial cell-derived host factors, we studied the influence of TNFα and LPS on pulmonary vascular endothelial barrier function.

BODY:

A. **EXPERIMENTAL METHODS:**

Recombinant Human Tumor Necrosis Factor α (rTNFα) Preparation: rTNFα was generously provided by Knoll Pharmaceuticals/BASF K&K Corp., Whippany, NJ 07981. The molecule was produced in *Escherichia coli* and purified. The rTNFα had a specific activity, in an actinomycin D-free L929 cytotoxicity assay, of 9.8 X 10^6 units per mg protein and contained <5 Endotoxin units/mg protein in the Limulus Amoebocyte Lysate Assay (Whittaker, M.A. Bioproducts, Walkersville, M.D.) The rTNFα was received lyophilized and frozen for storage at -70 C. The rTNFα was thawed only once for each experiment without re-freezing. The rTNFα was reconstituted in a 2% BSA solution in sterile nonpyrogenic normal saline (Travenol Laboratories). The BSA was globulin-and fatty acid-free (Sigma).

LPS AND LIPID A PREPARATIONS:

Purified native LPS phenol-extracted from *Escherichia coli* serotype 0111:B4 (Sigma) was dissolved in phosphate- buffered saline (PBS) st 1 mg/ml and stored at -20 C. For experiments, the LPS stock solution was further dissolved into supplemented tissue culture media as described below.

Salmonella minnesota lipopolysaccharide (LPS) chemotypes Ra, Rb, Rc, Rd, Re, and wild type; *E. coli* 0111:B4 LPS, *E. coli* J5 (Rc chemotype) LPS, and *E. coli* K12 lipid A were purchased from List Biological Laboratories Inc. (Campbell, CA). Monophosphoryl lipid A (MPL) and synthetic diphosphoryl lipid A (DPL) were purchased from ICN Biomedicals Inc. (Costa Mesa, CA).

De-o-acylated LPS: *E. coli* J5LPS (10.3mg) was suspended in 1.8ml of 0.1M NaOH solution. The cloudy suspension was heated in a water bath at 65°C for 2h. The reaction mixture was cooled in an ice/water bath, neutralized with 1.0M HCl to pH 6.8 and centrifuged at 10,000 x g for 10min. to remove insoluble material. The clear supernate was desalted on a PD-10 column (Pharmacia-LKB Biotechnology Inc. Piscataway, NJ) using water as eluant. The desalted sample was lyophilized. Yield of J5-DLPS was 4.5mg.

De-o-acylated lipid A: 1.0mg of lipid A from *E. coli* K12 strain D31M4 was suspended in 1.0 ml of 0.1M NaOH solution and the suspension was heated in a water bath at 65°C for 2h. The solution was cooled in an ice/water bath and was neutralized with 1.0M HCl to pH 7.0. The neutral solution was centrifuged at 10,000 X g for 10min. to remove insoluble material. The clear supernate was desalted on a PD-10 column using water as eluant. The desalted sample was lyophilized. Yield of de-o-acylated lipid A was 0.45mg.

Lipid A solution: Lipid A from *E. coli* K12 (1.0mg) was dissolved in 100ul of a mixture of chloroform (69%), methanol (27%), water (4%) in a small tube. The clear solution was evaporated to dryness by passing a slow stream of N_2 over the solution. The dry residue was

resuspended in 1.0ml of water. The resulting suspension was sonicated in an ultrasonic bath (Branson model 5200) for 10min. It gave a slightly hazy solution. A control sample was prepared by taking 100ul of the solvent mixture in a similar tube (without lipid A) and processed as described above.

Murine SPARC Preparation: Briefly, mouse PYS-2 cells, a teratocarcinoma cell line derived from parietal yolk sac endoderm, was used as a source for SPARC. Subconfluent PYS-2 cells were incubated in serum-free Dulbecco's Modified Eagles medium for 24-48h. The conditioned medium was harvested, clarified of cell debris, and concentrated by precipitation with 50% (w/v) ammonium sulfate in the presence of protease inhibitors. The precipitated proteins were then pelleted and dissolved in and dialyzed against 4M urea-50mM Tris-HC1 buffer (pH 8). The proteins were first separated by diethylamine ethyl (DEAE) - cellulose ion exchange chromatography (SPARC eluted with NaC1, 175mM). The peak containing SPARC was dialyzed vs. distilled H_2O for preferential precipitation of SPARC. The precipitate was dissolved in Tris-buffered saline and further purified by molecular sieve chromatography over Sephadex G-200 at 4°C. Several SPARC preparations were pooled for use in these studies. The SPARC preparations contained 0.0005-0.02ng endotoxin/μg protein as determined by the Limulus Amoebocyte Lysate Assay. To monitor the SPARC purification, selected cell cultures were radiolabeled with ^{35}S-methionine.

EC Culture: Bovine pulmonary artery EC were obtained from the American Tissue Culture Collection (Rockville, MD). EC were grown at 37°C under 5% CO_2 in Dulbecco's Modified Eagles Medium (DMEM) (Sigma) enriched with 20% heat-inactivated (56°C, 30 min) fetal bovine serum (FBS) (Hyclone Laboratories, Inc.; Logan, UT), L-glutamate 4mM, nonessential amino acids, and vitamins in the presence of penicillin (50 u/ml) and streptomycin (50 μg/ml) (Sigma). The cells were washed and gently detached with a brief (1-2 min) trypsin (0.5 mg/ml) (Sigma) exposure with gentle agitation followed immediately by neutralization with FBS-containing medium. The cells were counted and suspended in medium for immediate seeding of assay chambers (4 X 10^5 cells/ml) or 6-well tissue culture plates (2.9 x 10^5 cells/ml). Cultures were determined to be endothelial by uniform morphology and by quantitative determination of angiotensin-converting enzyme activity with commercially available ^{3}H-benzoyl-Phe-Ala-Pro substrate (Ventrex Laboratories, Inc., Portland, Maine 04103).

Assay of Transendothelial Albumin Flux: Transendothelial ^{14}C-BSA flux was assayed as we have previously described (3). Polycarbonate filters (13 mm diameter, 0.4 μm pore size) (Nucleopore, Inc., Pleaston, CA) were treated with 0.5% acetic acid (50°C 20 min), washed in distilled H_2O and immersed in boiling pig skin gelatin (Fisher Scientific, Pittsburgh, PA) solution (5mg/L distilled H_2O) for 60 min. The filters were then dried, glued to polystyrene chemotactic chambers (ADAPS, Inc., Dedham, MA), and gas sterilized with ethylene oxide. These chambers which served as the upper compartment for the assay chambers were inserted into wells of 24-well plates, each well containing 1.5 ml media and serving as the lower compartment of the assay chamber. Each upper compartment was seeded with 2 X 10^5 EC in 0.5 ml media and cultured for 72 hr (37°C, 5% CO_2). We used ^{14}C-BSA (Sigma) with a specific activity of 30.1 μCi per mg protein as the tracer molecule. The baseline barrier function of each

monolayer was determined by applying an equivalent and reproducible amount of ^{14}C-BSA (4,800 dpm/0.5 ml) to each upper compartment for 1 hr at 37°C, after which 0.5 ml from the lower compartment was added to 4.5 ml of Optifluor Scintillation fluid (Packard Instruments Co., Downers Grove, IL) and counted in a Tri-carb 1500 Liquid Scintillation Analyzer (Packard). Only endothelial monolayers retaining $\geq$ 97% of the ^{14}C-BSA were studied. The monolayers were then exposed to increasing rTNFα, LPS or SPARC concentrations for 6 h. Based on the established dose-response relationship, other monolayers were exposed to agonist at a fixed concentration for 0.5, 1, 2, 4, and 6h exposure times. Simultaneous controls with medium alone were performed for each time point. Transfer of ^{14}C-BSA across endothelial monolayers was again assayed.

In selected experiments, the monolayers were pretreated with the specific F-actin stabilizing agent, 7-nitrobenz-2-oxa-1, 3-diazole (NBD)-phallicidin (Molecular Probes, Eugene, OR), 0.3 μM for 3h prior to and throughout the standard rTNFα, LPS, SPARC, or medium exposure. Incorporation of NBD-phallicidin into EC actin filaments was confirmed by epifluorescence microscopy. In other experiments, monolayers were pretreated with protein synthesis inhibitor, cycloheximide (Sigma) 50 μg/ml, 0.5 h prior to and throughout the rTNFα, LPS, SPARC, or media exposures. This concentration of cycloheximide inhibited > 95% EC protein synthesis as measured by [^{35}S] methionine (New England Nuclear; Du Pont; Boston, MA) incorporation into trichloracetic acid-precipitable protein as we have previously described (3). Simultaneous NBD-phallicidin (0.3 μM) and cycloheximide (50 μg/ml) controls were also included.

Effect of LPS on Endothelial Cell Viability: To determine whether LPS-induced changes in endothelial barrier function could be explained by cell injury or loss of viability, LPS-exposed and medium control monolayers were serially studied for trypan blue exclusion and lactate dehydrogenase (LDH) release (3-6). EC were seeded into the wells of 24-well plates (2 X 10^5 cells/well) and cultured for 72h to achieve confluence. The media was decanted and replaced with media containing rTNFα, LPS, SPARC, or media alone for increasing exposure times. For trypan blue exclusion, supernatants were harvested from experimental and media control monolayers which were then washed with Hanks' balanced salt solution (HBSS). The supernatant and wash from each well were centrifuged (300g, 10 min) and the cell pellet suspended with respective detached monolayers for staining with trypan blue 0.4% (Sigma) for 5 min. Viable and nonviable cells were counted in triplicate using a hemocytometer. For the LDH release assay, supernatants were harvested from experimental and media control monolayers and the monolayers solubilized (Triton X-100 3%, 0.5h). LDH activity was assayed in the medium and the cell lysate. Test samples were mixed with reconstituted LD-L reagent (Lactate 50 mM, NAD 7mM, pH 9.8) (Sigma) and ΔA_{340nm} was measured at 37°C over 1.5 min in a Gilford Response II Spectrophotometer (Ciba Corning Diagnostics). LDH release was expressed as percent of total LDH (LDH in medium plus LDH in cells). Correction was made for LDH in FBS.

Assays for EC ^{51}Cr and ^{3}H-Adenine Release: To determine whether rTNFα-, LPS-, or SPARC-induced changes in endothelial barrier function could be explained by EC injury, treated and medium control monolayers were studied for ^{51}Cr and ^{3}H-adenine release. EC were seeded

into the wells of 24-well plates (2 X 10^5 cells/well) and cultured for 72h to achieve confluence. For the ^{51}Cr release assay, confluent monolayers labeled with [^{51}Cr]-sodium chromate (Amersham Arlington, IL), 12 μCi per well, for 3 hours at 37°C as we have previously described (3). The labeled monolayers were washed and the washes were counted for 2 minutes in a gamma counter (Pharmacia LKB, Piscataway, NJ). The ^{51}Cr-labeling efficiency was calculated as total CPM per well-CPM in washes/total CPM per well x 100% to be 3%. The washed, labeled monolayers were incubated with either rTNFα, LPS, or medium alone for increasing exposure times after which the supernatants were counted. To differentiate between actual cell release of ^{51}Cr and cell detachment into supernatants, aliquots of washes were centrifuged (300g, 10 min) before counting. All washed monolayers were solubilized with 1% Triton X-100 (Sigma) to induce maximum release. The lysates were centrifuged and the supernatants counted for ^{51}Cr-activity. EC injury was expressed as: (^{51}Cr supernatant)/(^{51}Cr supernatant + ^{51}Cr cell lysate) X 100%.

For the ^3H-adenine release assay, confluent monolayers were labeled with [8 - ^3H] adenine (Amersham) 1.0 μCi/ml (Specific activity = 25 Ci/mmol) for 1h at 37°C. This brief labeling time with postconfluent stationary phase cells avoids significant ^3H-adenine incorporation into the nucleus. The monolayers were washed x 3 and incubated with either LPS 10 ng/ml or medium alone for increasing exposure times. Selected ^3H-adenine-labeled media control monolayers were solubilized with Triton X-100 for 30 min to determine maximum ^3H-adenine release. At each time point, supernatants were harvested, and together with washes, centrifuged (1000g, 5 min), and 0.5 ml of resultant supernatant added to 4.5 ml Optifluor scintillation fluid (Packard) to determine ^3H-activity in a liquid scintillation counter (Packard). The 1h ^3H-adenine incubation followed by three washes yielded a labeling efficiency of 13%. ^3H-adenine was expressed as percent of maximum release.

F-actin Epifluorescence Microscopy: To maintain endothelial monolayers under identical experimental conditions to our permeability assay (4,5), we directly stained and visualized the monolayers on polycarbonate filters (4,5,7). EC grown to confluence on filters were exposed to media, rTNFα, LPS or SPARC for 0.5, 1, 2, 4, and 6h. The monolayers were fixed (formaldehyde 3.7%, 20 min), permeabilized (Triton X-100 0.5% in HEPES buffer, 5 min), and stained with the F-actin probe, fluorescein-phalloidin (1.65 x 10^{-7}M, 20 min) (Molecular Probes). The filters and their attached monolayers were mounted cell-side up on microscope slides and photographed through a Zeiss Axioskop 20 Microscope equipped for epifluorescence.

EC Numbers and Total Protein Concentrations in EC Monolayers: Methodologies for determining F- and G-actin pools involve fixation, permeabilization and extraction procedures which preclude cell counts and protein determinations on the same monolayers. Further, TNFα and LPS are each known to alter EC growth, to induce EC cytotoxicity, and to influence protein synthesis. Therefore, additional simultaneously plated EC were cultured under identical conditions as the monolayers to be assayed for the F- and G-actin pools. Postconfluent monolayers in the wells of 6-well plates were washed twice with phosphate-buffered saline (PBS), trypsin-detached as above, and counted in triplicate. The cells were centrifuged (600g, 10 min), again washed in PBS X 2, and lysed in lysing buffer [Sodium dodecyl sulfate (SDS)

3%, dithiothreitol (DTT) 1mM, phenylmethylsufonyl fluoride (PMSF) 10μM, ethylenediaminetetra acetic acid (EDTA) 1mM, Tris-HC1 50 mM, pH 8.0]. Lysates were assayed for protein concentration with the standard Bio-Rad DC Protein Assay (Bio-Rad Chem. Div., Richmond, CA). Total EC protein was used to standardize F- and G-actin measurements.

F-Actin Quantification by Spectrofluorometry: EC F-actin was fluorometrically measured as previously described (5). EC (5.8×10^5 cells in 2 ml media) were seeded into the wells of 6-well plates and cultured for 72h (37°C, 5% CO_2). The monolayers were exposed to varying concentrations of TNFα, LPS, SPARC, or medium alone for varying exposure times after which they were washed twice in a buffer (KCl 75mM, $MgSO_4$ 3mM, ethylene glycol tetraacetic acid (EGTA) 1mM, imidazole 10mM, DDT 0.2mM, aprotinin 10μg/ml, PMSF 0.1 mM) and fixed with formaldehyde 3.7% for 15 min. Monolayers were permeabilized (Triton X-100 0.2% in buffer, 5 min), stained with NBD-phallicidin (1.65×10^{-7}M, 20 min), and extracted with ice cold methanol (overnight,-20 C). Staining and extractions were performed in the dark. Extracts were harvested into cuvettes and intraendothelial fluorescence was measured in a Perkin-Elmer LS30 Luminescence Spectrometer at room temperature at 465 nm excitation (10 nm slit) and 535 nm emission (10 nm slit) and expressed in arbitrary fluorescence units per mg total EC protein. Application of NBD-phallicidin to fixed permeabilized endothelial monolayers resulted in 78.8% penetration of the probe into cells and 99.98% of intracellular probe was extracted with a single methanol treatment as measured by fluorometry. In other experiments, monolayers again were pretreated with cycloheximide 50μg/ml 30 min prior to and throughout the standard rTNFα, LPS, or medium exposure.

Deoxyribonuclease (DNAse) 1 Inhibition Assay: EC G-actin was measured using the DNAse 1 inhibition assay as we have described (5). This assay utilizes the ability of monomeric G-actin to inhibit DNAse 1 hydrolysis of type 1 DNA into its component nucleotides. DNAse 1 obtained from bovine pancreas (Sigma) was dissolved at 10 mg protein/ml in 0.125M Tris-HCl (pH 7.5) 5mM $MgCl_2$, 2mM $CaCl_2$, 1mM NaN_3, and 0.1mM PMSF to increase its stability. The stock solution was then diluted 100X with 20mM imidazole, pH 7.5, 30mM $NaCl_2$, and 15% glycerol. The enzyme was freshly made every 2 h and kept on ice. Calf thymus DNA (Type 1, Sigma) was used as substrate for the DNAse 1. The fibrous DNA preparation was cut into fine pieces and suspended in 0.1M Tris-HCl (pH = 7.5), 4mM $MgSO_4$, 1.8mM $CaCl_2$ at a concentration of 80μg DNA/ml. The DNA was brought into solution by slow stirring at 4°C for 48h after which the solution was sequentially passed through 0.45 and 0.22μM pore size filters and stored at 4°C. The absorbance of the final substrate at 260 nm varied between 1.05 and 1.15. The DNAse 1 was mixed with DNA substrate in the cuvette of a Gilford Response II Spectrophotometer (Ciba Corning Diagnostics) and the slope of the linear portion of the ΔA 260 recorded. Purified bovine skeletal muscle actin (Sigma) was used as the G-actin standard to calibrate the assay. This preparation was > 90% G-actin by SDS PAGE, had a MW of 43,000, and was dissolved in 20 mM Tris-HCl (pH 7.5), 1 M Na Acetate, 1 mM $CaCl_3$, 1.0 mM ATP, 0.75 M guanidine HCl. DNAse 1 inhibitory activity within a range of 30-70% inhibition is directly proportional to monomeric G-actin. Endothelial monolayers grown in 6-well plates were exposed to media or varying concentrations of rTNFα or LPS for varying exposure times. The monolayers were washed with Dulbecco's PBS (without Ca^{2+} and Mg^{2+})

and permeabilized with lysing buffer (HBSS with 1% Triton X-100, 2mM $MgCl_3$, 2mM EGTA, 0.2 mM ATP, 0.5 mM DTT, 0.1 mM PMSF) 0.5 ml/well for 5 min. The G-actin-containing supernatants then were tested in the DNAse 1 inhibition assay to generate inhibitory activities that fell on the linear portion of the standard curve (i.e., 30-70% inhibition). The inhibitory activities were interpolated to G-actin concentrations which were used to calculate G-actin expressed in μg per mg total EC protein. In selected experiments, monolayers were preincubated with NBD-phallicidin 0.3 μM for 3h prior to standard rTNFα, LPS, or media exposure. In other experiments, monolayers were pretreated with cycloheximide 50 μg/ml 30 min prior to and throughout the rTNFα, LPS, or media exposures.

Quantitative Immunoblotting for Total Actin: Postconfluent monolayers grown in 6-well plates were exposed to rTNFα, LPS, or media alone for 6h. Cell counts and total protein concentrations were determined as described above. Cell lysates were solubilized in 2% SDS, 10% 2-mercaptoethanol, 10% glycerol, 20mM Na_2PO_4, and bromophenol blue 0.001% and boiled at 100°C for 10 min. Cell lysates and known concentrations (10-500ng) of pure bovine skeletal muscle actin standard (Sigma) were loaded onto a 10% SDS-PAGE vertical slab gel, electrophoresed, and transferred onto nitrocellulose. The nitrocellulose membrane blots were blocked (2% BSA, 0.2% Tween-20 in PBS, pH 7.4), rinsed, and incubated with murine anti-avian actin IgG_1 kappa chain (ICN, Costa Mesa, CA) at 1:1000 dilution for 1hr at room temperature. The blots were washed 3 times and incubated with Protein G-Horseradish Peroxidase conjugate (BioRad, Richmond, CA) at 1:3000 dilution for 1 hr at room temperature. The blots were again washed, incubated with Enhanced Chemiluminescence substrates (Amersham, Arlington Heights, Il), and exposed to Kodak XAR X-Ray film for varying exposure times. Autoradiographs were scanned by laser densitometry (Molecular Dynamics, Sunnyvale, CA) and actin was quantified by interpolation from the actin standard curve. The correlation coefficients for all standard curves simultaneously run with each immunoblot were within range of 0.97 to 0.99. The actin concentrations were standardized to total EC protein and expressed as μg actin/mg total protein.

Actin Immunoprecipitation of ^{35}S-Methionine Labeled Endothelial Cells: Postconfluent endothelial monolayers grown in 6-well plates were washed and metabolically labeled with ^{35}S-methionine (Amersham, Arlington Heights, IL) in supplemented methionine-free DMEM (Gibco, Grand Island, NY) and stimulated with rTNFα, LPS, or media alone for 6h. Monolayers were washed in HBSS x 3, trypsin-detached, resuspended in DMEM with 10% FBS and the cells counted. The cells were then washed x 3 in HBSS (200g, 10 min, RT). The final cell pellets were aspirated dry and placed on ice. Cell pellets were lysed with 1 ml ice-cold lysis butter (3% SDS, 1% 2-mercaptoethanol, 50mM Tris-Hcl, pH 8.0, 10μM PMSF, 10μg/ml leupeptin, 1mM EDTA) and vortexted rigorously. For immunoprecipitation of actin, 200 μl lysate was incubated with rabbit anti-avian actin polyclonal antibody (Sigma) in Na_2HPO_4 50mM, pH 7.4, and deinonized H_2O used to bring the final volume up to 500 μl. The samples were equilibrated 15 min/RT followed by an 18h incubation at 4°C. Actin:antibody complexes were then incubated with precleaned and prewashed Protein G (Omnisorb™, Calbiochem, LaJolla, CA) for 30 min on ice with vortexing every 10 min. Each sample was microfuged (10,000 rpm, 5 min), the supernatants decanted, and the pellets washed and suspended in Tris buffered saline. The

resuspended pellets were transferred to scintillation vials into Optifluor Scintillation fluid (Packard) and β counts obtained ($^{35}S/^{14}C$ window). ^{35}S-methionine incorporation into actin immunoprecipitates, i.e., new actin synthesis, was expressed as dpms per immunoprecipitate.

Filter Detachment Assay: Polycarbonate filters (25mm diameter, 0.4μm pore size) (Nucleopore) which were gelatin impregnated and mounted in polystyrene chemotactic chambers (ADAPS) as described above, were inserted into the wells of 6-well plates. Each filter was seeded with 3.5 x 10^5 EC in 3ml media and cultured for 72h (37°C, 5% CO_2). The postconfluent monolayers were either exposed for 6h to increasing concentrations of LPS or SPARC or to LPS 10ng/ml or medium alone for increasing exposure times. In selected experiments, EC were subjected to an ambient temperature of 4°C or serum deprivation as described above. The supernatant and one wash from each well were pooled and the cells counted in duplicate. The remaining monolayers were trypsin-detached (0.5mg/ml, 15min), and counted. After trypsin treatment, filters were stained with Coumassie's blue to document complete cell detachment. Percent detachment was expressed as [total cells in the supernatant and wash]/[total cells in supernatant, wash, and filter] x 100%.

Statistical Methods: The mean response of each experimental group was compared to its simultaneous control by two-tailed student's t test. Analyses of variance were used to compare the mean responses among experimental and control groups.

B. **RESULTS:**

Role of TNFα (*In Vivo*): As a first test of the direct involvement of TNFα in acute pulmonary vascular endothelial injury, we administered human rTNFα to rabbits in 5 equivalent 200,000-unit bolus infusions every 0.5h over the first 2h of a 5h study period (i.e., 2.5 x 10^5 units or 5 ug per kg BW) (2). At this dose, rTNFα-challenged animals displayed no significant granulocytopenia or pulmonary leukostasis as determined by both histological (alveolar septal wall granulocytes per high power field) and biochemical markers (myeloperoxidase activity per gm lung tissue) compared to saline-infused controls. rTNFα increased lung wet/dry weight ratios (a gravimetric index of pulmonary edema formation) ($p<0.02$) and pulmonary extravasation of ^{125}I-labeled rabbit serum albumin ($p<0.01$). Electron microscopy of lung sections from rTNFα-challenged rabbits demonstrated endothelial gap formation with extravasation of a preinfused permeability tracer through the gaps. These findings implicated the pulmonary vascular endothelial surface as a major target for TNFα and a paracellular route for movement of macromolecules across the endothelial barrier.

Role of TNFα (*In Vitro*): To study the mechanisms of cytokine-induced changes in pulmonary vascular endothelial permeability and/or injury on a cellular/molecular level, we studied the influence of human rTNFα on movement of ^{14}C-BSA across confluent bovine PA EC monolayers (3).

Dose-, Time-, and Temperature-Dependence: rTNFα dose-dependently increased transendothelial ^{14}C-BSA flux, which significantly ($p<0.02$) correlated with the concentration of 24h rTNFα exposure (Fig. 1). Maximum ^{14}C-BSA flux of 0.74 pmoles/h or 13.16% transfer of the tracer was seen after rTNFα exposure with 2000 u with subsequent plateauing. The effect of rTNFα (200 u/ml) on transendothelial ^{14}C-BSA flux was also time-dependent (Fig. 2 and 3). Only after an incubation time of $\geq$4h did rTNFα significantly ($p<0.005$) increase transendothelial albumin flux (Fig. 2) and rTNFα pulse exposures as brief as 5 min induced significantly ($p<0.005$) increased albumin transfer detectible at 6h (Fig. 3). Note: Unless otherwise stated, rTNFα 200 u/ml x 6h was used in subsequent experiments. To determine whether the change in ^{14}C-BSA transfer was temperature-dependent, monolayers were exposed to rTNFα for 20 minutes at 4°C, 20°C, and 37°C (Fig. 4). rTNFα significantly ($p<0.001$) increased ^{14}C-BSA transfer only at 37°C (Fig. 4A). To determine whether the initial rTNFα exposure and/or the subsequent $\geq$ 4h lag time was temperature-dependant, monolayers were exposed to rTNFα for 20 minutes at 4°C, washed at 4°C and then incubated at either 4°C or 37°C (Fig. 4B). Monolayers incubated at 37°C after brief rTNFα exposure at 4°C displayed a significant ($p<0.005$) increase in ^{14}C-BSA transfer compared to simultaneous controls. These experiments suggest that the initial rTNFα-EC interaction was not temperature-dependent but that the subsequent cellular events were.

Contribution of LPS: To exclude any contribution of LPS, transendothelial ^{14}C-BSA flux was assayed after exposure to rTNFα, rTNFα preincubated with neutralizing rabbit anti-human rTNFα polyclonal antibody (Knoll Pharmaceuticals/BASF K&K Corp., Whippany, NJ 07981), boiled rTNFα, a 100,000-fold greater concentration of *Escherichia coli* 0111:B4 LPS (1.0 ng/ml

media) (Difco Lab, Detroit, MI) than the maximum but undetectable LPS concentration that could be present in the rTNFα preparation, or media alone (Fig. 5). The cytokine preparation and media contained no detectible LPS activity by Limulus Amoebocyte Lysate Assay (LAL) (Whittaker, MA Bioproducts, Walkersville, MD). Only the fresh rTNFα in the absence of antisera significantly ($p < 0.001$) increased transendothelial ^{14}C-BSA flux. Although the changes in barrier function cannot be ascribed solely to LPS, a synergistic action between rTNFα and undetectable amounts of LPS cannot be excluded.

Prolonged Stimulus-to-Response Time: To address the stimulus-to-response lag time intrinsic to rTNFα-induced changes in endothelial barrier function, we studied the impact of rTNFα on EC proliferation, injury, and viability (Fig. 6-9). EC at subconfluent density were exposed to rTNFα or media alone for increasing time intervals, detached for trypan blue staining, and viable and nonviable EC counted (Fig. 6). rTNFα did not alter EC populations after 3,6, or 12h exposures compared to media controls. rTNFα exposures of $\geq$24h significantly ($p < 0.02$) inhibited EC growth and exposures of $\geq$36h significantly ($p < 0.04$) decreased EC viability. To study the effect of rTNFα on EC proliferation, ^{3}H-thymidine was added to subconfluent (Fig. 7) or postconfluent (Fig. 8) cultures in the presence or absence of rTNFα and ^{3}H-thymidine incorporation serially determined. Under subconfluent conditions, rTNFα was not cytostatic at 3 or 6h but at $\geq$12 it was ($p < 0.001$). Under postconfluent conditions, rTNFα had to effect on ^{3}H-thymidine incorporation over 6h. Using a ^{51}Chromium release assay as a measure of EC injury, no significant differences between rTNFα-exposed postconfluent monolayers and media controls were demonstrated over 24h (Fig. 9). These data demonstrate that rTNFα-induced alterations in endothelial barrier function seen at 4-6h cannot be ascribed to EC growth inhibition, cell injury or loss of cell viability. In fact, we have now demonstrated that after either 5 min or 6h TNFα exposures, endothelial barrier function returns to basal levels 16h after removal of rTNFα (Fig. 10). To address the potential issue of "unstirred layers" contributing to a prolonged stimulus-to-response time, the effects of rTNFα in agitated and nonagitated assay chambers were compared and no difference was found (Fig. 11).

Role of Protein Synthesis: We then determined whether the rTNFα-induced alterations in endothelial barrier function were protein synthesis-dependent (Fig. 12). Monolayers were preincubated with cycloheximide at concentrations (25-200 ug/ml media) that inhibited >95% protein synthesis as measured by ^{35}S-methionine incorporation into trichloroacetic acid-(TCA)-precipitable protein. The monolayers were then exposed to rTNFα and assayed for ^{14}C-BSA transfer. Prior protein synthesis inhibition failed to block rTNFα-induced alterations in endothelial barrier function, suggesting that *de novo* protein synthesis is not essential to the process. In fact, the protein synthesis inhibition at all cycloheximide concentrations tested significantly ($p < 0.001$) enhanced the rTNFα-induced increments in ^{14}C-BSA flux. Similar results were demonstrated using actinomycin D (0.125-1.0 ug/ml) to inhibit mRNA synthesis (Fig. 12). In addition, we have shown that a subthreshold rTNFα exposure significantly ($p < 0.01$) protects against a subsequent suprathreshold rTNFα challenge (Fig. 13). These combined data are compatible with a rTNFα-induced protein synthesis-dependent process protective against loss of endothelial barrier function.

Tracer Specificity: To determine whether rTNFα-induced changes in endothelial barrier function were specific to albumin, assays were simultaneously performed using equimolar amounts of ^{14}C-BSA (MW=66,000) and ^{3}H-Dextran (average MW=70,000; Specific Activity=214 uCi/mg) (Amersham Corp., Arlington Heights, IL) (Fig. 14). Transfer of both ^{14}C-BSA and ^{3}H-Dextran were significantly ($p<0.01$) increased across endothelial monolayers exposed to all 3 rTNFα concentrations compared to the control and ^{14}C-BSA flux was not significantly different than ^{3}H-Dextran flux at all concentrations tested. Therefore, the effect of rTNFα on movement of macromolecules across the endothelium is not albumin-specific.

Actin Cytoskeletal Structure-Function Relationship: We have demonstrated that human rTNFα induces changes in endothelial barrier function temporally coincident with EC actin depolymerization (Fig. 15) and intercellular gap formation (Fig. 16) (4). Preloading EC with a selective probe that binds to and stabilizes F-actin against depolymerization protects against the rTNFα-induced G-actin incement (Fig. 17) and barrier dysfunction (Fig. 18). In contrast, prior protein synthesis inhibition greatly enhances them (Fig. 17 and 18). The rTNFα-induced changes in endothelial barrier function were clearly time-dependent. Coincident with these rTNFα-induced increments in permeability, we demonstrated thinning of cytoplasmic actin microfilaments and intraendothelial cell gap formation (Fig. 16). rTNFα increased the G-actin pool with a reciprocal, although delayed, decrease in the endothelial F-actin pool (Fig. 15). The rTNFα-induced decrement in F-actin could only be detected at 6h, with a maximal mean percent decrease of -7% (Fig. 15). rTNFα concentrations of up to 10,000u/ml failed to induce greater F-actin decrements (Fig. 19). This decrease in F-actin was greatly enhanced by prior protein synthesis inhibition, with a mean percent decrease of -44% (Fig. 20). This suggested that new actin synthesis might partially compensate for and mask the rTNFα-induced F-actin decrement. The rTNFα-induced increment in G-actin could be first detected at 2h, with a maximal percent mean increase of +51% (Fig. 17). This G-actin increment was reversible (Fig. 21). The G-actin increment was, in part, blocked by prior F-actin stabilization with phallicidin and, in part, by protein synthesis inhibition (Fig. 17). These findings suggested that the G-actin increment could be explained by both F-actin depolymerization and new actin synthesis. That rTNFα stimulated actin synthesis was further substantiated by an increased total actin pool (Fig. 22) as well as increase [^{35}S]-methionine incorporation into actin immunoprecipitates (Fig. 23).

The shift from the F- to G-actin pools was not perfectly reciprocal. The increment in G-actin both preceded and exceeded the decrement in F-actin. First, although the stoichiometries between phallicidin and actin monomers incorporated into microfilaments and between DNase I and G-actin are comparable, it is not possible to reconcile micrograms in the DNase I inhibition assay for G-actin with arbitrary fluorescence units in the fluorometric assay for F-actin. Second, new actin synthesis contributes to the increment in G-actin without cost to the F-actin pool and possibly increases it. In the face of protein synthesis inhibition, the F-actin decrement was -44% (vs. -8%) and the G-actin increment was +13% (vs. +51%). Therefore, in the absence of new actin synthesis, the F-actin decrement was enhanced and the G-actin increment lessened, making the reciprocal changes more comparable. Third, actin pool measurements reflect mean changes over an entire monolayer, although area-to-area differences within the same monolayer may exist. Although cultured cells can behave differently from

experiment to experiment, the pretreatment baselines for mean (± SE) F-actin for the three different data sets (266.1±5.3,270.4±7.9, 272.4±7.44) were not significantly different, and the mean percent changes from baseline at 6h were -6.9, -8.7, and -8.3%, respectively. Similarly, there was no significant differences between the pretreatment baselines for mean (±SE) G-actin (168.7±6.52, 179.2±6.10, and 173.5±5.00), and at 2h the mean percent changes from the baseline were +50.7, +36.4, and 44.8%, respectively. Therefore, the two assays were reproducible. More important than the absolute F- and G-actin values are their relative changes over time.

Effects of LPS on Endothelial Barrier Function: We studied the effect of native LPS derived from *Escherichia coli* 0111:B4 on movement of ^{14}C-bovine serum albumin (BSA) across postconfluent bovine pulmonary artery EC monolayers (6). In the presence of serum, LPS augmented transendothelial ^{14}C-BSA flux in a dose-, time-, and temperature-dependent manner. A 6h LPS exposure increased ($p<0.001$) ^{14}C-BSA flux compared to the media controls at concentrations $\geq$0.5 ng/ml with plateauing at $\geq$10 ng/ml (Fig. 24-see hatched bars). Continuous LPS (10 ng/ml) exposures of $\geq$2h increased ($p<0.005$) ^{14}C-BSA flux with further increments at 4h and 6h (Fig. 25). We have also demonstrated that LPS exposure times as brief as 10min was sufficient to induce a biological response demonstrable only after a considerable lag time (Fig. 26). LPS exposure increased ($p<0.0001$) ^{14}C-BSA flux compared to the isothermal media control at 37°C but not at 4°C (Fig. 27). That LPS-induced changes in endothelial barrier function are saturable, temperature-dependent, and can be elicited after very brief LPS exposures, is compatible with a receptor-mediated process. When bovine pulmonary arterial, aortic, and retinal microvascular EC monolayers were each exposed to LPS, ^{14}C-BSA flux across all three endothelia increased ($p<0.001$) compared to their respective media controls (Fig. 28)-i.e., extrapulmonary endothelia, including a microvascular endothelium that is part of the blood-brain barrier, responded similarly to LPS. Lastly, three cytotoxicity/viability assays of varying sensitivity and specificity were used to determine whether LPS-induced changes in barrier function could be ascribed to EC injury or death (Table 1). On the basis of trypan blue exclusion and LDH release, there was no loss of membrane integrity or viability in LPS-exposed monolayers. When the more sensitive but less stringent ^{51}Cr detection system was used, LPS increased ^{51}Cr release at 4 and 6h ($p<0.04$). LPS induced ^{3}H-adenine release at all time points tested suggesting a selective effect on nucleotide pools and transport. These data suggest that LPS can induce EC membrane perturbation without frank loss of viability.

Influence of Serum on LPS-Induced Changes in Endothelial Barrier Function: The LPS-induced changes in endothelial barrier function were profoundly serum-dependent (6). In the presence of 10% FBS, LPS concentrations as low as 0.5 ng/ml increased ^{14}C-BSA flux ($p<0.001$) (Fig. 24-see hatched bars). In the absence of FBS, only LPS concentrations $\geq 10^5$ ng/ml increased flux ($p<0.0001$) (Fig. 24-see open bars). Therefore, the presence of serum increased EC sensitivity to the LPS stimulus by ~20,000-fold. Albumin flux across serum-starved monolayers was also measured after a 6h exposure to a fixed LPS concentration (10 ng/ml) or media, both in the presence of increasing FBS concentrations (Fig. 29). LPS increased ($p<0.04$) ^{14}C-BSA flux at serum concentrations $\geq$0.5% reaching the maximum effect at 2.5%. At the intervening FBS concentrations, i.e., 0.5 to 2.5%, the LPS effect on flux increased with

increasing FBS concentrations.

Role of LPS-Binding Protein (LBP) in LPS-Induced Changes in Endothelial Barrier Function: The ability of LBP to support the LPS-induced EC response was studied (6). Albumin flux was determined across serum-starved monolayers exposed for 6h to serum-free media, LPS 100 ng/ml without serum, media enriched with 10% FBS, LPS and FBS, LPS 100 ng/ml with an estimated equimolar concentration of rabbit LBP (1.2μg/ml), LPS with human LBP, or media with rabbit or human LBP alone, as well as species-matched protein controls (Fig. 30). LPS only in the presence of FBS or either species LBP increased transendothelial ^{14}C-BSA flux ($p<0.002$). When monolayers were exposed for 6h to a fixed LPS concentration (100 ng/ml) in the presence of varying rabbit LBP concentrations, the LPS/LBP effect increased as the LBP concentration increased (Fig. 31). The maximal LPS/LBP effect was seen in the presence of LBP 1.0μg/ml, a close approximation of the estimated equimolar concentration of LBP (MW=60 kDa) for LPS 100 ng/ml (estimated ave. MW=5,000 Da). These data are compatible with an optimal LPS:LBP ratio of 1:1 or 1 lipid A-binding site per LBP molecule. In the presence of human serum, anti-human LBP antisera blocked the LPS-induced endothelial barrier dysfunction ($p<0.00005$) (Fig. 32). Therefore, the single protein, LBP, could replace whole serum in the promotion of the LPS effect.

Role of sCD14 in LPS-Induced Changes in Endothelial Barrier Function: The ability of sCD14 to support the LPS-induced changes in the absence of serum or LBP was studied (6). Albumin flux was determined across serum-starved monolayers exposed for 6h to serum-free media, LPS 100ng/ml without serum, LPS with human sCD14 50 ng/ml, LPS with human LBP 100 ng/ml, LPS with both sCD14 and LBP, sCD14 alone, LBP alone, sCD14 and LBP, as well as species-matched protein control (Fig. 33). LPS with sCD14 in the absence of serum or LBP increased ^{14}C-BSA flux compared to either LPS or sCD14 controls ($p<0.001$). · When monolayers were exposed for 6h to a fixed LPS concentration (100 ng/ml) in the presence of varying sCD14 concentrations, the LPS/sCD14 effect increased as the sCD14 concentration increased (Fig. 34). Soluble CD14 concentrations $\geq$25 ng/ml in the presence of LPS increased albumin flux compared to sCD14 alone ($p<0.02$). The LPS/sCD14 effect plateaued at sCD14 concentrations of $\geq$500 ng/ml. LBP further enhanced the LPS-sCD14 induced increment compared to that seen after exposure to LPS-sCD14 alone ($P=0.0003$) (Fig. 33). Again, in the presence of human serum, antihuman CD14 antibody blocked the LPS-induced barrier dysfunction ($p<0.00005$) (Fig. 32). In a serum-free reconstituted LPS-human LBP system, anti-CD14 antibody had no effect. In addition, HS immunodepleted of sCD14 with immobilized anti-human CD14 antibody failed to support the LPS effect (Fig. 35). This CD14-depleted HS contained suprathreshold concentrations of LBP and no anti-CD14 antibody. Therefore, immunoblockade with anti-CD14 antibody prevented LPS-induced changes only in the presence of serum - i.e., it targeted sCD14, not EC membrane-associated CD14. These studies demonstrate that sCD14 participates in and is even essential to LPS-induced changes in endothelial barrier function.

Kinetic Analysis of LPS-Induced Changes in Endothelial Barrier Function in the Presence of LBP, sCD14, or Both: LBP, sCD14, or both accessory molecules together, were studied

for their ability to promote the LPS-induced changes in barrier function over time (Fig. 36) (6). LPS in the presence of either LBP or both LBP and sCD14 increased ^{14}C-BSA flux compared to LPS alone at all time points $\geq$ 1h ($p<0.0005$). LPS in the presence of sCD14 alone (50 or 500 ng/ml) did not increase ^{14}C-BSA flux until 6h ($p<0.0001$). Therefore, the LPS-induced changes in endothelial barrier function in the presence of either LBP or sCD14 alone are kinetically distinct. Again, LPS in the presence of both LBP and sCD14 for 6h induced greater ^{14}C-BSA flux than did LPS with either accessory molecule alone ($p<0.01$).

Structure-Function Relationship Between the LPS Molecule and Endothelial Function: To determine which portion of the LPS molecule was responsible for changes in endothelial barrier function, LPS derived from well-defined mutants as well as biochemically purified LPS components were employed. When LPS obtained from the *E. coli* J5 Rc mutant was compared on the basis of KDO content to LPS derived from the wild type, *E. coli* 0111:B4, there was no significant difference; deacylation of J5 reduced its activity ($p<0.01$) (Fig. 37). LPS derived from series of *Salmonella minnesota* mutants with varying O-polysaccharide chain lengths all displayed similar bioactivities (Fig. 38). When a wide range of concentrations of purified *E. coli* lipid A and O-polysaccharide devoid of lipid A were compared on a dry weight-for-weight basis, lipid A induced dose-dependent increments in endothelial permeability whereas the O-polysaccharide preparation did not (Fig. 39). These data suggest that lipid A is the portion of the LPS molecule required to induce an EC response, that the acyl chains on lipid A are essential for the LPS-EC interaction, and O-polysaccharide of varying chain lengths does not interfere.

Actin Cytoskeletal Structure-Function Relationship: We have studied whether LPS regulates endothelial barrier function through actin reorganization (5). Postconfluent EC monolayers were exposed to LPS 10 ng/ml or media alone for up to 6h and evaluated for: (1) transendothelial ^{14}C-albumin flux, (2) F-actin organization with fluorescence microscopy, (3) F-actin quantitation by spectrofluorometry and (4) monomeric G-actin levels by the DNAse 1 inhibition assay. LPS induced increments in ^{14}C-albumin flux ($p<0.001$) (Fig. 25), G-actin ($p<0.002$) (Fig. 40), and intercellular gap formation at $\geq$2-6h (Fig. 41). During this same time period the EC F-actin pool was not significantly changed (Fig. 40). LPS concentrations up to 10^5 ng/ml all failed to significantly decrease F-actin (Fig. 42). Prior F-actin stabilization with phallicidin protected against the LPS-induced increments in G-actin ($p=0.040$) (Fig. 43) as well as changes in barrier function ($p<0.0001$) (Fig. 44). Prior protein synthesis inhibition unmasked an LPS-induced decrement in F-actin ($p=0.0044$) (Fig. 45), blunted the G-actin increment ($p=0.010$) (Fig.43), and increased LPS-induced changes in barrier function ($p<0.0001$) (Fig. 44). These data are compatible with LPS-induced endothelial F-actin depolymerization, intercellular gap formation, and barrier dysfunction. Over the same time period, LPS increased total actin ($p=0.0017$) (Fig. 46) and new actin synthesis ($p=0.0063$) (Fig. 47) which may be a compensatory EC response to LPS-induced F-actin disassembly.

Effect of LPS on EC Detachment: The effect of LPS on both transendothelial ^{14}C-BSA flux and EC detachment were studied in parallel (Fig. 48-52). The dose (Fig. 48), time (Fig. 49), temperature (Fig. 50), and serum (Fig. 51) requirements for these two EC responses were

similar. Further, when EC detachment (%) was correlated with transendothelial ^{14}C-BSA flux (pmol/hr), the correlation coefficient = 0.925 (Fig. 52).

SPARC - A Postulated Mediator for LPS-Induced Increments in Endothelial Permeability:
Another potential mechanism for LPS-induced changes in EC shape and barrier function involves increased EC expression of SPARC (Secreted Protein Acidic and Rich in Cysteine) (7). SPARC, known also as osteonectin and BM-40, is a 43KDa glycoprotein constitutively secreted by EC at 1-3% of total secreted protein. Exposure of cells to picogram concentrations of LPS induces up to a 3-fold increase in expression of this protein in $\geq$1.5h. Exogenous SPARC induces dose-dependent rounding of confluent EC in the absence of cell injury. We have now studied whether SPARC, through its ability to regulate EC shape, might regulate endothelial barrier function (7). We studied the effect of exogenous murine SPARC, which shares an amino acid sequence identity of 92% with bovine SPARC, on the movement of ^{14}C-BSA across bovine EC monolayers (Fig. 53-59). SPARC increased ^{14}C-BSA flux compared to controls ($p < 0.02$) in a dose-dependent manner at all concentrations $\geq$0.5 μg/ml (Fig. 53). At 15 μg/ml, exposure times of $\geq$1h increased ^{14}C-BSA flux ($p < 0.005$) with further time-dependent increments (Fig. 54). The SPARC-induced changes in barrier function could be blocked ($p < 0.01$) by prior incubation with neutralizing rabbit anti-murine SPARC polyclonal antibody, trypsin digestion, and heat treatment (Fig. 55) but not by protein synthesis inhibition (Fig. 56). Thus, the SPARC-induced changes in endothelial barrier function could not be ascribed to either LPS contamination or, *de novo* synthesis of a second protein mediator. In addition, SPARC exposure was not associated with loss of cell viability (Table 2). Scanning electron microscopy of SPARC-exposed monolayers revealed cell rounding and intercellular gaps (Fig. 57). F-actin fluorescence microscopy of SPARC-exposed, phalloidin-probed monolayers confirmed the rounded morphology and intercellular gap formation (Fig. 58 A-C). Prior F-actin stabilization with phallicidin protected against the SPARC-induced changes in barrier function ($p = 0.0001$) (Fig. 58D). Therefore, SPARC induced specific dose-, time, and F-actin-dependent changes in endothelial barrier function temporally coincident with intercellular gap formation. Although LPS upregulates EC SPARC expression and SPARC can regulate EC shape and barrier function, a causal role for SPARC in LPS-induced barrier dysfunction has yet to be proven.

(7) CONCLUSIONS:

A. Summary of Completed Research

1. **Influence of TNFα on Endothelial Barrier Function:**
   a. TNFα increases transendothelial ^{14}C-BSA flux in a dose-, time-, and temperature-dependent manner.
   b. TNFα-induced barrier dysfunction requires a brief exposure time but a prolonged stimulus-to-response lag time.
   c. The TNFα-induced changes in barrier function were saturable, were not protein synthesis-dependent, could not be ascribed to cytotoxicity or loss of EC viability, and was, in fact, reversible.
   d. The TNFα effect on transendothelial flux of macromolecules was not specific for albumin.
   e. A structure-function relationship exists between TNFα-induced changes in endothelial barrier function and EC actin reorganization. TNFα induces depolymerization of filamentous F-actin to soluble, monomeric G-actin and this actin depolymerization is a prerequisite to TNFα-induces barrier dysfunction.
   f. TNFα induces EC actin synthesis which may be a host cell compensatory response to TNFα-induced F-actin disassembly.

2. **Influence of LPS on Endothelial Barrier Function:**
   a. LPS induces dose-, time-, and temperature-dependent increments in endothelial permeability.
   b. LPS-induced barrier dysfunction requires a brief exposure time but a prolonged stimulus-to-response lag time.
   c. The LPS effect was saturable, was not protein synthesis-dependent, and could not be explained through loss of EC viability.
   d. The LPS effect was profoundly serum-sensitive. The addition of low concentrations of serum increased the EC sensitivity to the LPS stimulus many fold.
   e. LBP and sCD14 could each satisfy this serum requirement.
   f. A causal structure-function relationship exists between LPS-induced loss of barrier function and EC actin depolymerization.
   g. LPS induces *de novo* actin synthesis in EC.

3. **Influence of SPARC on Endothelial Barrier Function:**
   a. SPARC induces changes in endothelial barrier function in a dose-, time-, and temperature-dependent manner.
   b. The SPARC effect was comparable for endothelia harvested from systemic and pulmonic large vessels as well as the blood-brain barrier microvasculature.
   c. The SPARC effect was F-actin dependent and protein synthesis-independent.

B. Recommendations for Future Work

Important overlap exists between TNFα and LPS and their abilities to regulate endothelial barrier function. These include a prolonged stimulus-to-response lag time, actin depolymerization, endothelial cell shape changes, and intercellular gap formation. A logical next step(s) will be to delineate intracellular effector mechanisms that are activated by TNFα/LPS that lead to actin depolymerization and intercellular gap formation i.e. opening of the paracellular pathway. These include established signal transduction pathways as well as phosphorylation of target protein substrates within the specialized apparatus found at the cell-cell (zonula adherence, zonula occludens) and cell-matrix (focal adhesions) interfaces. These should address the role of adherence junction and/or focal adhesion disassembly in intercellular gap formation and loss of barrier function.

(8) REFERENCES PUBLISHED BY THE PRINCIPAL INVESTIGATOR RELEVANT TO THIS GRANT:

1. **Goldblum SE**, Jay M, Yoneda K, Cohen DA, McClain CJ, Gillespie MN. Monokine-induced acute lung injury in rabbits. *Journal Applied Physiology*; 1987, 63, 2093-2100.

2. **Goldblum SE**, Hennig B, Jay M, Yoneda K, McClain CJ. Tumor necrosis factorα-induced pulmonary vascular endothelial injury. *Infection and Immunity*; 1989, 57:1218-1226.

3. **Goldblum SE**, Sun WL. Human recombinant tumor necrosis factorα augments pulmonary artery transendothelial albumin flux *in vitro*. *Am. J. Physiology (Lung Cellular and Molecular Physiology)*; 1990, 258:L57-L67.

4. **Goldblum SE**, Ding X, Campbell-Washington J. Tumor necrosis factorα induces endothelial cell F-actin depolymerization, new actin synthesis, and barrier dysfunction. *Am. J. Physiol. (Cell Physiol.:33)*; 1993, 264:C894-C905.

5. **Goldblum SE**, Ding X, Brann TW, Campbell-Washington J. Bacterial lipopolysaccharide induces actin reorganization, intercelluar gap formation and endothelial barrier dysfunction in pulmonary vascular endothelial cells. Concurrent F-actin depolymerization and new actin synthesis. *J. Cell Physiol.*; 1993, 157;13-23.

6. **Goldblum SE**, Brann TW, Ding X, Pugin J, Tobias PS. Lipopolysaccharide (LPS)-binding protein (LBP) and soluble CD14 function as accessory molecules for LPS-induced changes in endothelial barrier function. *J. Clin. Invest.*; 1994, 93:692-702.

7. **Goldblum SE**, Ding X, Funk S, Sage EH. SPARC Regulates Cell Shape and Endothelial Barrier Function. *Proc. Natl. Acad. Sci. (USA)*; 1994, 91:3448-3452.

APPENDIX A: TABLES

Table 1

TABLE 1: MEASUREMENTS OF ENDOTHELIAL CELL INJURY OR DEATH AFTER LPS EXPOSURE

TIME	1h	(n)	2h	(n)	4h	(n)	6h	(n)
TRYPAN BLUE EXCLUSION[1] (% NONVIABLE)								
MEDIA CONTROL	7.02 ± 0.52	(9)	8.49 ± 2.10	(9)	7.48 ± 0.70	(9)	8.34 ± 1.31	(9)
LPS (10 ng/ml)	6.99 ± 1.17	(9)	5.73 ± 0.80	(9)	4.21 ± 0.40	(9)	6.79 ± 1.12	(9)
LDH RELEASE (%)[2]								
MEDIA CONTROL	4.93 ± 1.74	(9)	1.98 ± 0.77	(9)	2.97 ± 0.79	(9)	2.22 ± 0.81	(23)
LPS (10 ng/ml)	2.14 ± 0.72	(9)	3.30 ± 1.87	(9)	2.98 ± 1.33	(9)	4.40 ± 0.99	(23)
^{51}CHROMIUM RELEASE (%)[3]								
MEDIA CONTROL	5.83 ± 0.51	(10)	8.13 ± 0.28	(10)	8.76 ± 0.23	(10)	13.00 ± 0.50	(10)
LPS (10 ng/ml)	6.73 ± 0.29	(10)	7.60 ± 0.44	(10)	13.10 ± 0.42*	(10)	16.26 ± 1.33*	(10)
^{3}H-ADENINE RELEASE (%)[4]								
MEDIA CONTROL	4.02 ± 0.53	(6)	5.00 ± 0.89	(6)	5.77 ± 0.76	(6)	6.70 ± 0.52	(10)
LPS (10 ng/ml)	7.61 ± 1.31*	(6)	10.08 ± 0.39*	(6)	36.39 ± 1.07*	(6)	50.20 ± 1.72*	(10)

1 Mean (± SE) percent cells failing to exlude trypan blue.
2 Mean (± SE) percent LDH release calculated as LDH in medium/LDH in medium + LDH in cell lysate x 100%;
3 Mean (± SE) percent ^{51}Chromium release calculated as ^{51}Chromium activity in supernatant/total ^{51}Chromium activities in supernatant and cell lysate x 100%.
4 Mean (± SE) percent ^{3}H-adenine release into the medium relative to maximum release from Triton X-100 solubilized cells;
* Significantly increased compared to simultaneous media controls at $p < 0.04$.

TABLE 2: EFFECT OF SPARC ON EC DETACHMENT AND CYTOTOXICITY

	Medium Control*	(n)	SPARC†	(n)
Total EC Counts($x10^6$) per monolayer‡	1.11±0.07	(11)	1.05±0.09§	(12)
EC Detachment(%)‡	2.0±0.17	(6)	3.5±0.37¶	(6)
Trypan Blue Exclusion‖ (%nonviable)	2.45±0.26	(6)	2.56±0.26§	(6)
LDH Release(%)**	3.58±0.55	(8)	3.65±0.85§	(8)

*Media controls were after 6h; † SPARC exposure was 15 μg/ml for 6h; ‡Mean (± SE) cell counts or percent detachment determined for postconfluent monolayers cultured on 25mm filters suspended in 6-well plates; §Not significant compared to medium control; ¶ significantly increased compared to medium control at p=0.0028; ‖ Mean (± SE) percent cells failing to exclude trypan blue; **Mean (± SE) percent LDH release calculated as [LDH in medium]/[LDH in medium + LDH in cell lysate] x 100%.

APPENDIX B: FIGURE LEGENDS

Figure 1: Dose-dependent effect of human rTNFα on transendothelial [^{14}C]BSA flux. 1-h transfer of [^{14}C]BSA across endothelial monolayers immediately after a 24-h exposure to increasing concentrations of rTNFα. Transendothelial [^{14}C]BSA flux was expressed as pmol/h. Vertical bars represent means (±SE) transendothelial [^{14}C]BSA flux. Mean (± SE) pretreatment baseline transendothelial [^{14}C]BSA flux is represented by closed bar and mean (± SE) [^{14}C]BSA flux across naked membrane filters by open bar.

Figure 2: Time-dependent effect of rTNFα on transendothelial [^{14}C]BSA flux. 1-h transendothelial [^{14}C]BSA flux in pmol/h immediately after increasing exposure times to rTNFα, 200 U/ml (cross-hatched bars) and simultaneous media controls (open bars). Vertical bars represent means (±SE) transendothelial [^{14}C]BSA transfer. Mean (±SE) pretreatment baseline transendothelial [^{14}C]BSA transfer is shown by closed bar. *Significantly increased compared with simultaneous media control at $P<0.005$.

Figure 3: rTNFα exposure time requirements. 1-h transfers of [^{14}C]BSA across endothelial monolayers all determined 6 h after onset of increasing rTNFα exposure times (200 U/ml) (cross-hatched bars) and their simultaneous media controls (open bars). Vertical bars represent means (±SE) transendothelial [^{14}C]BSA transfer. Mean (±SE) pretreatment baseline transendothelial [^{14}C] BSA transfer is shown by closed bar. *Significantly increased compared with simultaneous media control at $P<0.005$.

Figure 4: Temperature-dependent effect of rTNFα on transendothelial [^{14}C]BSA flux. *A*: transendothelial [^{14}C]BSA transfer across monolayers exposed to rTNFα, 200 U/ml for 6 h at 37,20, and 4°C (▨) and their simultaneous media controls studied at respective temperatures (□). *B*: endothelial monolayers were exposed to rTNFα, 4,000 U/ml for 20 min at 4°C, washed at 4°C, and after replacing the media, incubated at either 4 or 37°C (▨). Again, simultaneous control monolayers were performed with media alone under identical temperature conditions (□). Simultaneous rTNFα or media treatment and incubations were also performed at 37°C. Vertical bars represent means (±SE) transendothelial [^{14}C]BSA transfer. Mean (±SE) pretreatment baseline transendothelial [^{14}C]BSA transfer is represented by closed bars (■). *Significantly increased compared with media control at $P<0.001$.

Figure 5: Exclusion of endotoxin contamination. 1-h transfers of [^{14}C]BSA across endothelial monolayers after 6-h exposures to rTNFα 200 U/ml, boiled rTNFα, rTNFα preincubated with neutralizing rabbit antihuman rTNFα polyclonal antibody, *E. coli* lipopolysaccharide 1ng/ml, or media alone. Vertical bars represent means (±SE) transendothelial [^{14}C]BSA flux. Mean (±SE) pretreatment baseline transendothelial [^{14}C]BSA flux is represented by closed bar. *Significantly increased compared with the simultaneous media control at $P<0.001$.

Figure 6: Viable and nonviable EC counts of postconfluent EC monolayers after exposure to rTNFα 200 U/ml media or media alone were serially determined over 72h in triplicate using trypan blue exclusion.

Figure 7: Effect of rTNFα on ^{3}H-thymidine incorporation by subconfluent EC.

Figure 8: Effect of rTNFα on ^{3}H-thymidine incorporation by postconfluent EC.

Figure 9: Effects of rTNFα on EC ^{51}Cr release. ^{51}Chromium-loaded EC were exposed to either rTNFα, 200 U/ml (-■-) or media (-□-) for increasing time intervals up to 24 h. Mean (±SE) EC ^{51}Chromium release was determined in rTNFα-exposed endothelial monolayers and media controls at each time point in triplicate. ^{51}Chromium release was expressed as a percentage of maximum or 100% release from monolayers treated with Triton X-100.

Figure 10: Reversibility. 1-h transfers of [^{14}C]BSA across endothelial monolayers at 0 h (baseline) and at time points after a 6-h exposure to rTNFα 200 U/ml or media control. Symbols represent means (±SE) transendothelial [^{14}C]BSA transfer at each time point. *Significantly increased compared with simultaneous media control at $P < 0.05$.

Figure 11: Effect of agitation on rTNFα-induced endothelial barrier dysfunction.

Figure 12: Effect of protein synthesis inhibition on rTNFα-induced increments in transendothelial [^{14}C]BSA flux. Transendothelial [^{14}C]BSA transfer was determined across monolayers incubated with media alone, media containing cycloheximide 25,100, or 200μg/ml, media containing rTNFα, 200 U/ml, and cycloheximide pretreatment with subsequent rTNFα exposure. Vertical bars present means (±SE) transendothelial [^{14}C]BSA transfer. Mean (±SE) pretreatment baseline transendothelial [^{14}C]BSA transfer is represented by closed bar. *Significantly increased compared with rTNFα 200 U/ml without prior protein synthesis inhibition at $P<0.001$.

Figure 13: Ability of rTNFα pre-exposure to protect *vs* subsequent rTNFα challenge.

Figure 14: Comparison of transendothelial transfer of two permeability tracers of similar molecular weight. 1-h transfers of equimolar amounts of [^{14}C]BSA (open bars) and [^{3}H]dextran (cross-hatched bars) across endothelial monolayers immediately after 6h exposures to rTNFα (0,20,200, and 2,000 U/ml). Vertical bars represent means (±SE) transendothelial transfers. Mean (± SE) pretreatment baseline transendothelial transfers are also represented.

Figure 15: Time-dependent effect of rTNF-α on EC F- and G-actin pools. For F-actin studies, EC monolayers were exposed to 1,000 U/ml rTNF-α for increasing exposure times, fixed, permeabilized, incubated with 7-nitrobenz-2-oxa-1,3-diazole (NBD)-phallicidin, and extracted with methanol. Extracts were spectrofluorometrically assayed and F-actin concentrations at each time point expressed as means (±SE) fluorescent units per mg total EC protein (○). For G-actin measurements, similarly treated monolayers were permeabilized, and the supernatants were tested in a DNase I inhibition assay standardized with purified actin. Each point represents mean (±SE) G-actin in μg per mg total EC protein (●). *Significantly changed from pretreatment baseline at $P<0.01$.

Figure 16: Fluorescein-phalloidin staining of endothelial monolayers grown on filters before and after rTNF-α exposure (1,000 U/ml). *A*: medium control (x500). *B*: medium control (x800). *C*: rTNF-α, 2 h (x500). *D*: rTNF-α, 2h (x800). *E*: rTNF-α, 6 h (x500). *F*: rTNF-α, 6 h (x800). After above treatments, monolayers were fixed, permeabilized, stained with fluorescein-phalloidin, and examined by epifluorescence microscopy. Small arrows point to cytoplasmic actin filaments; large arrows point to peripheral actin bands; arrowheads point to focal disruptions in actin lattice and intercellular gaps.

Figure 17: Effect of F-actin stabilization and protein synthesis inhibition on cytochalasin B- and rTNF-α-induced increments in G-actin. EC monolayers were exposed to media, 0.5% DMSO, 0.3μM NBD-phallicidin, 50μg/ml cycloheximide, 20μg/ml cytochalasin B in DMSO, or 1,000 U/ml rTNF-α. Selected monolayers were pretreated with either NBD-phallicidin for 3h or cycloheximide for 0.5h before and throughout exposure to either cytochalasin B or rTNF-α. After 2h, monolayers were permeabilized, and supernatants were tested in the standardized DNase I inhibition assay. Each hatched bar represents mean (±SE) G-actin in μg per mg total EC protein.

Figure 18: Effect of F-actin stabilization and protein synthesis inhibition on cytochalasin B- and rTNF-α-induced increments in transendothelial [^{14}C]BSA flux. Endothelial monolayers grown on filters were pretreated with 0.3μM NBD-phallicidin or media alone for 3 h before either cytochalasin B (20μg/ml, 2 h) or rTNF-α exposure (1,000 U/ml, 6 h). In other experiments, monolayers were pretreated with 50μg/ml cycloheximide for 0.5 h before and throughout rTNF-α exposure. Simultaneous controls for media, 0.5% DMSO, 0.3μM NBD-phallicidin, 50μg/ml cycloheximide, 20μg/ml cytochalasin B, and 1,000 U/ml rTNF-α are each represented. Hatched bars represent means (±SE) transendothelial [^{14}C]BSA flux in pmol/h. Mean (±SE) pretreatment baseline transendothelial [^{14}C]BSA transfer is shown by solid bar.

Figure 19: Dose-dependent effect of rTNF-α on EC F- and G-actin pools. Endothelial monolayers were exposed to increasing concentrations of rTNF-α for exposure times at which maximum changes in F-actin (6 h) and G-actin (2 h) occur. Each symbol represents mean (±SE) F-actin in fluorescent units per mg total protein (○) or mean (±SE) G-actin in μg per mg total protein (●). *Significantly changed from simultaneous media control at $P < 0.005$.

Figure 20: Effect of protein synthesis inhibition on rTNF-α-induced decrements in EC F-actin. EC monolayers were exposed for 6h to media, 50μg/ml cycloheximide, or 1,000 U/ml rTNF-α, or to cycloheximide for 0.5h before and throughout a 6h rTNF-α exposure. Monolayers were fixed, permeabilized, incubated with NBD-phallicidin, and extracted with methanol. Extracts were fluorometrically assayed and F-actin concentrations expressed as means (±SE) fluorescent units per mg total EC protein.

Figure 21: Reverisbility of rTNFα-induced increments in the G-actin pool.

Figure 22: Quantitative immunoblotting for total EC actin. Endothelial monolayers were exposed to 1,000 U/ml rTNF-α or media alone for 6 h. Endothelial extracts were

electrophoresed on SDS-polyacrylamide gels, transferred onto nitrocellulose, incubated with murine anti-avian actin immunoglobulin G_1 followed by protein G-horseradish peroxidase conjugate with enhanced chemiluminescence substrates, and exposed to film. A simultaneous standard curve with known concentrations of pure bovine skeletal muscle actin was run on each gel. Autoradiographs were scanned by laser densitometry, and total actin extracted from each monolayer was quantified by interpolation from the actin standard curve.

Figure 23: Effect of rTNF-α on total actin pool and new actin synthesis. *A.* quantitative immunoblotting was performed on extracts obtained from rTNF-α (1,000 U/ml)-exposed monolayers as well as simultaneous media controls. Total EC cell actin was expressed as μg actin per mg total protein. *B*: [^{35}S]methionine-labeled EC were stimulated with rTNF-α (1,000 U/ml) or media alone for 6 h, immunoprecipitated with anti-actin antibody, and the actin immunoprecipitates counted for ^{35}S activity. [^{35}S]methionine incorporation into actin immunoprecipitates, i.e., new actin synthesis, is expressed as DPMs per immunoprecipitate.

Figure 24: Dose-Dependent Effect of LPS on Transendothelial ^{14}C-BSA Flux. Cross-hatched bars represent mean (±SE) transendothelial ^{14}C-BSA flux in pmol/h immediately after 6h exposures to increasing concentrations of LPS in the presence of 10% FBS. Open bars represent mean (±SE) ^{14}C-BSA flux across serum-starved monolayers exposed to increasing concentrations of LPS for 6h in the absence of FBS. Mean (±SE) pretreatment baseline transendothelial ^{14}C-BSA flux across both standard and serum-starved monolayers as well as mean (±SE) ^{14}C-BSA flux across naked filters (stippled bar) are also shown. n indicates the number of monolayers studied in the presence of FBS and (n) is the number of monolayers studied in serum-free conditions. * = significantly increased compared to the simultaneous media control at $p < 0.001$; ** = significantly increased compared to the serum-free media control at $p < 0.0001$.

Figure 25: Time-Dependent Effect of LPS on Transendothelial ^{14}C-BSA Flux. Vertical bars represent mean (±SE) transendothelial ^{14}C-BSA flux in pmol/h immediately after increasing exposure times to LPS 10 ng/ml (cross-hatched bars) and simultaneous medium controls (open bars). Mean (±SE) pretreatment baseline is shown by the closed bar.

Figure 26: LPS Exposure Time Requirements. Mean (±SE) transendothelial ^{14}C-BSA flux across endothelial monolayers all determined 6h after onset of increasing LPS exposure times (10ng/ml, 10min-6h) (cross-hatched bars) and their simultaneous media controls (open bars). Mean (±SE) pretreatment baseline transendothelial ^{14}C-BSA flux is shown by the closed bar. * = significantly increased compared with simultaneous media control at $p < 0.03$.

Figure 27: Temperature-dependence of LPS-induced barrier dysfunction.

Figure 28: Relative Responsiveness of Pulmonary Artery, Aortic, and Retinal Endothelia to LPS. Endothelial monolayers isolated from bovine pulmonary artery, aorta, and retina were exposed to LPS 10ng/ml for 6h. Vertical bars represent mean (±SE) transendothelial ^{14}C-BSA flux in pmol/h immediately after LPS exposure (cross-hatched bars) or simultaneous media

controls (open bars). Mean (±SE) pretreatment baseline transendothelial ^{14}C-BSA flux is shown by the closed bars. *= significantly increased compared to the simultaneous medium control at $p < 0.001$.

Figure 29: Serum-Dependent Effect of LPS on Transendothelial ^{14}C-BSA Flux. Transendothelial ^{14}C-BSA flux across serum-starved monolayers exposed to LPS 10 ng/ml or media for 6h in the presence of increasing FBS concentrations. Each symbol represents mean (±SE) transendothelial ^{14}C-BSA flux in the presence of a specific FBS concentration. Mean (±SE) pretreatment baseline transendothelial ^{14}C-BSA flux is shown by the open bar. Insert contains n values for both LPS-exposed monolayers and the media controls in the presence of increasing FBS concentrations. * = significantly increased compared to the simultaneous media control containing an equivalent FBS concentration at $p < 0.045$.

Figure 30: Effect of LPS-Binding Protein (LBP) on LPS-Induced Changes in Endothelial Barrier Function. Transendothelial ^{14}C-BSA flux was determined across serum-starved monolayers exposed for 6h to serum-free media, LPS 100 ng/ml in serum-free media, media enriched with 10% FBS, LPS 100 ng/ml in media with 10% FBS, LPS 100 ng/ml with an equimolar concentration of rabbit LBP (1.2 μg/ml) in serum-free media, LPS 100ng/ml with an equimolar concentration of human LBP in serum-free media, LPS 100 ng/ml with human C-reactive protein (CRP) (1.2 μg/ml), or serum-free media with either rabbit or human LBP or CRP, alone. Vertical cross-hatched bars represent mean (± SE) transendothelial ^{14}C-BSA flux in pmol/h immediately following stimulation and mean (± SE) pretreatment baseline is shown by the closed bar.

Figure 31: Dose-Dependent Effect of LBP on LPS-Induced Changes in Endothelial Barrier Function. Transendothelial ^{14}C-BSA flux was determined across serum-starved monolayers exposed for 6h to serum-free media, LPS 100 ng/ml in serum-free media, LPS 100 ng/ml in the presence of increasing concentrations of rabbit LBP, or rabbit LBP (3μg/ml) alone. Vertical cross-hatched bars represent mean (± SE) transendothelial ^{14}C-BSA flux in pmol/h immediately following stimulation and the mean (± SE) pretreatment baseline is shown by the closed bar. * = significantly increased compared to LPS in the absence of LBP at $p < 0.002$.

Figure 32: Effect of Anti-LBP and Anti-CD14 Immunoblockade on LPS-Induced Changes in Endothelial Barrier Function. Transendothelial ^{14}C-BSA flux was determined across serum-starved monolayers exposed for 6h to media enriched with 10% human serum (HS), LPS 100ng/ml in media with 10% HS, LPS in media with 10%HS in the presence of anti-human LBP antibody (1 mg/ml), LPS 100 ng/ml in media with 10% HS in the presence of anti-human CD14 antibody (10 μg/ml), LPS 100 ng/ml and human LBP 1.2 μg/ml in serum-free media, LPS 100 ng/ml and human LBP 1.2 μg/ml in serum-free media in the presence of anti-human CD14 antibody, LPS 100 ng/ml and human sCD14 100 ng/ml in serum-free media, LPS 100 ng/ml and human sCD14 in serum-free media in the presence of anti-LBP antibody, or media with either antibody or their species-matched controls alone. Vertical cross-hatched bars represent mean (±SE) transendothelial ^{14}C-BSA flux in pmol/h immediately following stimulation and mean (±SE) pretreatment baseline is shown by the closed bar.

Figure 33: Effect of sCD14 on LPS-Induced Changes in Endothelial Barrier Function. Transendothelial ^{14}C-BSA flux was determined across serum-starved monolayers exposed for 6h to serum-free media, LPS 100ng/ml serum-free media, human sCD14 50 ng/ml, LPS 100 ng/ml with sCD14 50 ng/ml, LPS 100 ng/ml with human decay accelerating factor (DAF) 50 ng/ml, LPS 100 ng/ml with bovine folate binding protein (FBP) 50 ng/ml, human LBP 100 ng/ml, LPS 100 ng/ml with LBP 100 ng/ml, sCD14 and LBP, and LPS with both sCD14 and LBP. Vertical cross-hatched bars represent mean (±SE) transendothelial ^{14}C-BSA flux in pmol/h immediately following stimulation and mean (± SE) pretreatment baseline is shown by the closed bar.

Figure 34: Dose-Dependent Effect of sCD14 on LPS-Induced Changes in Endothelial Barrier Function. Transendothelial ^{14}C-BSA flux was determined across serum-starved monolayers exposed for 6h to serum-free media, LPS 100 ng/ml increasing sCD14 concentrations, or these same sCD14 concentrations in the presence of LPS 100 ng/ml. Vertical bars represent mean (±SE) transendothelial ^{14}C-BSA flux in pmol/h immediately following stimulation and mean (±SE) pretreatment baseline is shown by the closed bar. * = significantly increased compared to sCD14 in the absence of LPS at $p < 0.02$; ** = significantly increased compared to the media control at $p < 0.002$.

Figure 35: Effect of CD14-Depletion on Serum-Dependent LPS-Induced Changes in Endothelial Barrier Function. Transendothelial ^{14}C-BSA flux was determined across serum-starved monolayers exposed for 6h to media enriched with 10% HS, LPS 100 ng/ml in media with 10% HS, media with 10% CD14-depleted HS from the same donor, or LPS 100 ng/ml with 10% CD14-depleted HS. The LBP concentrations in the HS and CD14-depleted HS were 27 μg/ml and 23 μg/ml, respectively. Vertical bars represent mean (±SE) transendothelial ^{14}C-BSA flux in pmol/h immediately following stimulation and the mean (±SE) pretreatment baseline is shown by the closed bar.

Figure 36: Kinetic Analysis of Accessory Molecule(s) Regulation of LPS-Induced Changes in Endothelial Barrier Function. Transendothelial ^{14}C-BSA flux was determined across serum-starved monolayers immediately after increasing exposure times to serum-free media, LPS 100 ng/ml serum-free media, LPS with LBP (1.2 μg/ml), LPS with sCD14 (50 or 500 ng/ml), and LPS with both LBP and sCD14 (50 ng/ml). Each symbol represents the mean (±SE) transendothelial ^{14}C-BSA flux in pmol/h immediately after increasing exposure times.

Figure 37: Effect of LPS, rough LPS and deacylated LPS on endothelial barrier function.

Figure 38: Effect of wild type and mutant *S. minnesota* LPS with varying lengths of O-polysaccharide side chain on endothelial barrier function.

Figure 39: Effects of Lipid A and O-polysaccharide LPS fractions on endothelial barrier function.

Figure 40: Time-Dependent Effect of LPS on the EC F- and G-Actin Pools. A. For F-actin studies, endothelial cell monolayers were exposed to LPS 10ng/ml (●—●) or media alone (○—○) for increasing exposure times, fixed, permeabilized, incubated with NBD-phallicidin, and extracted with methanol: The extracts were spectrofluorometrically assayed and F-actin concentrations at each time point expressed as mean (±SE) fluorescent units per mg total

endothelial cell protein. B. For G-actin measurements, monolayers were exposed to LPS 10ng/ml (●—●) or media alone (○—○) for increasing exposure times, permeabilized, and the supernatants tested in DNAse 1 inhibition assay standardized with pure actin. Each point represents the mean (±SE) G-actin in μg per mg total endothelial cell protein. n, the number of control or LPS-exposed monolayers studied, is indicated by the (numeral) next to each symbol. *=significantly increased compared to the simultaneous media control at $p < 0.002$.

Figure 41: Fluorescein-Phalloidin Staining of LPS-Exposed Endothelial Monolayers. Endothelial monolayers grown on filters were exposed to media or LPS (10ng/ml) for increasing exposure times. the monolayers were fixed, permeabilized, stained with fluorescein-phalloidin, and examined by epifluorescence microscopy. A. medium control; B. LPS, 2h; C. and D. LPS, 6h. Arrows in A point to cycloplasmic actin filaments, arrows in B and C point to intercellular gaps, and arrows in D point to peripheral actin bands. (Magnification 400X).

Figure 42: Dose-Dependent Effect of LPS on the EC F- and G-Actin Pools. Endothelial monolayers were exposed to increasing concentrations of LPS for 6h. Each symbol represents mean (± SE) F-actin in fluorescent units/mg total protein (○—○) or mean (± SE) G-actin in μg/mg total protein (●—●). n, the number of monolayers studied, is indicated by the (numeral) next to each symbol. *=significantly changed from the simultaneous media control at $p < 0.03$.

Figure 43: Effect of F-Actin Stabilization and Protein Synthesis Inhibition on LPS-Induced Increments in G-Actin. EC monolayers were exposed to media, NBD-phallicidin 0.3μM, cycloheximide 50μg/ml, or LPS 10ng/ml. Selected monolayers were pretreated with either NBD-phallicidin for 3h or cycloheximide for 0.5h, prior to and throughout exposure to either media or LPS. After 2h, monolayers were permeabilized and the supernatants tested in the standard DNAse 1 inhibition assay. Each cross-hatched bar represents the mean (±SE) G-actin in μg per mg total EC protein.

Figure 44: Effect of F-Actin Stabilization and Protein Synthesis Inhibition on LPS-Induced Increments in Transendothelial ^{14}C-BSA Flux. EC monolayers grown on filters were pretreated with NBD-phallicidin 0.3μM or media alone for 3h prior to and throughout either LPS (10ng/ml, 6h) or media exposures. In other experiments, monolayers were pretreated with cycloheximide (50μg/ml) for 0.5h prior to and throughout LPS exposure. Simultaneous control for media, NBD-phallicidin (0.3μM), cycloheximide (50μg/ml), and LPS (10ng/ml), are each represented. Cross-hatched bars represent mean (±SE) pretreatment baseline transendothelial ^{14}C-BSA flux in pmol/h. The mean (±SE) pretreatment baseline transendothelial ^{14}C-BSA flux is shown by the closed bar.

Figure 45: Effect of Protein Synthesis Inhibition on the LPS-Induced Changes in EC F-Actin. EC monolayers were exposed for 6h to media, cycloheximide 50μg/ml, LPS 10ng/ml, or cycloheximide for 0.5h prior to and throughout a 6h LPS exposure. The monolayers were fixed, permeabilized, incubated with NBD-phallicidin, and extracted with methanol. The extracts were fluorometrically assayed and F-actin concentrations expressed as mean (±SE) fluorescent units per mg total EC protein.

Figure 46: Quantitative Immunoblotting for Total EC Actin. Endothelial extracts obtained

from LPS-exposed and medium control monolayers were electrophoresed on SDS polyacrylamide gels, transferred onto nitrocellulose, incubated with murine anti-avian actin IgG_1 followed by Protein G-HRP conjugate with enhanced chemiluminescence substrates and exposed to film. A simultaneous standard curve with known concentrations of bovine skeletal muscle actin were run on each gel. Autoradiographs were scanned by laser densitometry and actin quantified by interpolation from the actin standard curve.

Figure 47: Effect of LPS on the Total Actin Pool and New Actin Synthesis. A. Quantitative immunoblotting was performed on extracts obtained from LPS (10ng/ml) exposed monolayers as well as simultaneous media controls. Total EC actin was expressed as μg actin/mg total protein. B. ^{35}S-methionine-labeled EC were stimulated with LPS 10ng/ml or media alone for 6h, immunoprecipitated with anti-actin antibody, and the actin immunoprecipitates counted for ^{35}S-activity. ^{35}S-methionine incorporation into actin immunoprecipitates, i.e., new actin synthesis, is expressed as dpm's/immunoprecipitate.

Figure 48: Dose-Dependent Effect of LPS on Transendothelial ^{14}C-BSA Flux and EC Detachment. A. Vertical bars represent mean (±SE) transendothelial ^{14}C-BSA flux in pmol/h immediately after 6h exposures to increasing concentrations of LPS (cross-hatched bars). B. Vertical bars represent mean (±SE) percent EC detachment from gelatin-impregnated filters after 6h exposures to increasing concentration of LPS. n for each experimental group notated in each bar. *= significantly increased compared to the simultaneous medium control at $p < 0.001$.

Figure 49: Time-Dependent Effect of LPS on Transendothelial ^{14}C-BSA Flux and EC Detachment. A. Vertical bars represent mean (±SE) transendothelial ^{14}C-BSA flux in pmol/h immediately after increasing exposure times to LPS 10ng/ml (cross-hatched bars) or media alone (open bars). B. Vertical bars represent mean (±SE) percent EC detachment after increasing exposure times to LPS 10ng/ml (cross-hatched bars) or media alone (open bars). n for each group notated in each bar. *= significantly increased compared to the simultaneous media controls at $p < 0.03$.

Figure 50: Temperature-Dependent Effect of LPS on Transendothelial ^{14}C-BSA Flux and EC Detachment. A. Mean (±SE) transendothelial ^{14}C-BSA flux across in pmol/h monolayers exposed to LPS 10ng/ml (cross-hatched bars) or media alone (open bars) for 6h at 4°C or 37°C. B. Mean (±SE) percent EC detachment after exposure to LPS 10ng/ml (cross-hatched bars) or media alone (open bars) for 6h at 4°C or 37°C. n for each experimental group is notated in each bar. * = significantly increased compared to the simultaneous isothermal medium control at $p < 0.0001$.

Figure 51: Serum-Dependent Effect of LPS on Transendothelial ^{14}C-BSA Flux and EC Detachment. A. Vertical bars represent mean (±SE) transendothelial ^{14}C-BSA flux in pmol/h after exposure to LPS 10ng/ml (cross-hatched bars) or media alone (open bars) for 6h in the presence or absence of FBS. B. Mean (±SE) percent EC detachment after exposure to LPS 10ng/ml (cross-hatched bars) or media alone (open bars) for 6h in the presence or absence of FBS. The n for each experimental group is notated within each bar. * = significantly increased compared to the simultaneous medium control at $p < 0.0001$.

Figure 52: Correlation Between Endothelial Barrier Function and EC Detachment. The mean values from the experimental and control groups found in Figures 1,2,6, and 8 were used to plot.

Figure 53: Dose-Dependent Effect of SPARC on Transendothelial Flux of ^{14}C-BSA. Vertical bars represent mean (±SE) transendothelial flux of ^{14}C-BSA in pmol/h. Baseline ^{14}C-BSA flux is shown by a closed bar in each panel. n indicates number of monolayers studied. *indicates a significant increase compared to the simultaneous media control at $p < 0.02$.

Figure 54: Time-Dependent Effect of SPARC on Endothelial Barrier Function. ^{14}C-BSA flux immediately after increasing exposure times to SPARC (15μg/ml) (cross-hatched bars) and simultaneous controls (open bars) in the absence of FBS.

Figure 55: Exclusion of contribution of LPS to SPARC-induced changes in endothelial barrier function. Ability of anti-SPARC antibody, trypsin proteolysis, or heat treatment to abort the SPARC effect.

Figure 56: Effect of prior protein synthesis inhibition on SPARC-induced changes in endothelial barrier function.

Figure 57: Effects of SPARC on EC Morphology. SEM of postconfluent monolayers grown on filters in assay chambers after exposure to SPARC (15μg/ml for 6h) (B and C) or to medium alone (A). A. Control monolayers were in tight apposition and displayed the typical cobblestone appearance (x 2000). B. Monolayers exposed to SPARC remained attached to matrix-coated filters (closed arrowheads) but exhibited extensive interendothelial gaps (closed arrows). Occasional cells assumed an extremely rounded phenotype (open arrows) (x 2000). C. Selected cells (open arrows) became rounded with marked separation from neighboring cells and displayed numerous slender processes (small arrowheads) and extensive blebs (small closed arrows) (x 4000).

Figure 58: SPARC-Induced Actin Reorganization and Changes in Endothelial Barrier Function. Endothelial monolayers grown on filters were exposed to medium (A) or SPARC (15μg/ml for $\geq$ 2h) (B and C). The monolayers were fixed, rendered permeable, and stained with fluorescein-phalloidin (x800). A. Monolayers exposed to medium alone contained continuous transcytoplasmic actin cables and exhibited tight cellular apposition without intercellular gaps. B and C. Exposures of SPARC $\geq$ 2h induced intercellular gaps (closed arrows). C. Note circumferential F-actin redistribution (small closed arrows). D. Endothelial cell monolayers grown on filters were pretreated with NBD-phallicidin (0.3μM) or media alone for 3h prior to and throughout either a 6h exposure to SPARC or medium alone in the absence of FBS. Vertical bars represent mean (±SE) transendothelial flux of ^{14}C-BSA. Baseline (±SE) ^{14}C-BSA flux is shown by the closed bar.

APPENDIX C: FIGURES

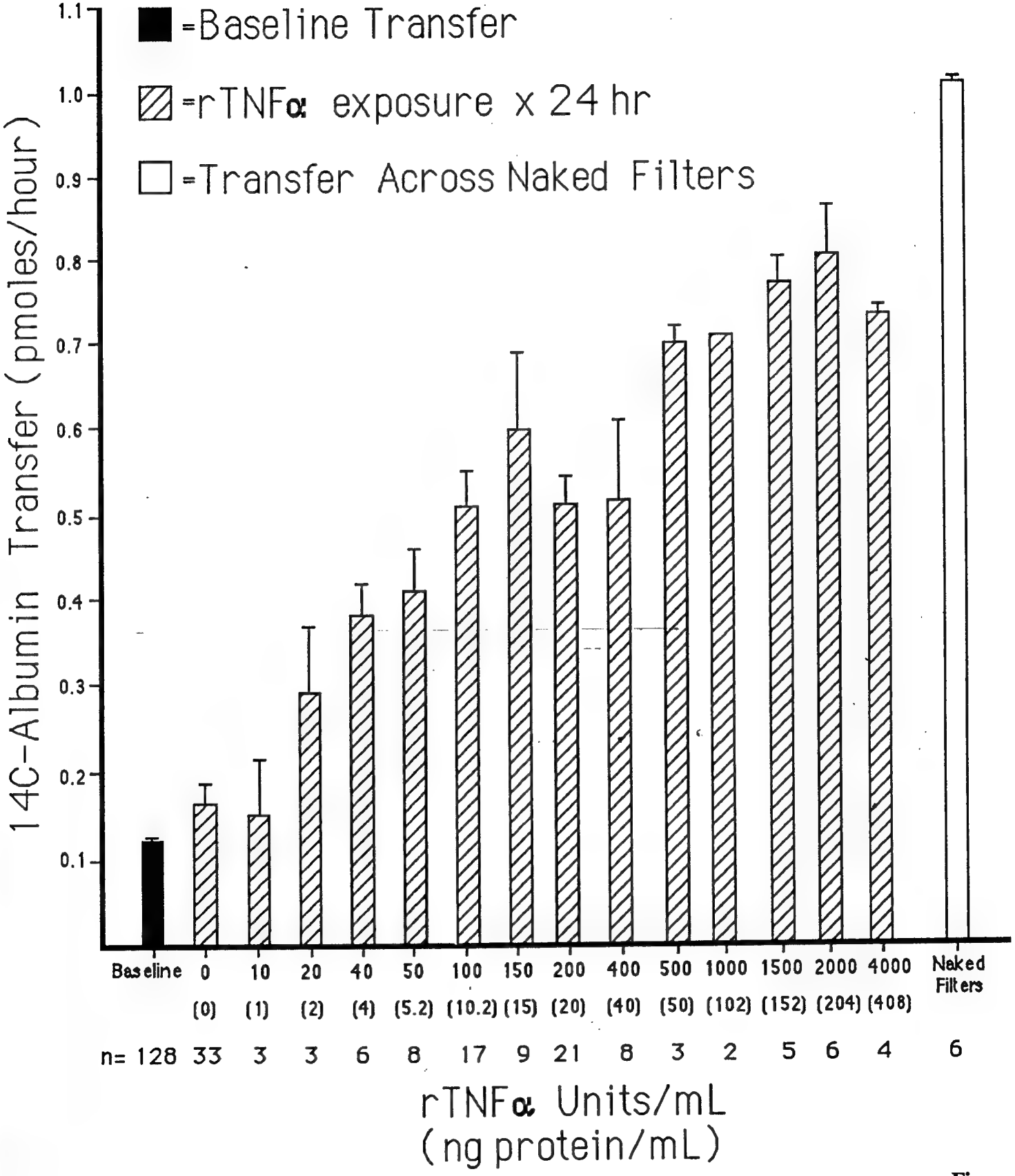
■=Baseline Transfer
▨=rTNFα exposure x 24 hr
□=Transfer Across Naked Filters
14C-Albumin Transfer (pmoles/hour)
1.1
1.0
0.9
0.8
0.7
0.6
0.5
0.4
0.3
0.2
0.1
Baseline
0 (0)
10 (1)
20 (2)
40 (4)
50 (5.2)
100 (10.2)
150 (15)
200 (20)
400 (40)
500 (50)
1000 (102)
1500 (152)
2000 (204)
4000 (408)
Naked Filters
n= 128 33 3 3 6 8 17 9 21 8 3 2 5 6 4 6
rTNFα Units/mL
(ng protein/mL)

Figure1

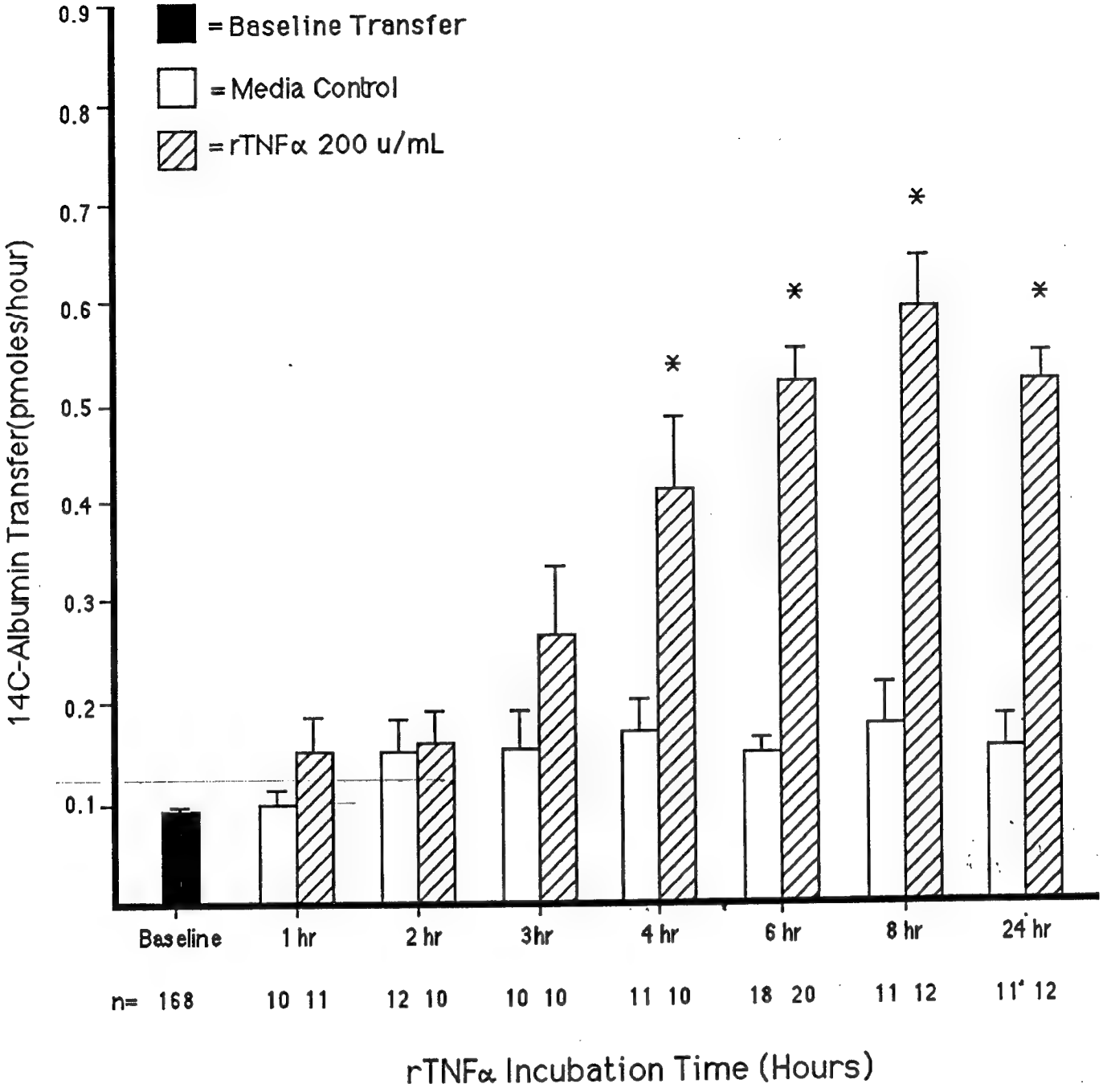
= Baseline Transfer
= Media Control
= rTNFα 200 u/mL
14C-Albumin Transfer(pmoles/hour)
0.9
0.8
0.7
0.6
0.5
0.4
0.3
0.2
0.1
*
Baseline
1 hr
2 hr
3hr
4 hr
6 hr
8 hr
24 hr
n= 168
10 11
12 10
10 10
11 10
18 20
11 12
11 12
rTNFα Incubation Time (Hours)

Figure 2

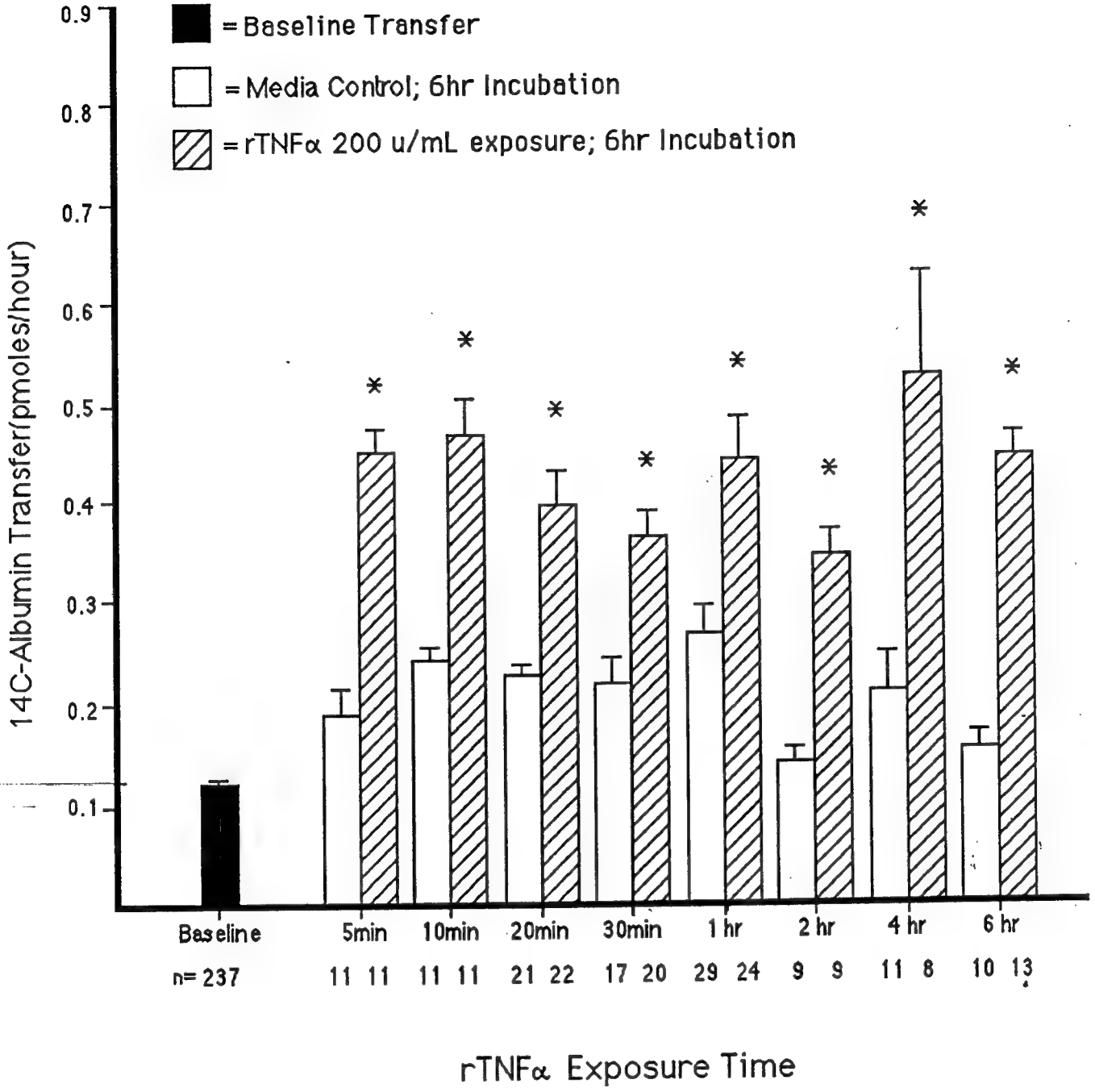
= Baseline Transfer
= Media Control; 6hr Incubation
= rTNFα 200 u/mL exposure; 6hr Incubation
14C-Albumin Transfer(pmoles/hour)
0.9
0.8
0.7
0.6
0.5
0.4
0.3
0.2
0.1
Baseline
5min
10min
20min
30min
1 hr
2 hr
4 hr
6 hr
n= 237
11 11
11 11
21 22
17 20
29 24
9 9
11 8
10 13
rTNFα Exposure Time

Figure 3

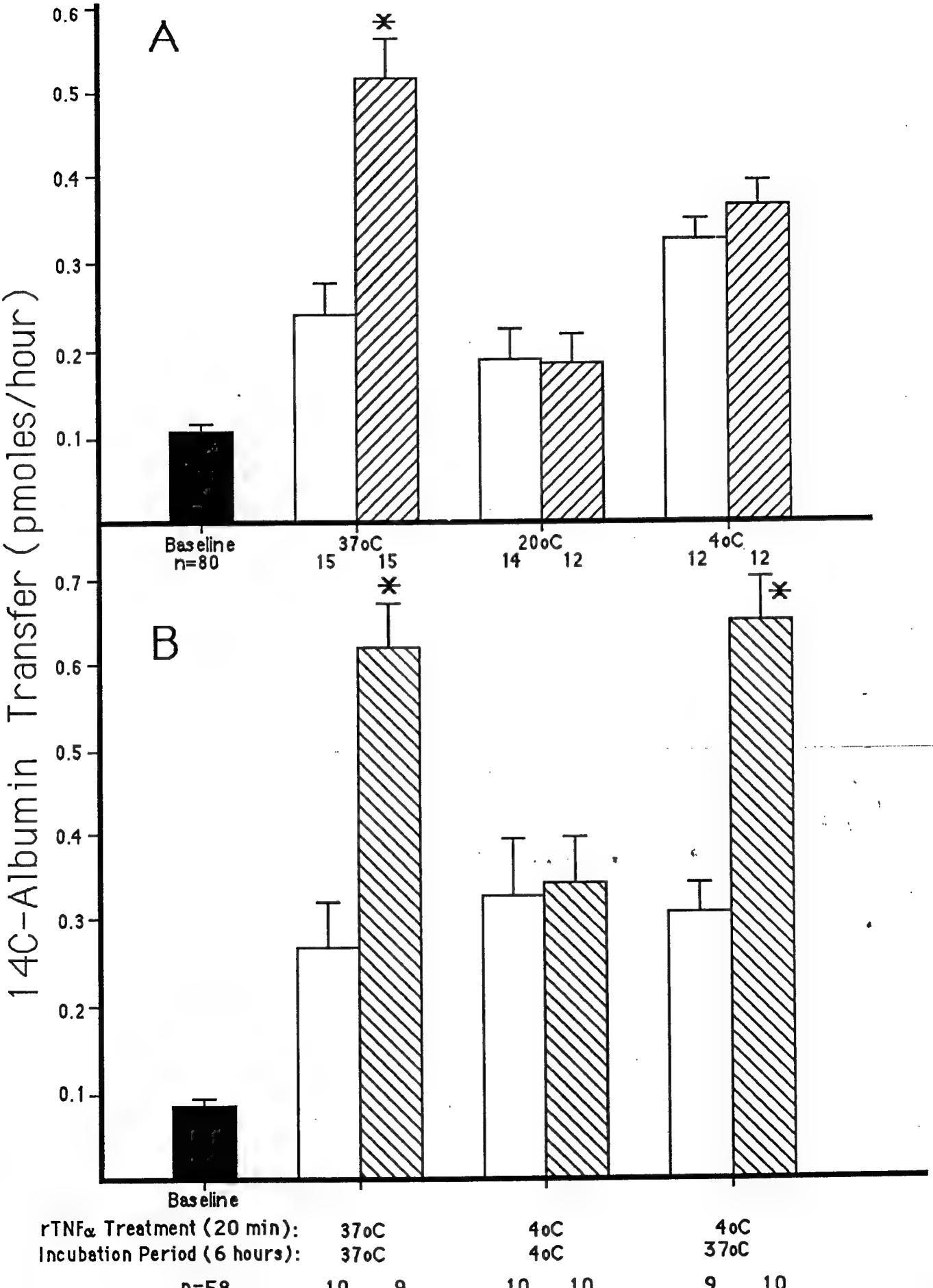
A
B
14C-Albumin Transfer (pmoles/hour)
0.6
0.5
0.4
0.3
0.2
0.1
0.7
Baseline
n=80
37oC
15
15
20oC
14
12
4oC
12
12
Baseline
rTNFα Treatment (20 min):
Incubation Period (6 hours):
n=58
37oC
37oC
10
9
4oC
4oC
10
10
4oC
37oC
9
10

Figure 4

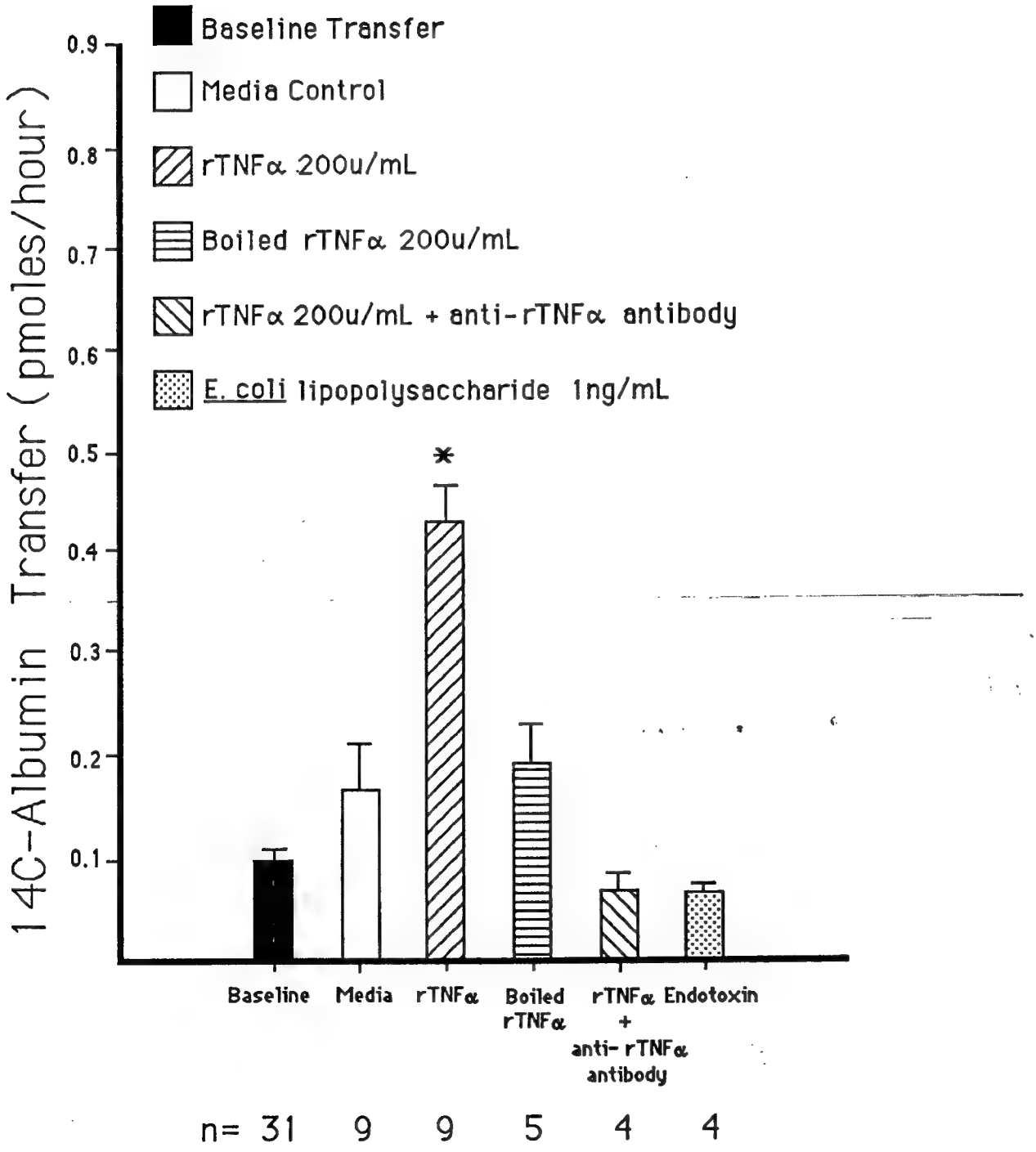
Baseline Transfer
Media Control
rTNFα 200u/mL
Boiled rTNFα 200u/mL
rTNFα 200u/mL + anti-rTNFα antibody
E. coli lipopolysaccharide 1ng/mL
14C-Albumin Transfer (pmoles/hour)
0.9
0.8
0.7
0.6
0.5
0.4
0.3
0.2
0.1
*
Baseline
Media
rTNFα
Boiled rTNFα
rTNFα + anti-rTNFα antibody
Endotoxin
n= 31 9 9 5 4 4

Figure 5

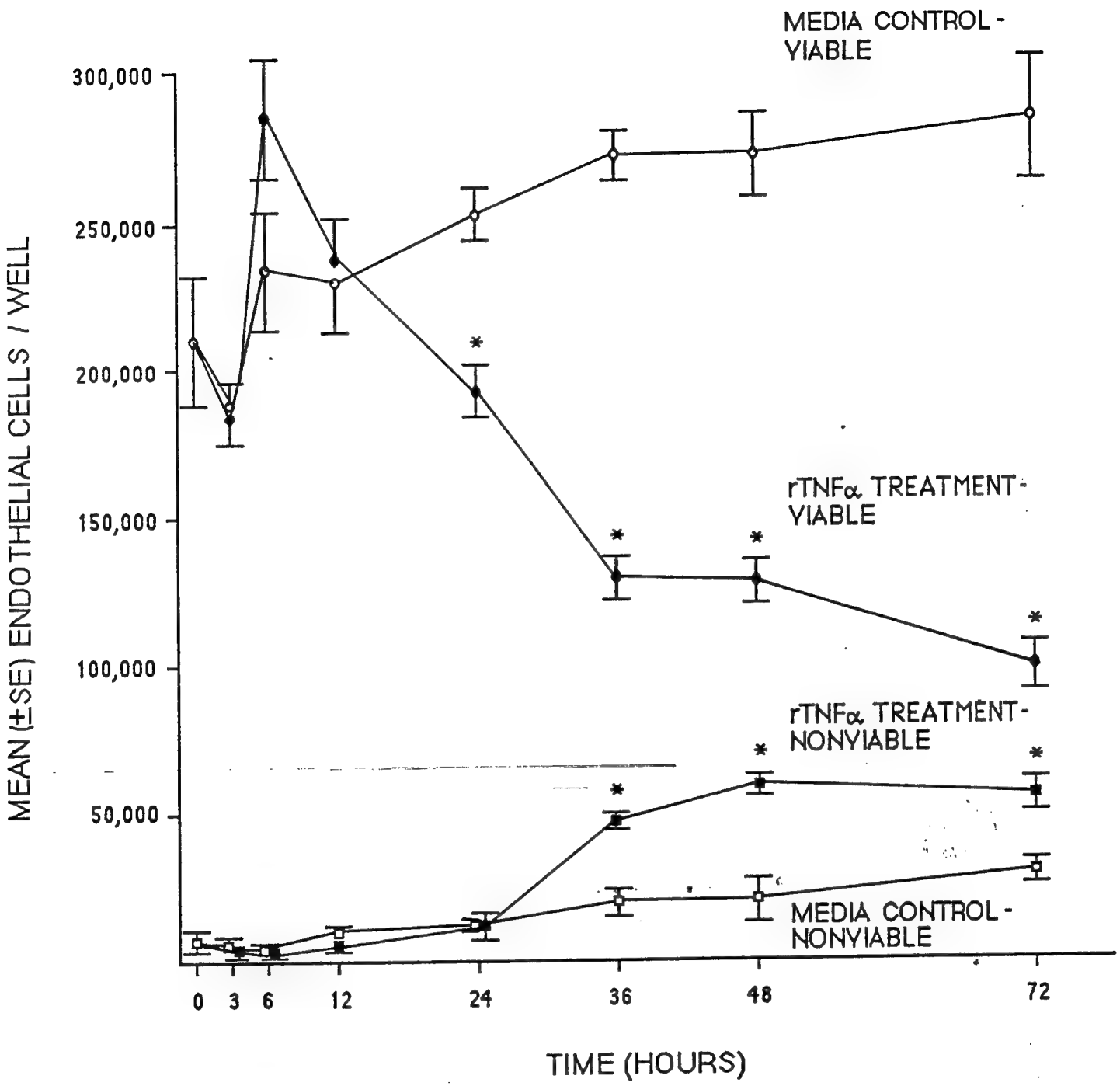
MEDIA CONTROL - VIABLE
rTNFα TREATMENT - VIABLE
rTNFα TREATMENT - NONVIABLE
MEDIA CONTROL - NONVIABLE
MEAN (±SE) ENDOTHELIAL CELLS / WELL
300,000
250,000
200,000
150,000
100,000
50,000
0
3
6
12
24
36
48
72
TIME (HOURS)

Figure 6

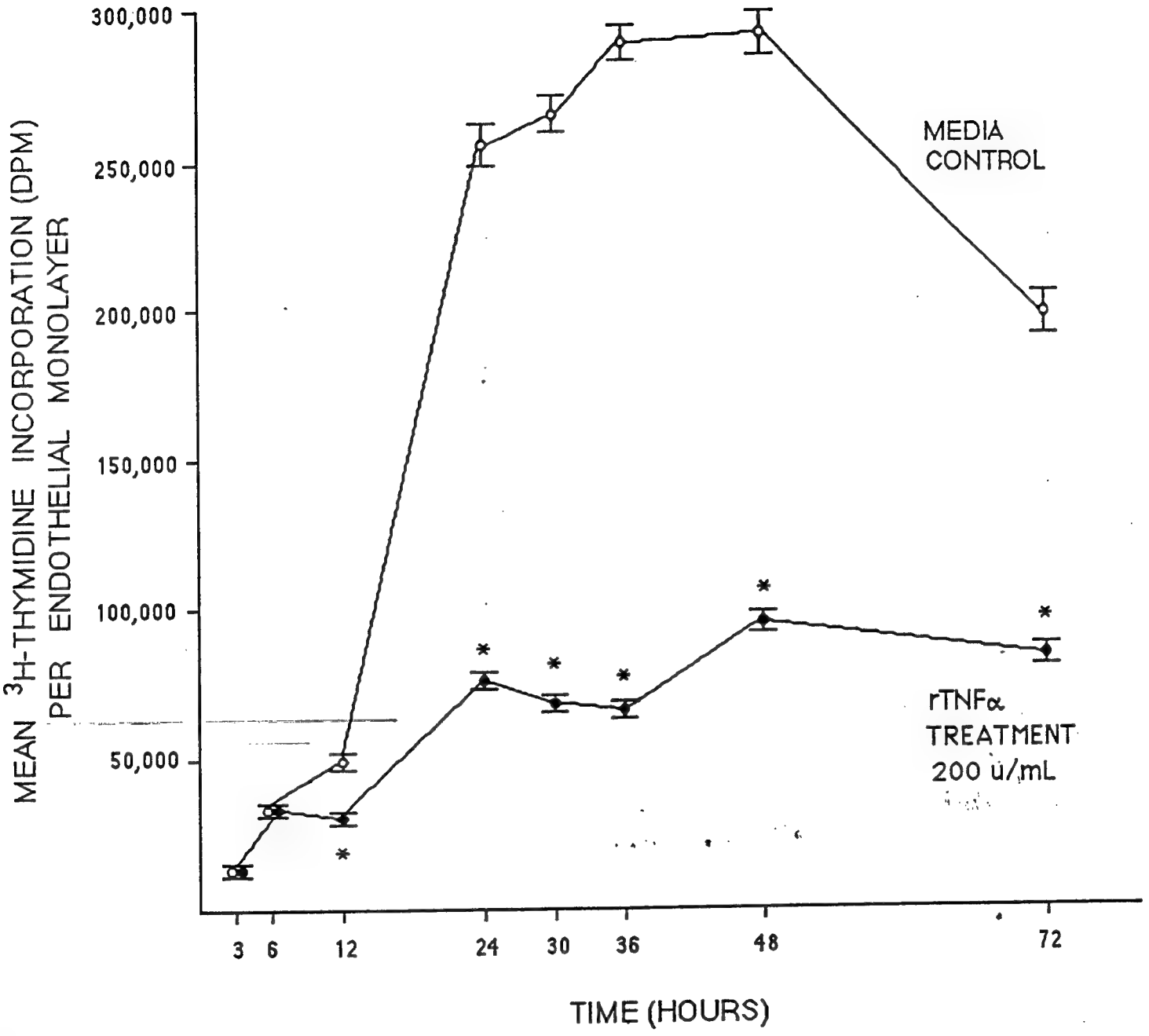
300,000
250,000
200,000
150,000
100,000
50,000
MEAN ^{3}H-THYMIDINE INCORPORATION (DPM) PER ENDOTHELIAL MONOLAYER
MEDIA CONTROL
rTNFα TREATMENT 200 u/mL
3
6
12
24
30
36
48
72
TIME (HOURS)

Figure 7

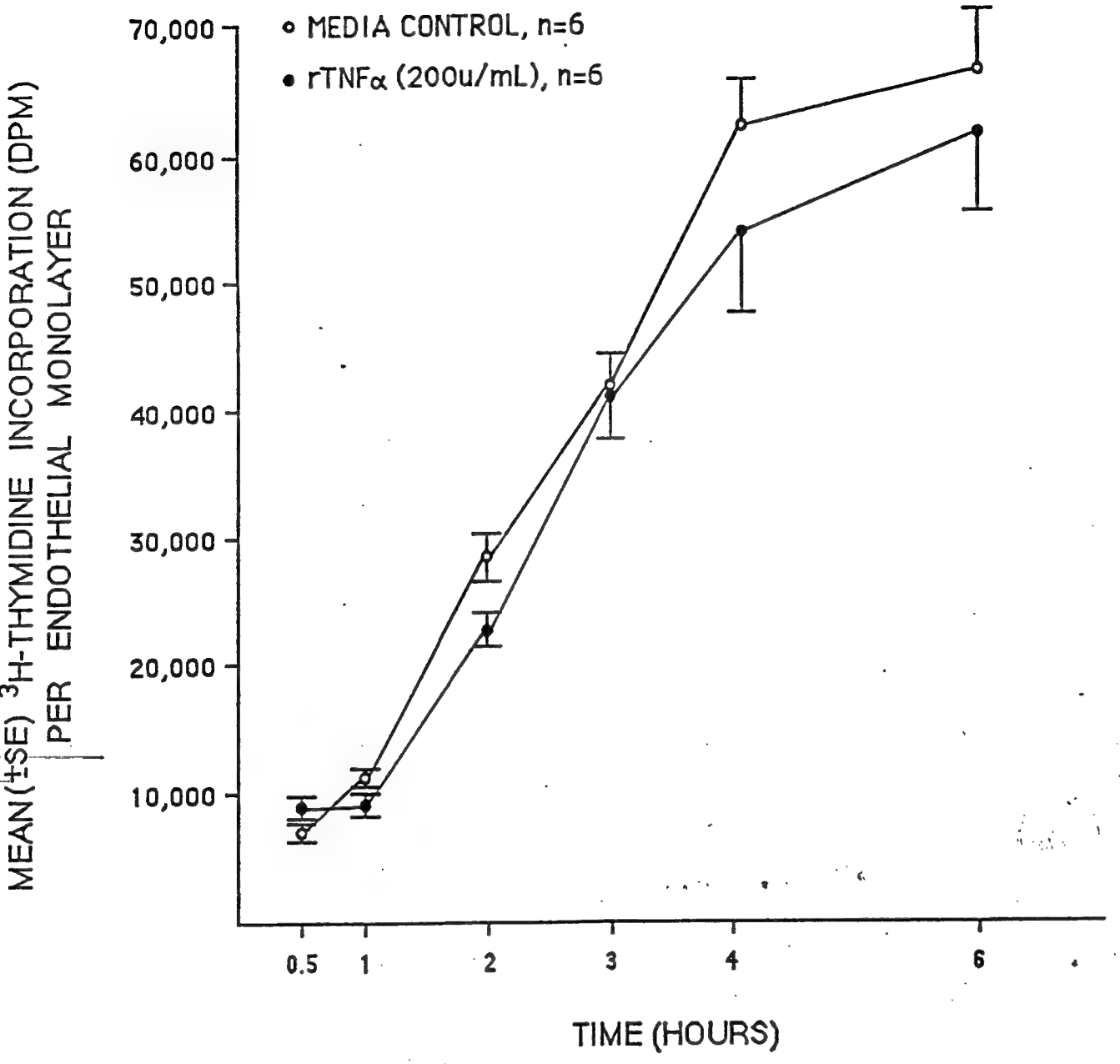
MEDIA CONTROL, n=6
rTNFα (200u/mL), n=6
MEAN (±SE) ^{3}H-THYMIDINE INCORPORATION (DPM) PER ENDOTHELIAL MONOLAYER
70,000
60,000
50,000
40,000
30,000
20,000
10,000
0.5
1
2
3
4
6
TIME (HOURS)

Figure 8

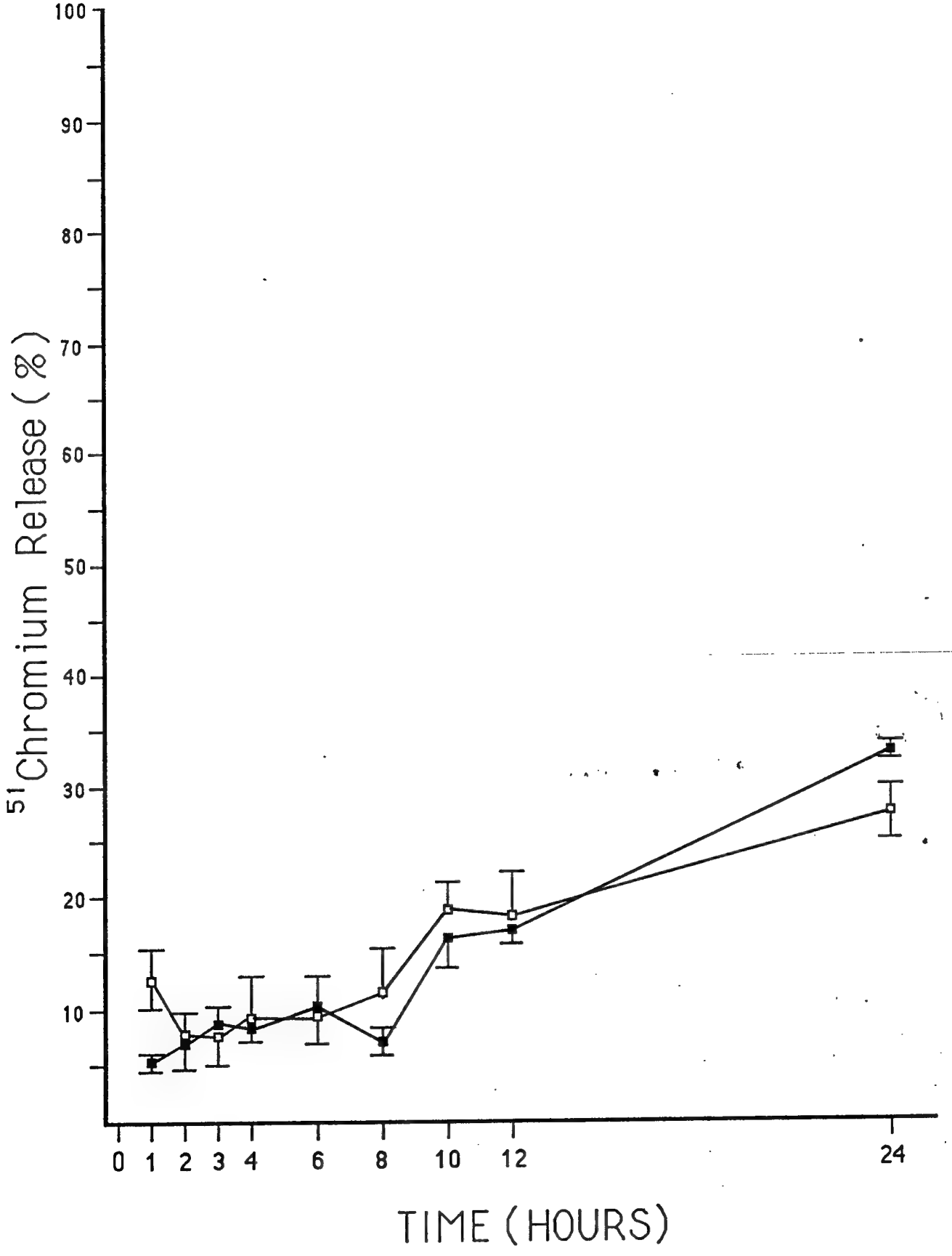
100
90
80
70
60
50
40
30
20
10
^{51}Chromium Release (%)
0 1 2 3 4 6 8 10 12 24
TIME (HOURS)

Figure 9

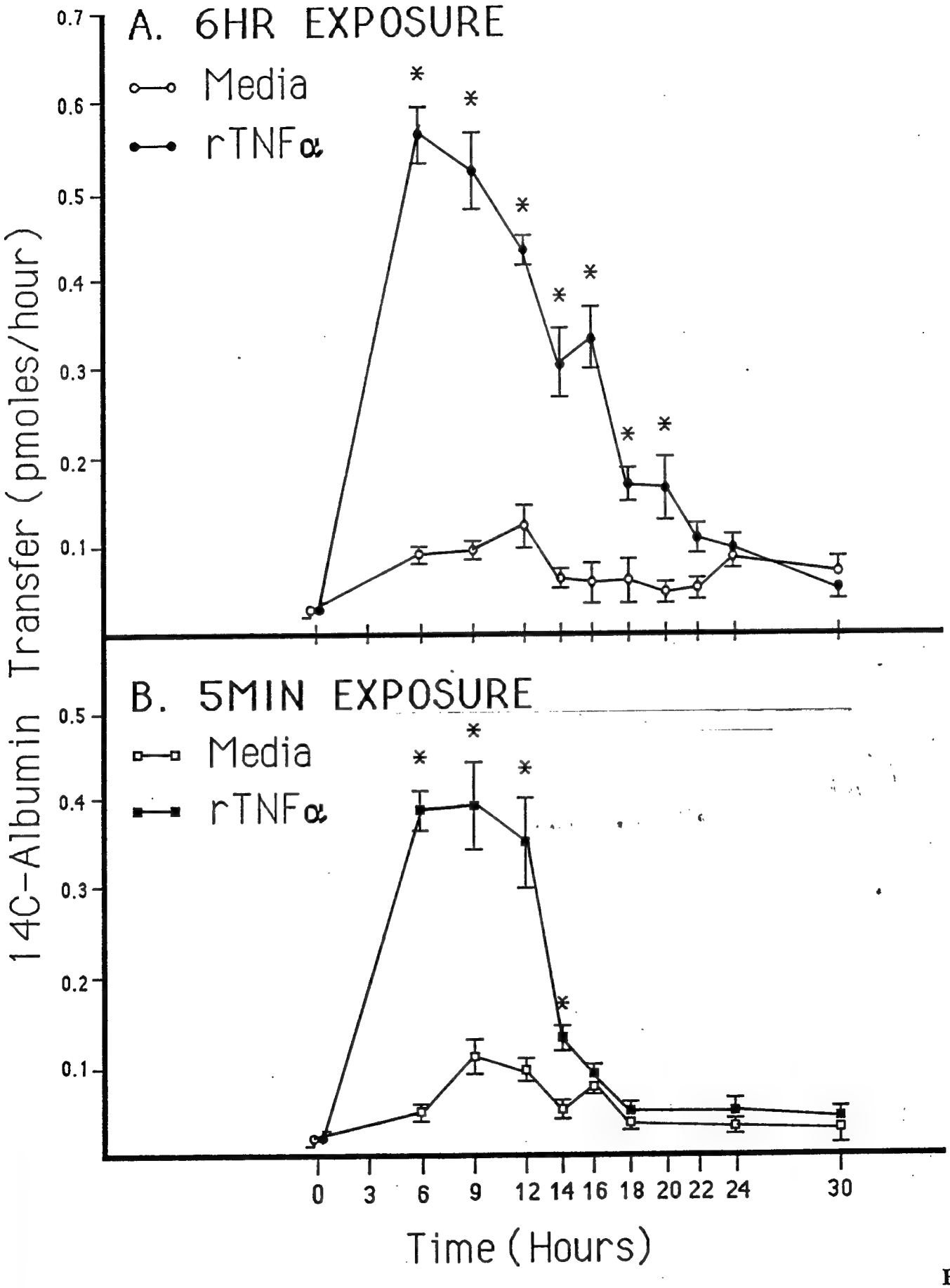
A. 6HR EXPOSURE
Media
rTNFα
B. 5MIN EXPOSURE
Media
rTNFα
14C-Albumin Transfer (pmoles/hour)
0.7
0.6
0.5
0.4
0.3
0.2
0.1
0.5
0.4
0.3
0.2
0.1
0 3 6 9 12 14 16 18 20 22 24 30
Time (Hours)

Figure 10

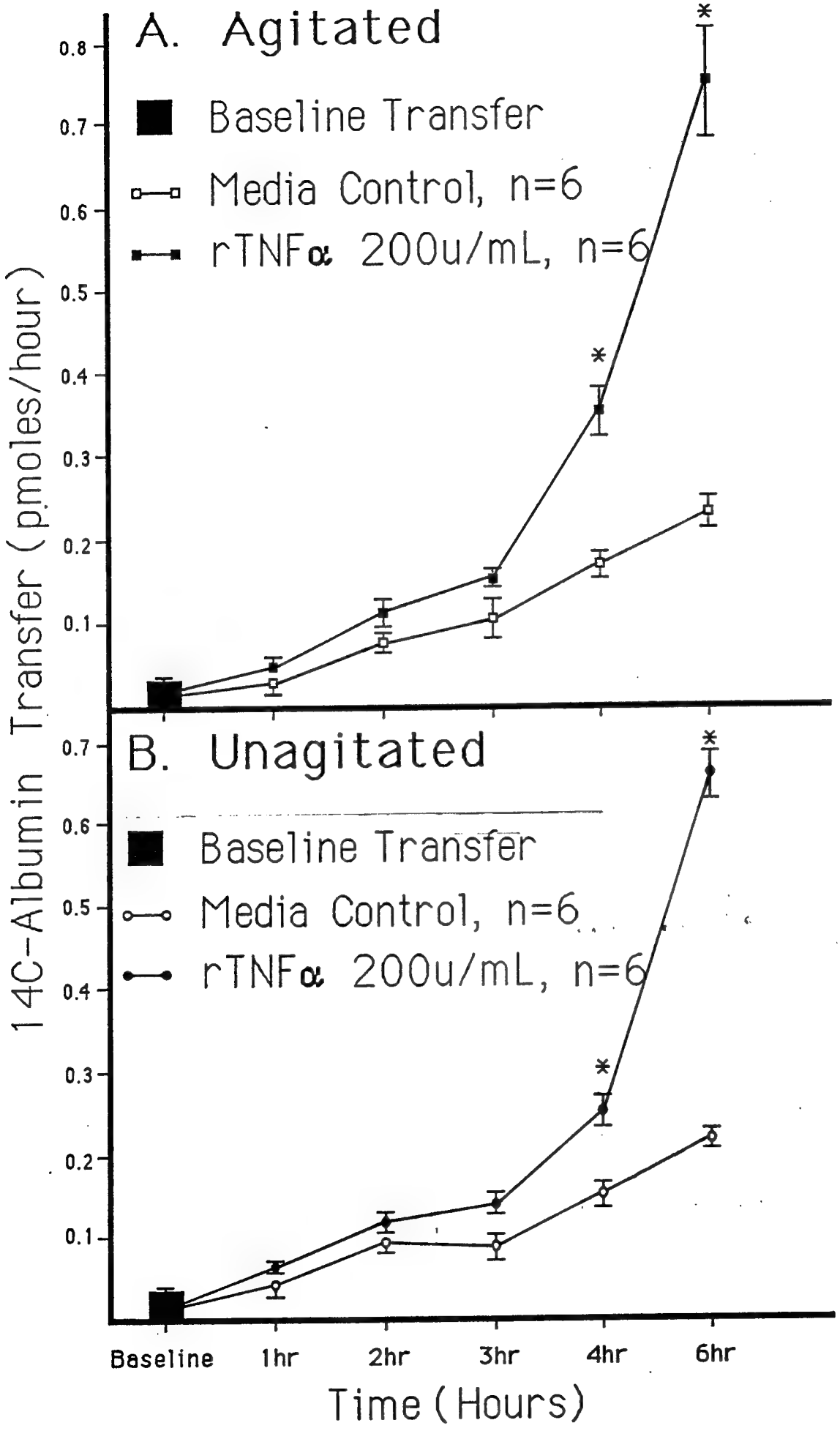
A. Agitated
Baseline Transfer
Media Control, n=6
rTNFα 200u/mL, n=6
B. Unagitated
Baseline Transfer
Media Control, n=6
rTNFα 200u/mL, n=6
14C-Albumin Transfer (pmoles/hour)
0.8
0.7
0.6
0.5
0.4
0.3
0.2
0.1
Baseline
1hr
2hr
3hr
4hr
6hr
Time (Hours)

Figure 11

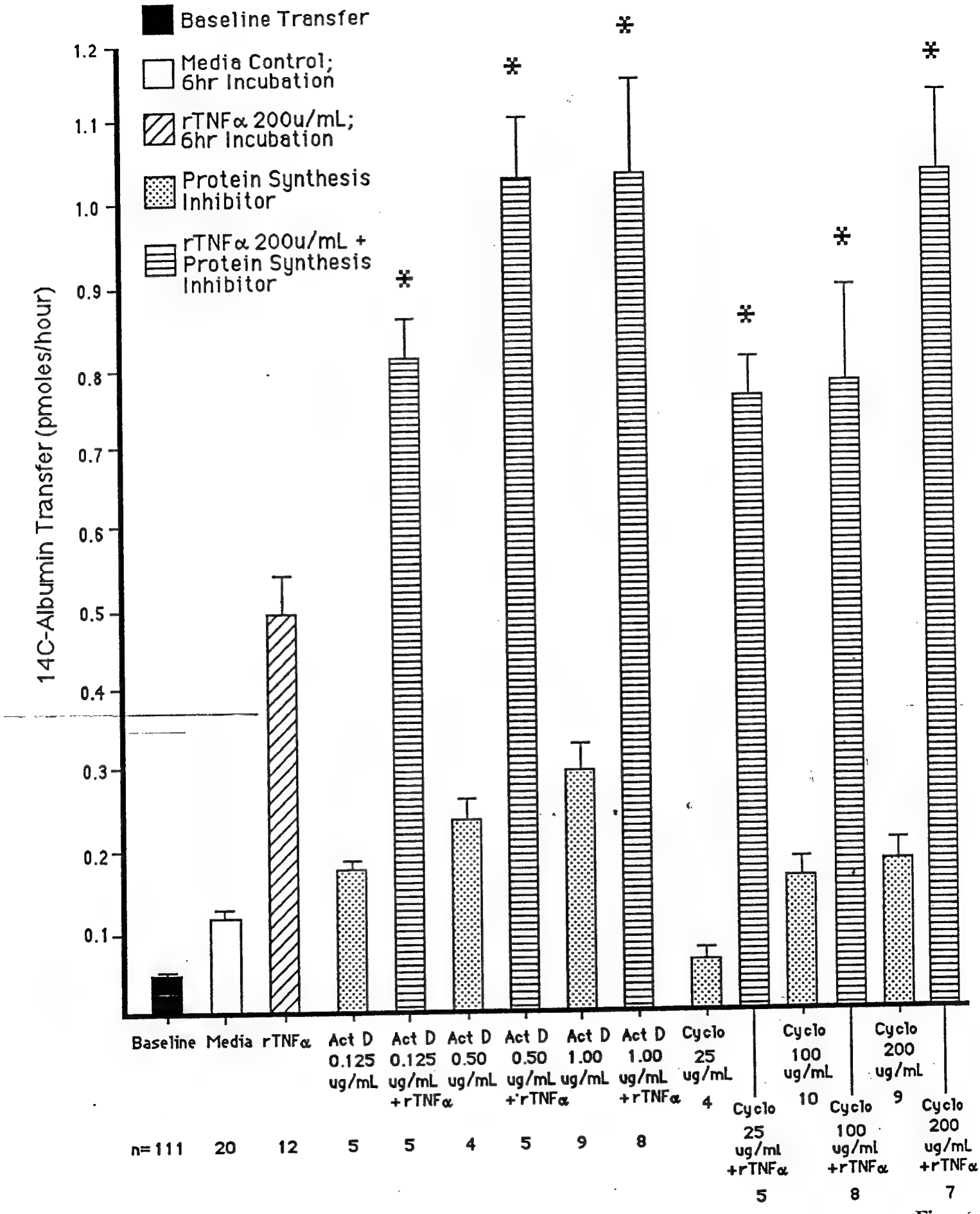
Baseline Transfer
Media Control; 6hr Incubation
rTNFα 200u/mL; 6hr Incubation
Protein Synthesis Inhibitor
rTNFα 200u/mL + Protein Synthesis Inhibitor
14C-Albumin Transfer (pmoles/hour)
1.2
1.1
1.0
0.9
0.8
0.7
0.6
0.5
0.4
0.3
0.2
0.1
Baseline
Media
rTNFα
Act D 0.125 ug/mL
Act D 0.125 ug/mL +rTNFα
Act D 0.50 ug/mL
Act D 0.50 ug/mL +rTNFα
Act D 1.00 ug/mL
Act D 1.00 ug/mL +rTNFα
Cyclo 25 ug/mL
Cyclo 100 ug/mL
Cyclo 200 ug/mL
Cyclo 25 ug/mL +rTNFα
Cyclo 100 ug/mL +rTNFα
Cyclo 200 ug/mL +rTNFα
n= 111 20 12 5 5 4 5 9 8 4 10 9 5 8 7

Figure 12

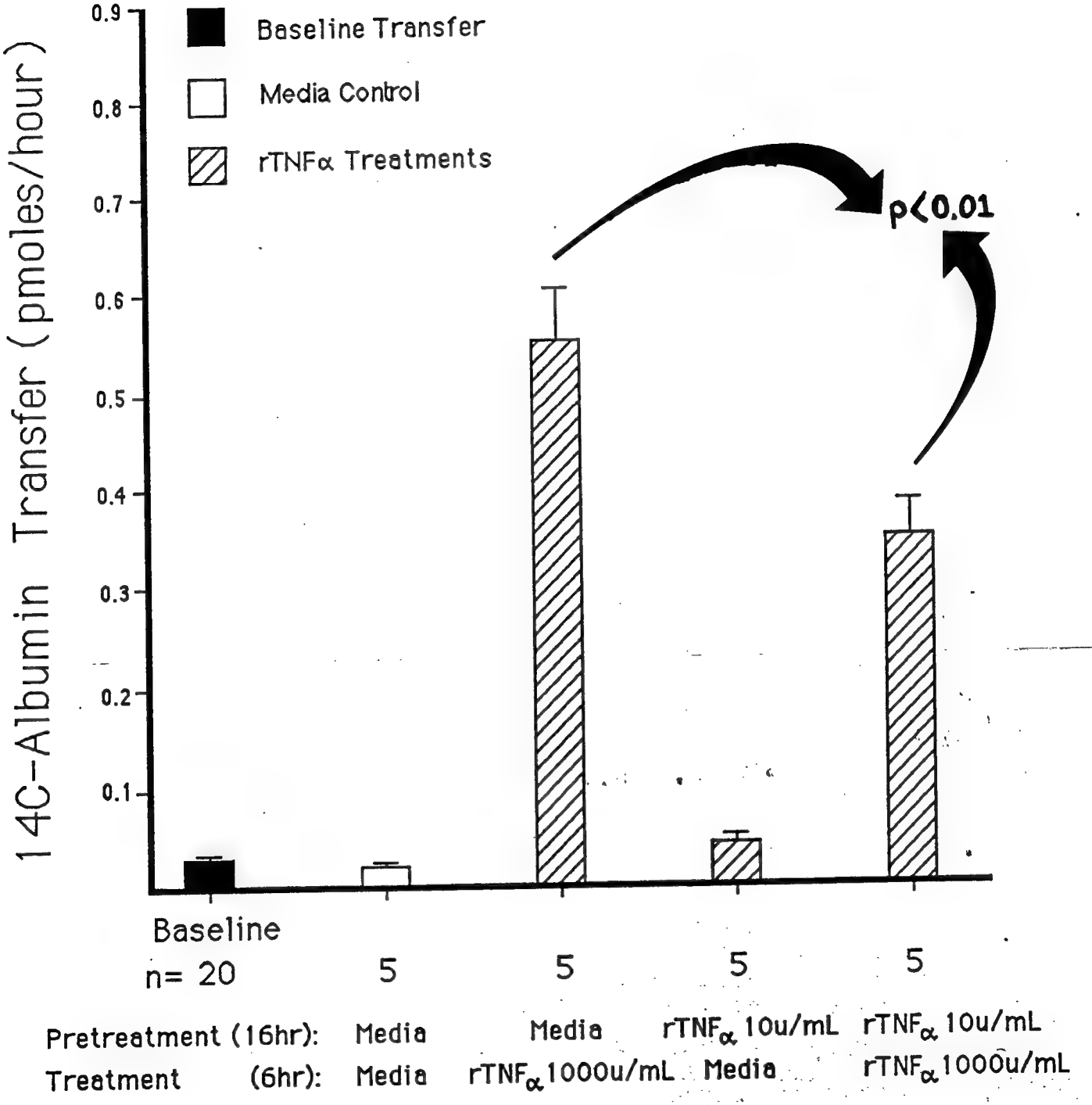
Baseline Transfer
Media Control
rTNFα Treatments
14C-Albumin Transfer (pmoles/hour)
0.9
0.8
0.7
0.6
0.5
0.4
0.3
0.2
0.1
p<0.01
Baseline
n= 20
5
5
5
5
Pretreatment (16hr): Media Media rTNFα 10u/mL rTNFα 10u/mL
Treatment (6hr): Media rTNFα 1000u/mL Media rTNFα 1000u/mL

Figure 13

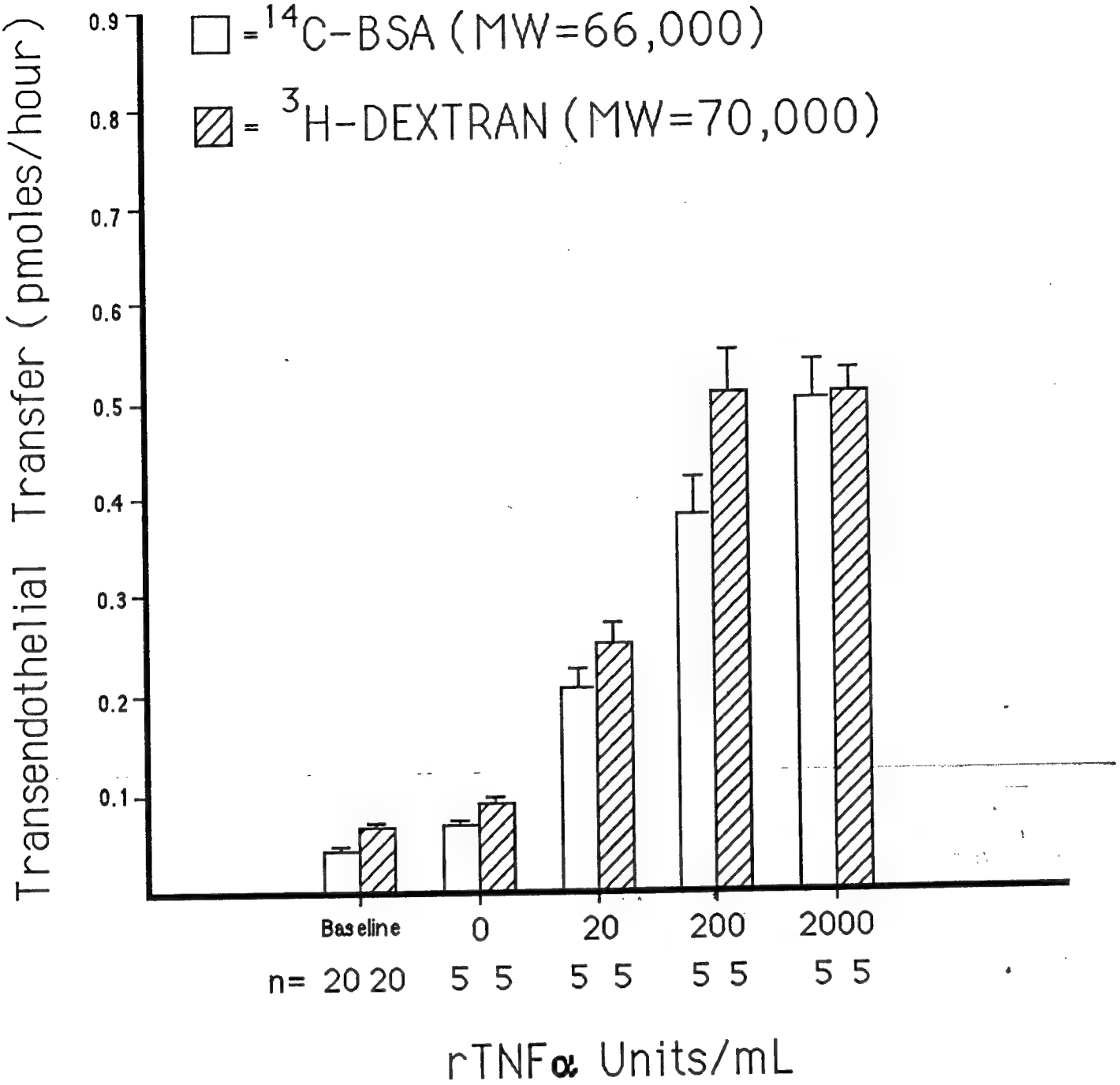
□ = ^{14}C-BSA (MW=66,000)
▨ = ^{3}H-DEXTRAN (MW=70,000)
Transendothelial Transfer (pmoles/hour)
0.9
0.8
0.7
0.6
0.5
0.4
0.3
0.2
0.1
Baseline
0
20
200
2000
n= 20 20 5 5 5 5 5 5 5 5
rTNFα Units/mL

Figure 14

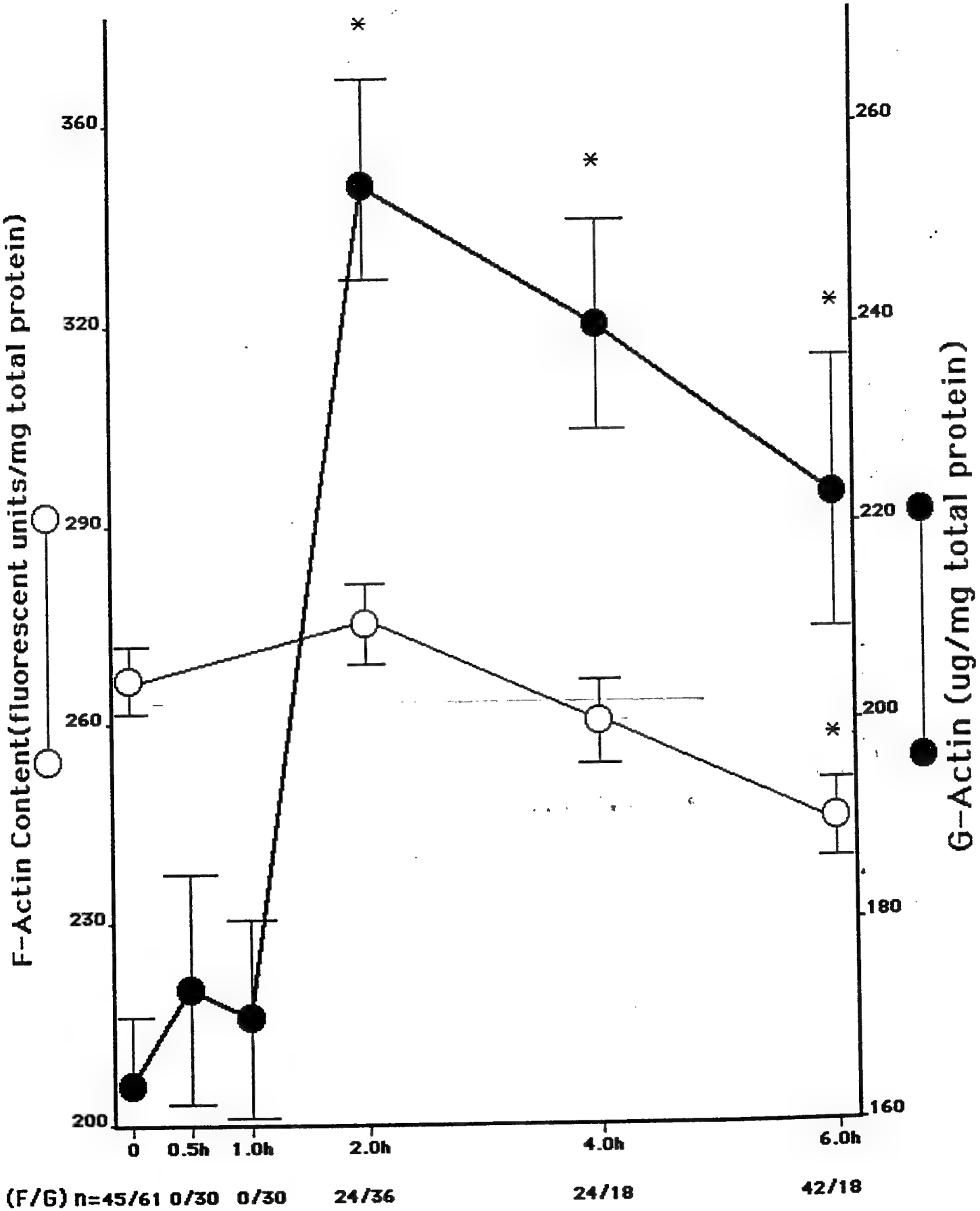
F-Actin Content(fluorescent units/mg total protein)
G-Actin (ug/mg total protein)
360
320
290
260
230
200
260
240
220
200
180
160
*
*
*
*
0
0.5h
1.0h
2.0h
4.0h
6.0h
(F/G) n=45/61 0/30 0/30 24/36 24/18 42/18
rTNFα Exposure Time (hours)

Figure 15

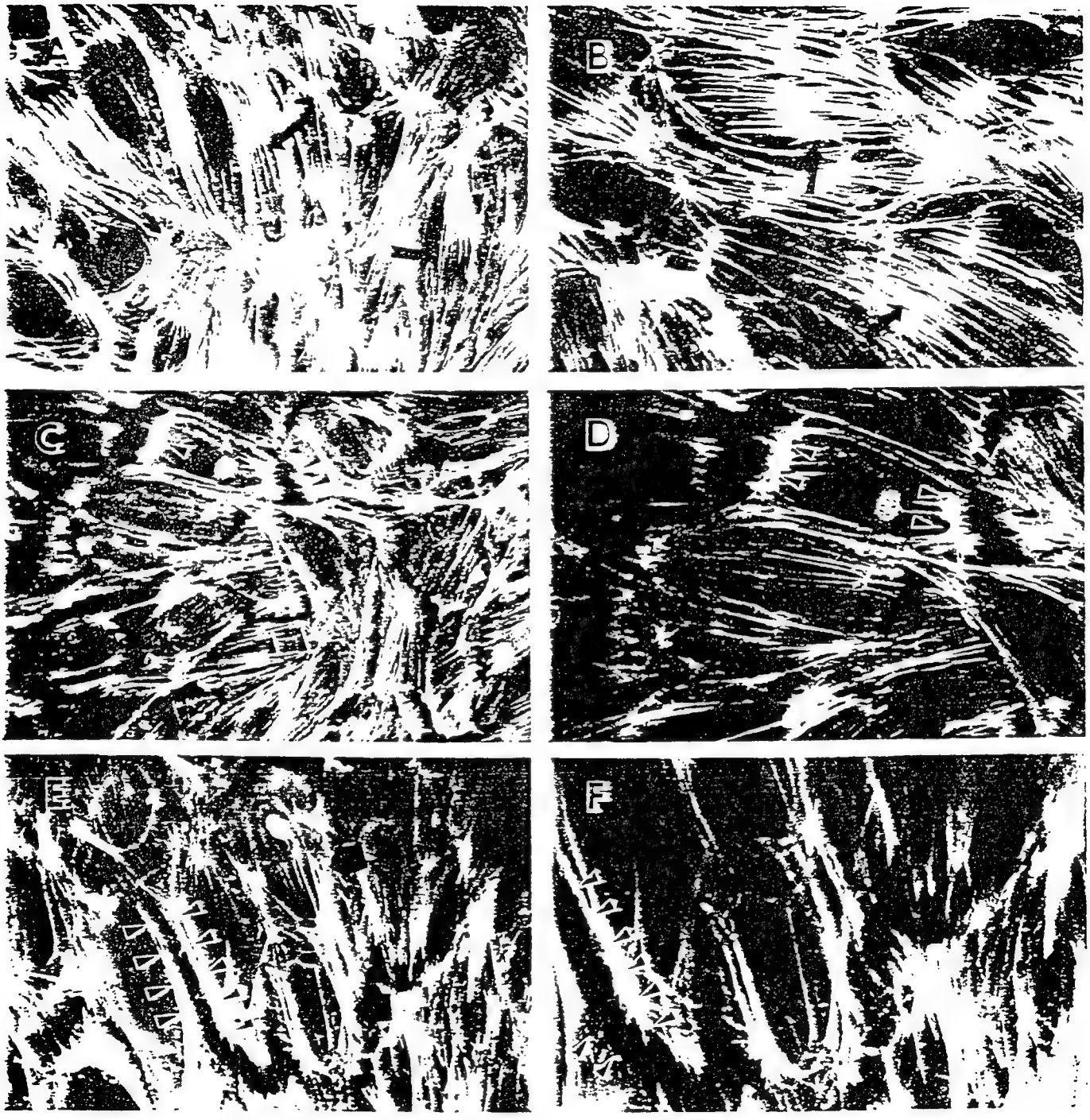

Figure 16

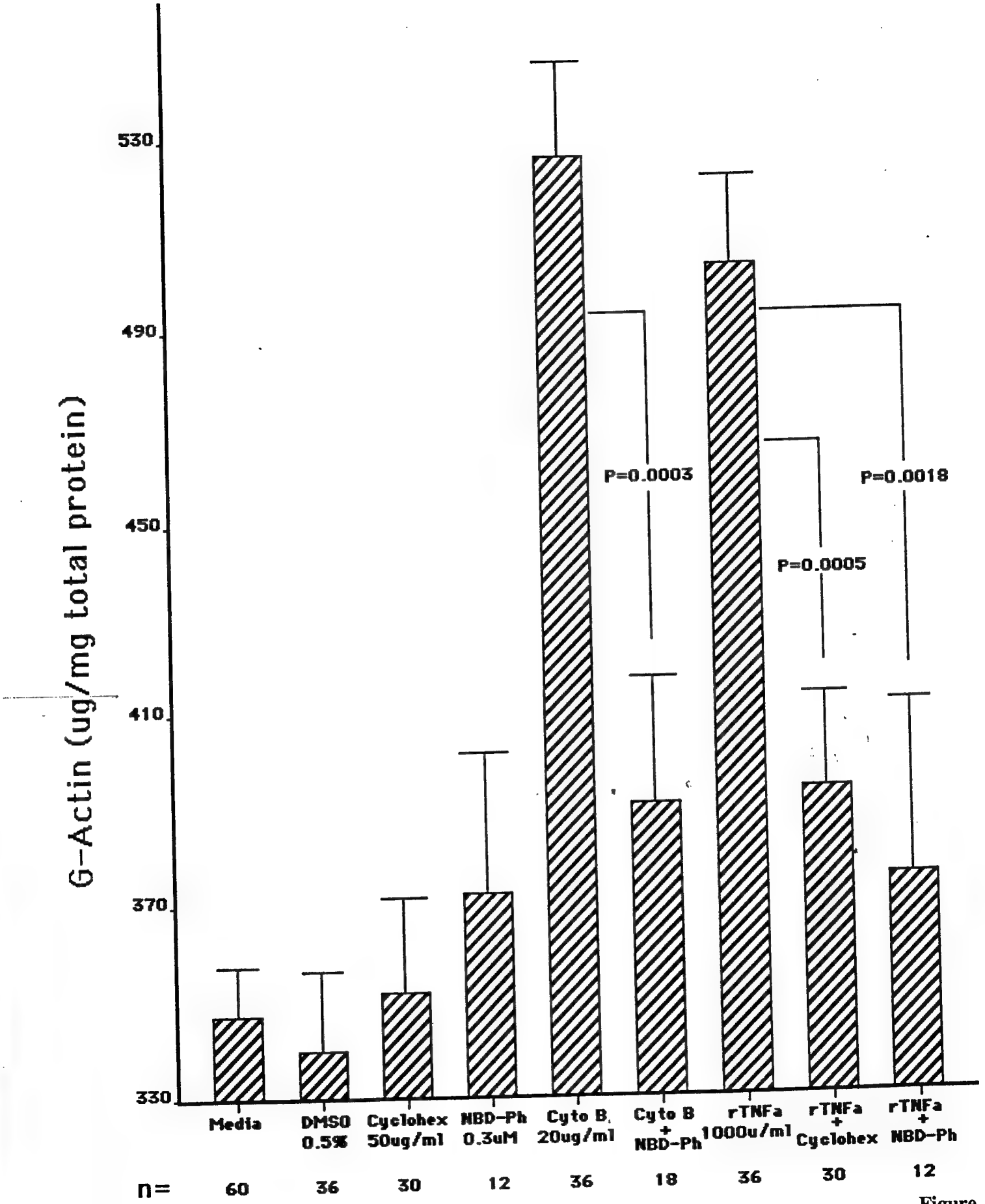
G-Actin (ug/mg total protein)
530
490
450
410
370
330
P=0.0003
P=0.0018
P=0.0005
Media
DMSO 0.5%
Cyclohex 50ug/ml
NBD-Ph 0.3uM
Cyto B 20ug/ml
Cyto B + NBD-Ph
rTNFa 1000u/ml
rTNFa + Cyclohex
rTNFa + NBD-Ph
n=
60
36
30
12
36
18
36
30
12

Figure 17

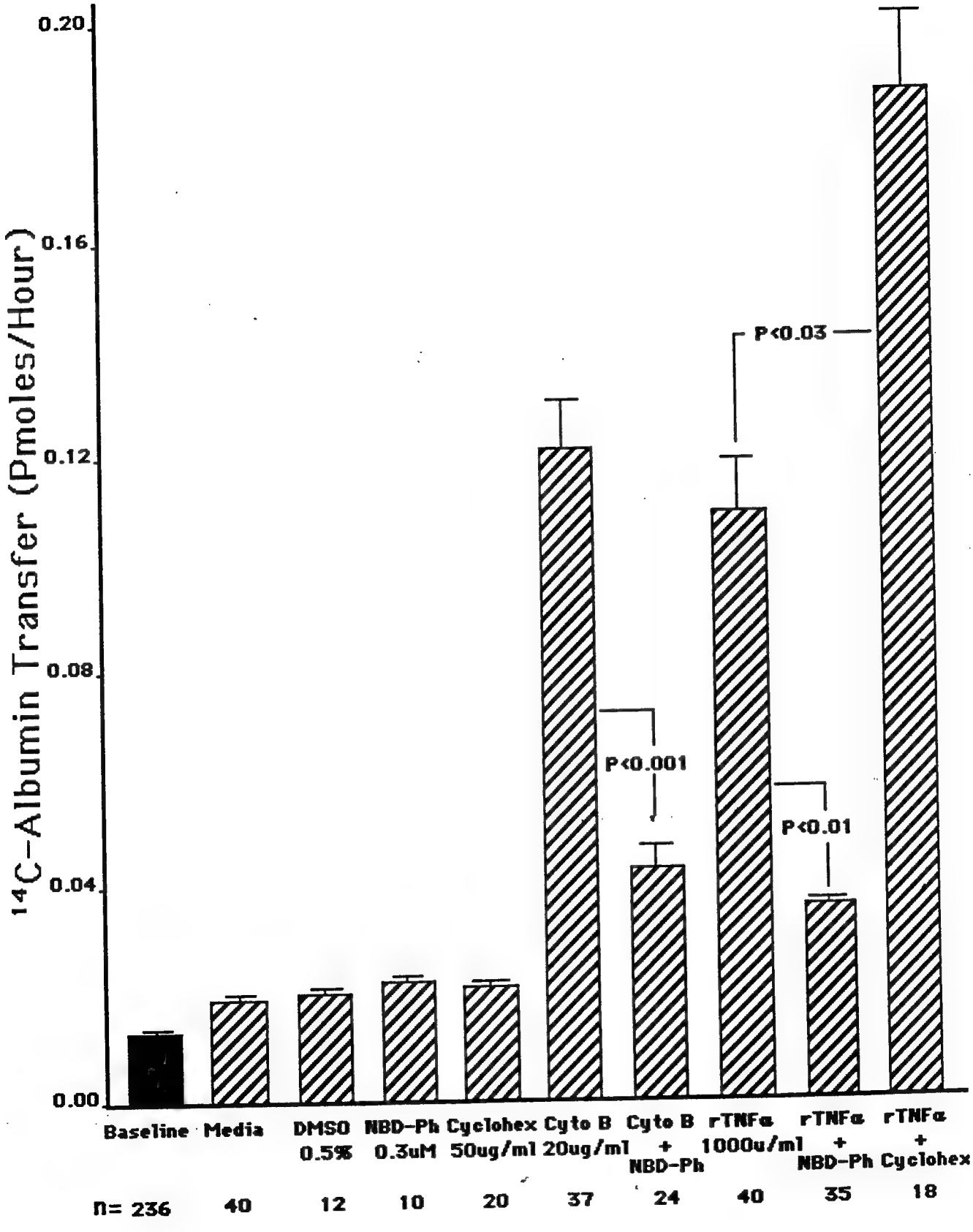
0.20
0.16
0.12
0.08
0.04
0.00
^{14}C-Albumin Transfer (Pmoles/Hour)
P<0.03
P<0.001
P<0.01
Baseline
Media
DMSO 0.5%
NBD-Ph 0.3uM
Cyclohex 50ug/ml
Cyto B 20ug/ml
Cyto B + NBD-Ph
rTNFα 1000u/ml
rTNFα + NBD-Ph
rTNFα + Cyclohex
n= 236
40
12
10
20
37
24
40
35
18

Figure 18

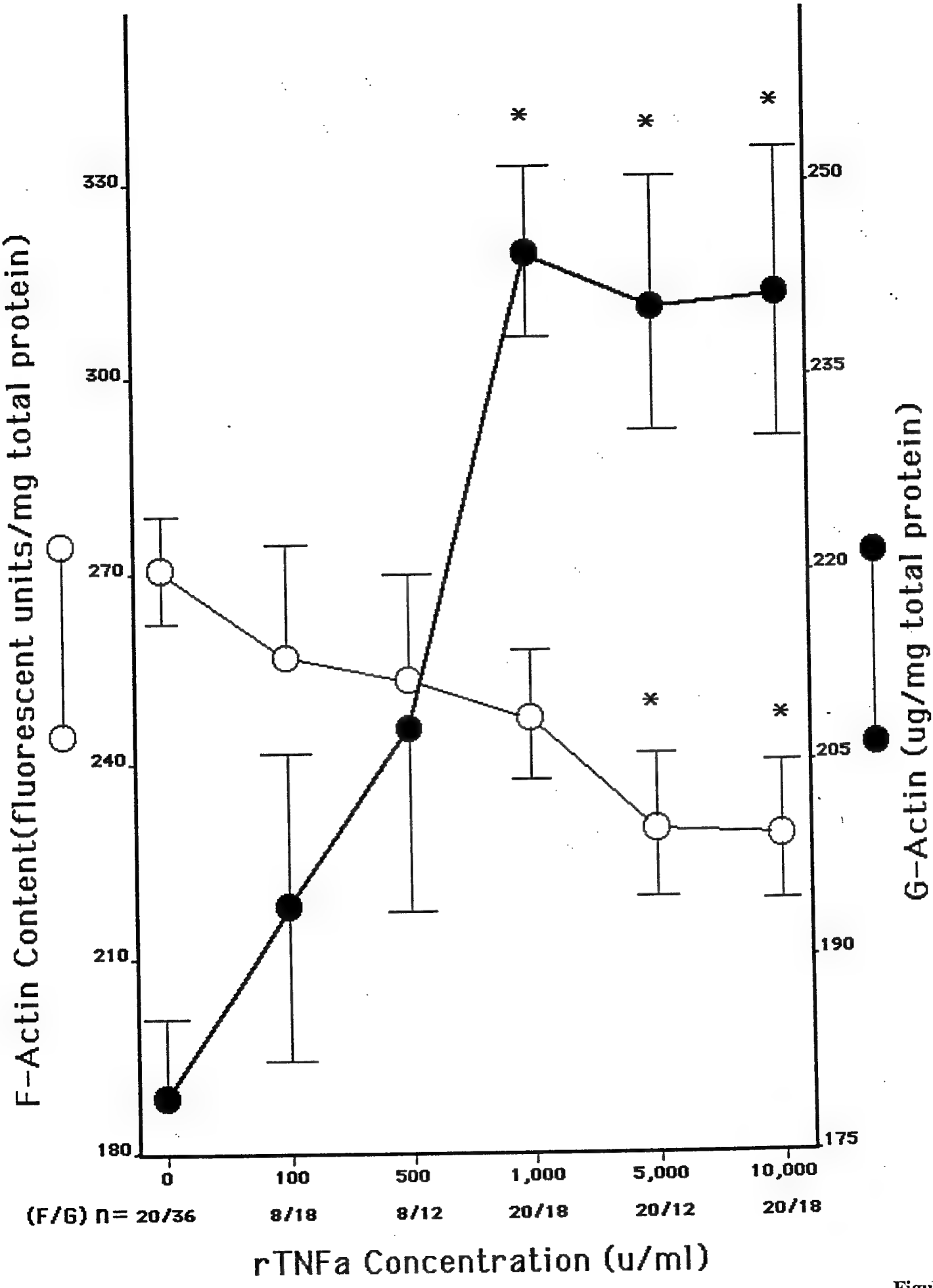
F-Actin Content(fluorescent units/mg total protein)
G-Actin (ug/mg total protein)
330
300
270
240
210
180
250
235
220
205
190
175
*
*
*
*
*
0
100
500
1,000
5,000
10,000
(F/G) n= 20/36
8/18
8/12
20/18
20/12
20/18
rTNFa Concentration (u/ml)

Figure 19

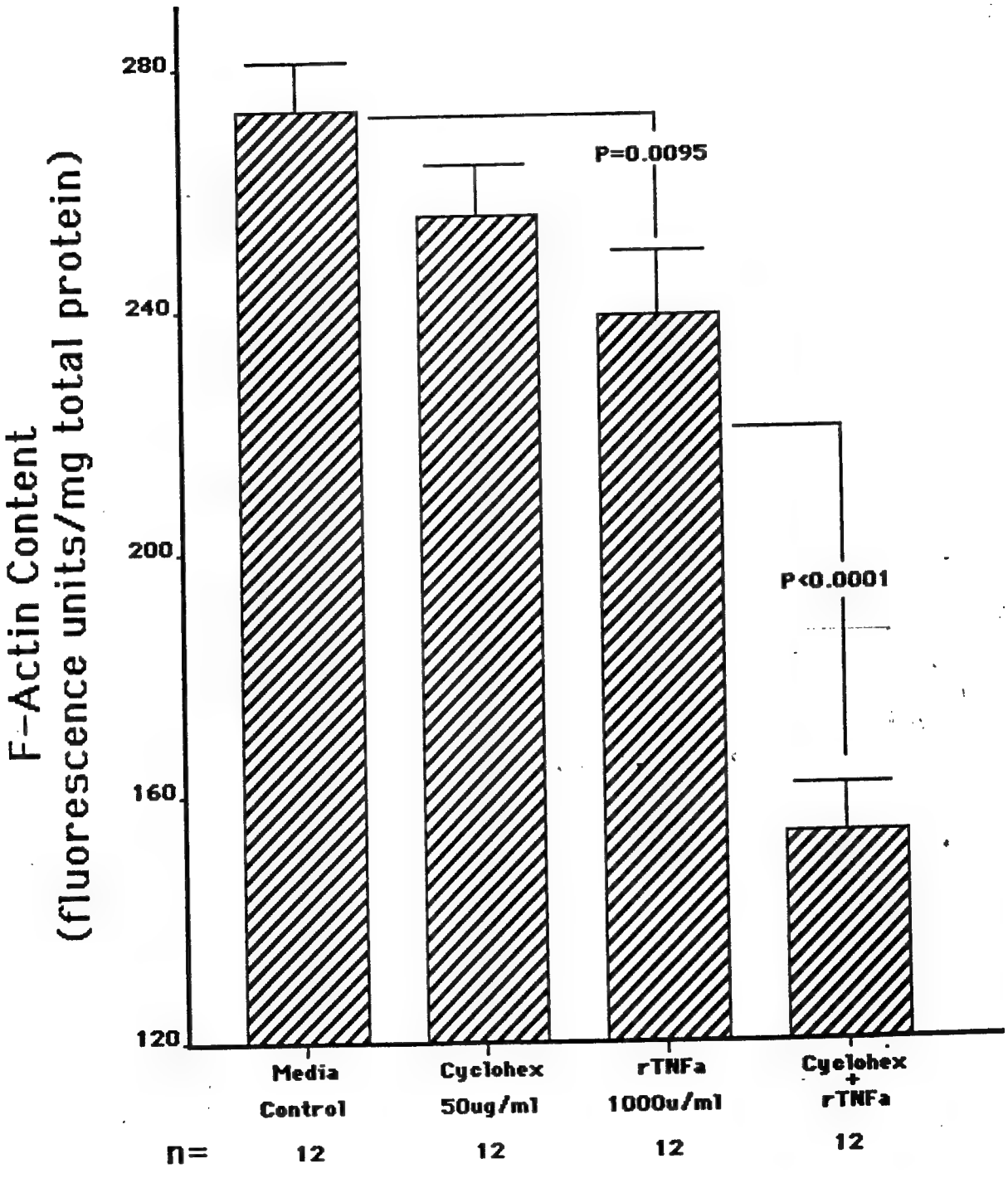
F-Actin Content
(fluorescence units/mg total protein)
280
240
200
160
120
P=0.0095
P<0.0001
Media Control
Cyclohex 50ug/ml
rTNFa 1000u/ml
Cyclohex + rTNFa
n=
12
12
12
12

Figure 20

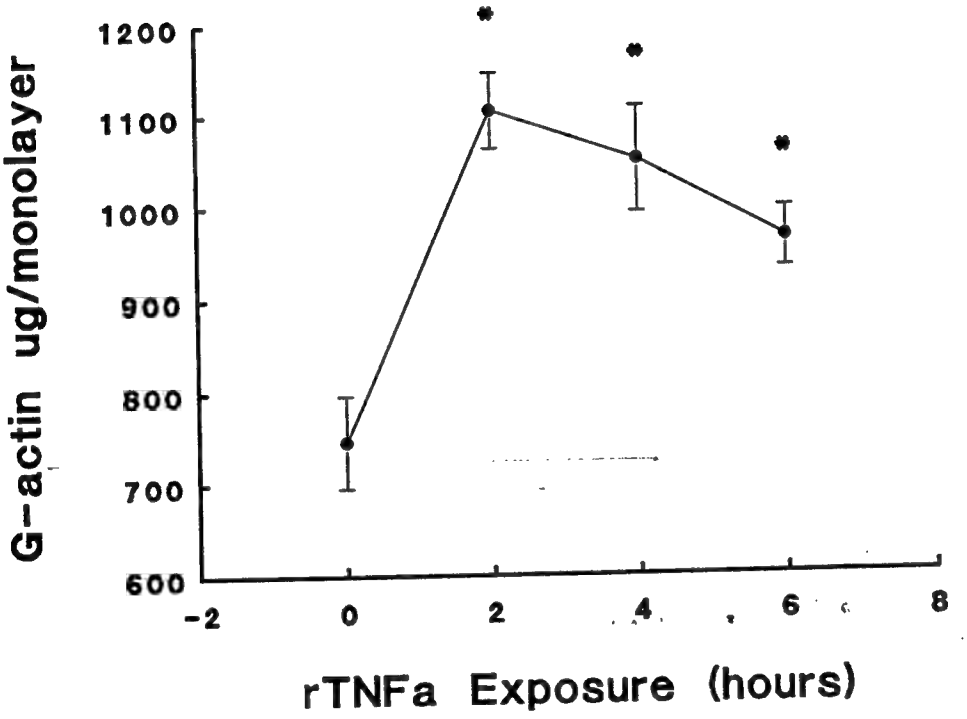
G-actin ug/monolayer
1200
1100
1000
900
800
700
600
-2
0
2
4
6
8
rTNFa Exposure (hours)

Figure 21

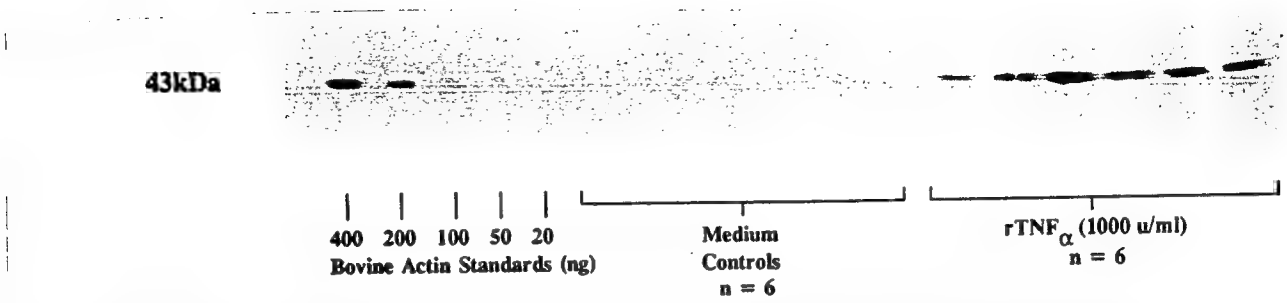

Fig. 7. Quantitative immunoblotting for total endothelial cell actin. Endothelial monolayers were exposed to 1,000 U/ml rTNF-α or media alone for 6 h. Endothelial extracts were electrophoresed on SDS-polyacrylamide gels, transferred onto nitrocellulose, incubated with murine anti-avian actin immunoglobulin G_1 followed by protein G-horseradish peroxidase conjugate with enhanced chemiluminescence substrates, and exposed to film. A simultaneous standard curve with known concentrations of pure bovine skeletal muscle actin was run on each gel. Autoradiographs were scanned by laser densitometry, and total actin extracted from each monolayer was quantified by interpolation from actin standard curve.

Figure 22

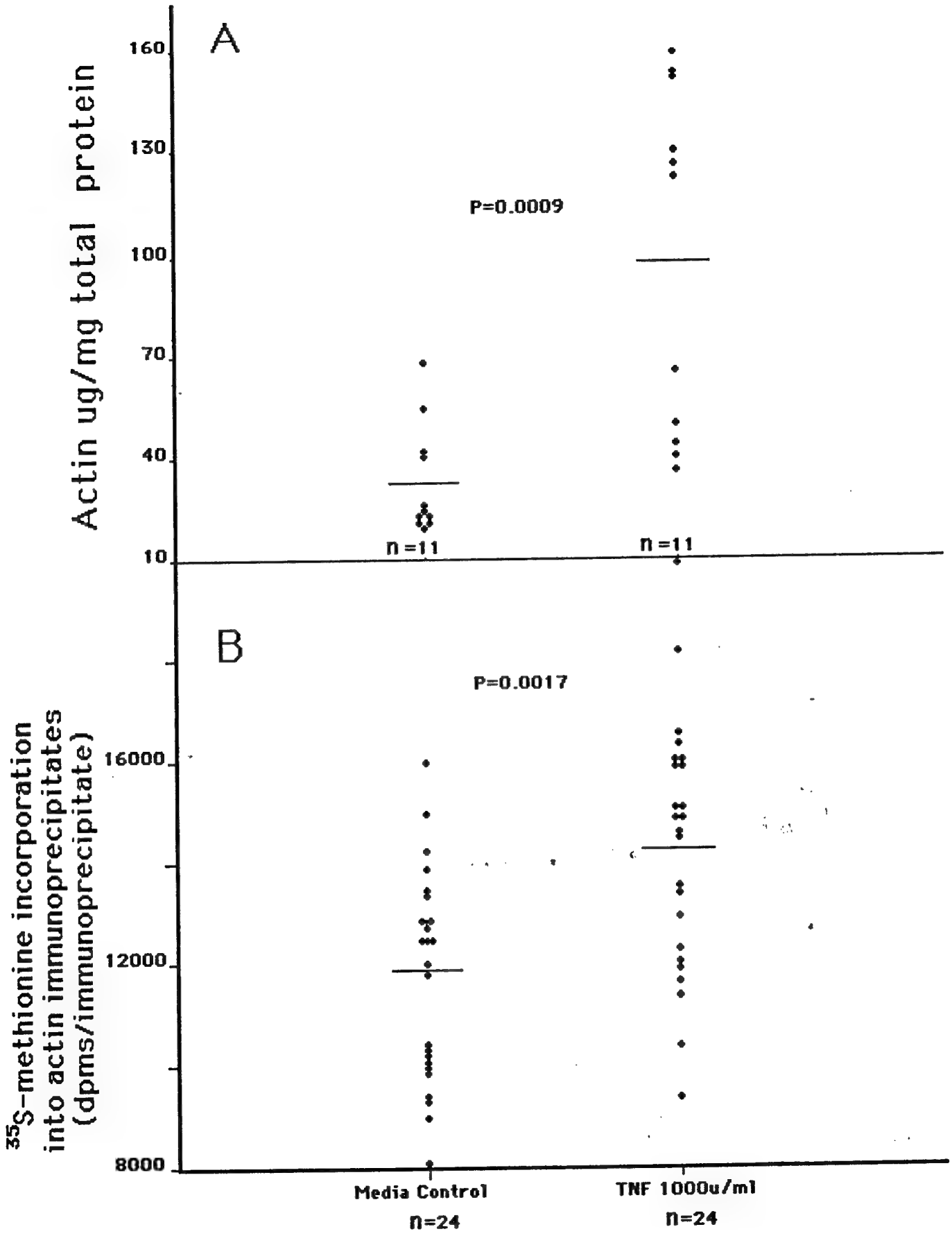
A
Actin ug/mg total protein
160
130
100
70
40
10
P=0.0009
n=11
n=11
B
^{35}S-methionine incorporation into actin immunoprecipitates (dpms/immunoprecipitate)
16000
12000
8000
P=0.0017
Media Control
n=24
TNF 1000u/ml
n=24

Figure 23

Figure 24

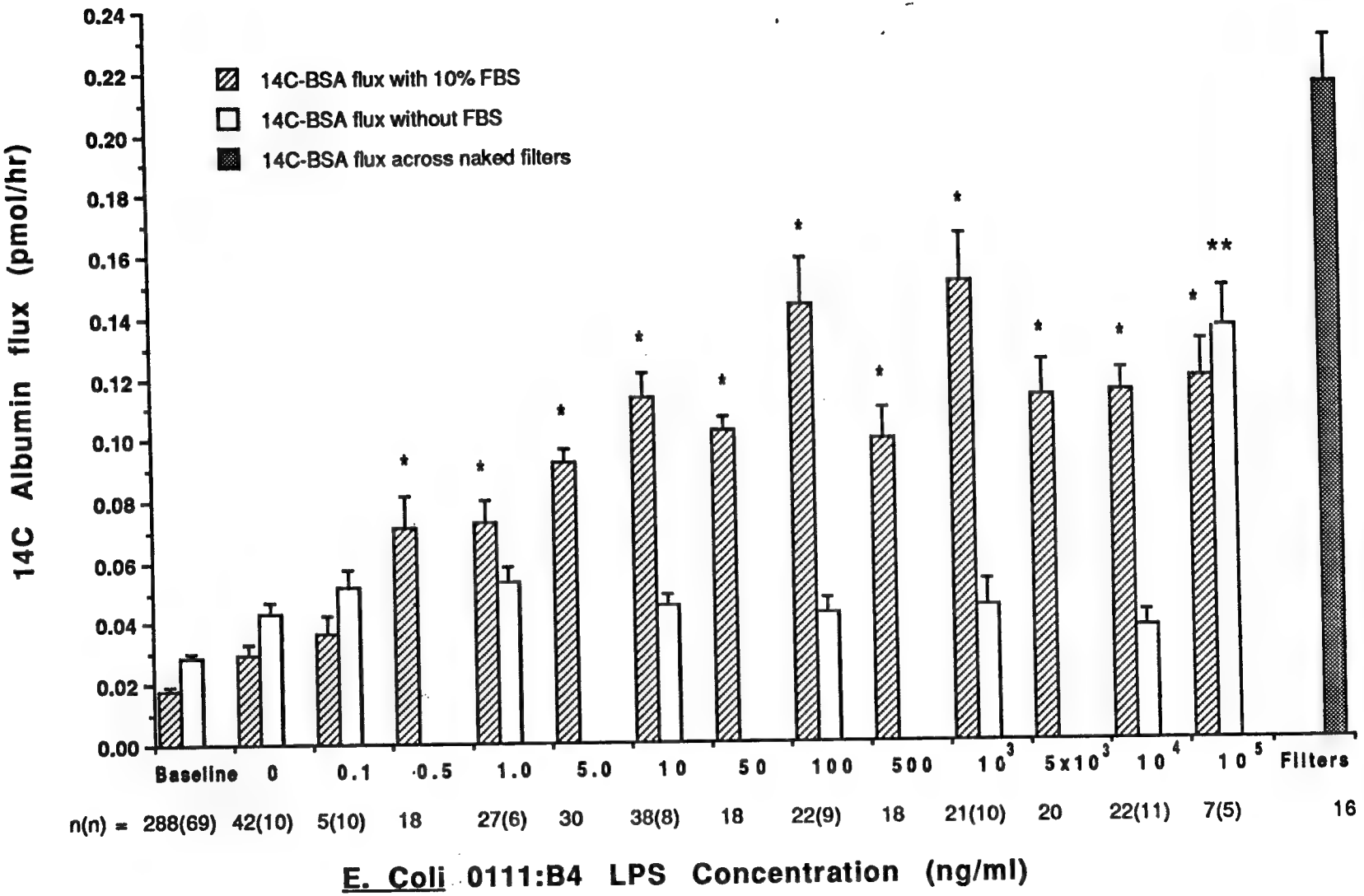
14C-BSA flux with 10% FBS
14C-BSA flux without FBS
14C-BSA flux across naked filters
14C Albumin flux (pmol/hr)
0.24
0.22
0.20
0.18
0.16
0.14
0.12
0.10
0.08
0.06
0.04
0.02
0.00
Baseline
0
0.1
0.5
1.0
5.0
10
50
100
500
10^3
5x10^3
10^4
10^5
Filters
n(n) = 288(69) 42(10) 5(10) 18 27(6) 30 38(8) 18 22(9) 18 21(10) 20 22(11) 7(5) 16
E. Coli 0111:B4 LPS Concentration (ng/ml)

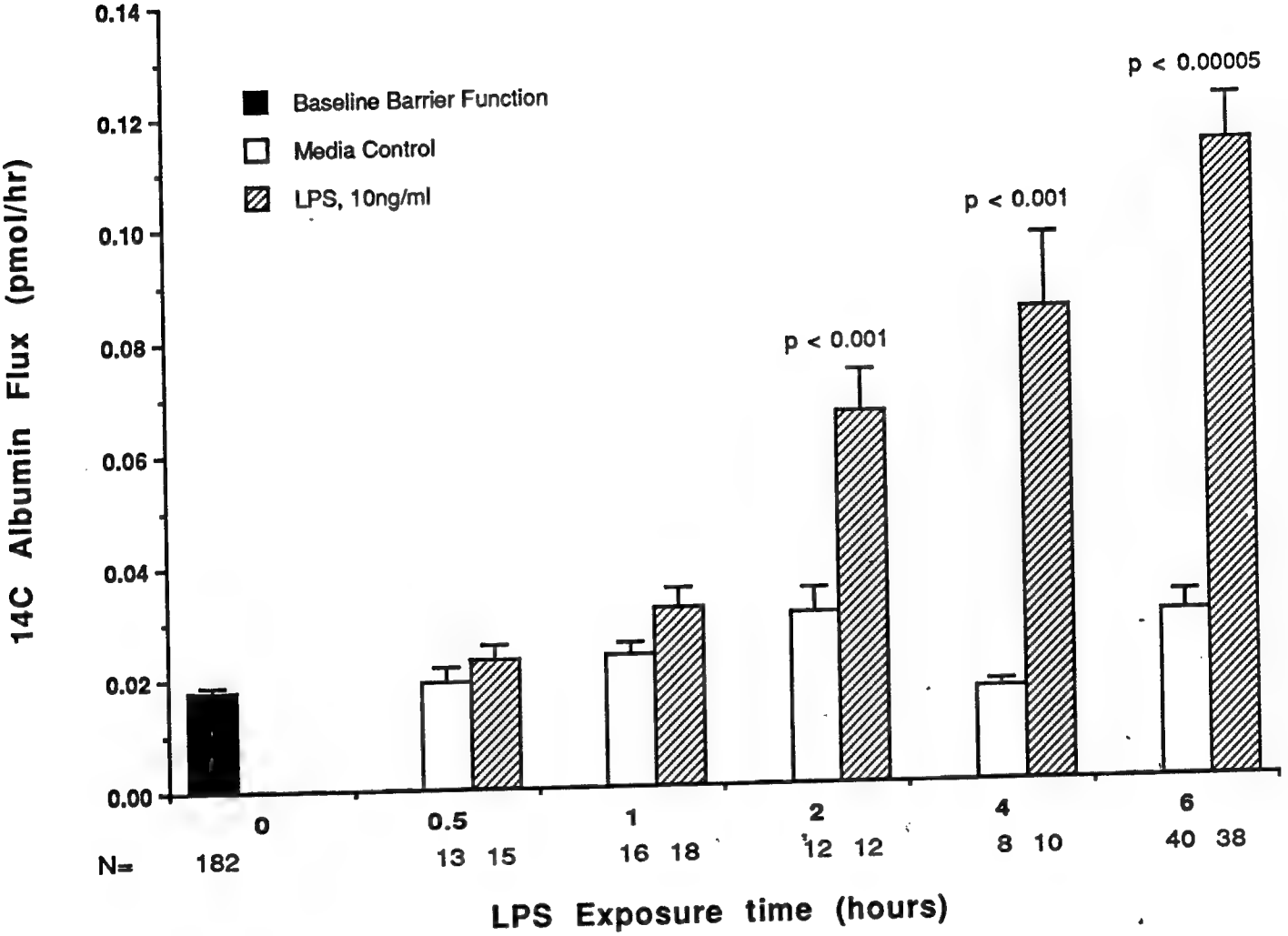
0.14
0.12
0.10
0.08
0.06
0.04
0.02
0.00
14C Albumin Flux (pmol/hr)
Baseline Barrier Function
Media Control
LPS, 10ng/ml
p < 0.00005
p < 0.001
p < 0.001
0
0.5
1
2
4
6
N=
182
13 15
16 18
12 12
8 10
40 38
LPS Exposure time (hours)

Figure 25

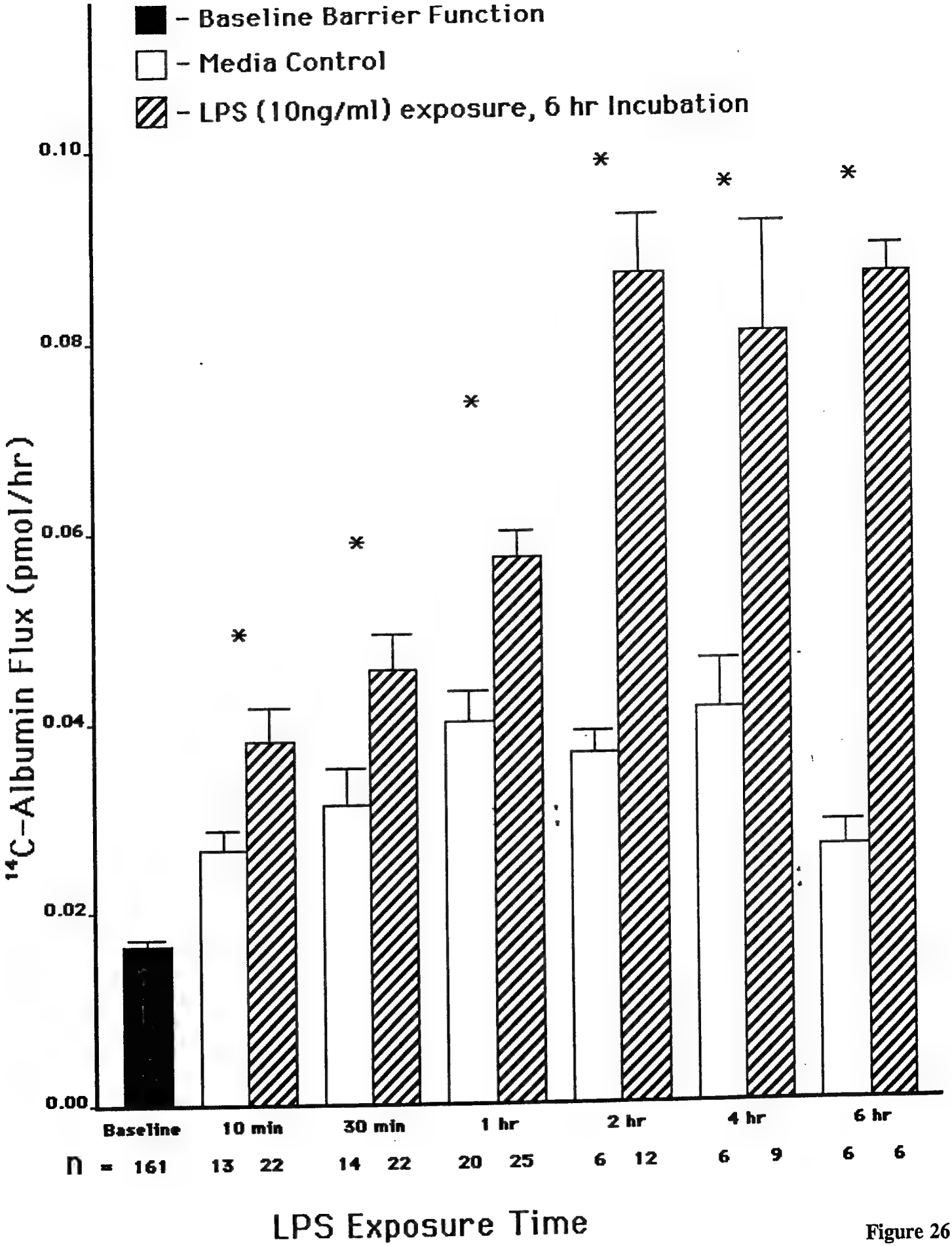
■ - Baseline Barrier Function
□ - Media Control
▨ - LPS (10ng/ml) exposure, 6 hr Incubation
0.10
0.08
0.06
0.04
0.02
0.00
^{14}C-Albumin Flux (pmol/hr)
*
Baseline
10 min
30 min
1 hr
2 hr
4 hr
6 hr
n = 161 13 22 14 22 20 25 6 12 6 9 6 6
LPS Exposure Time

Figure 26

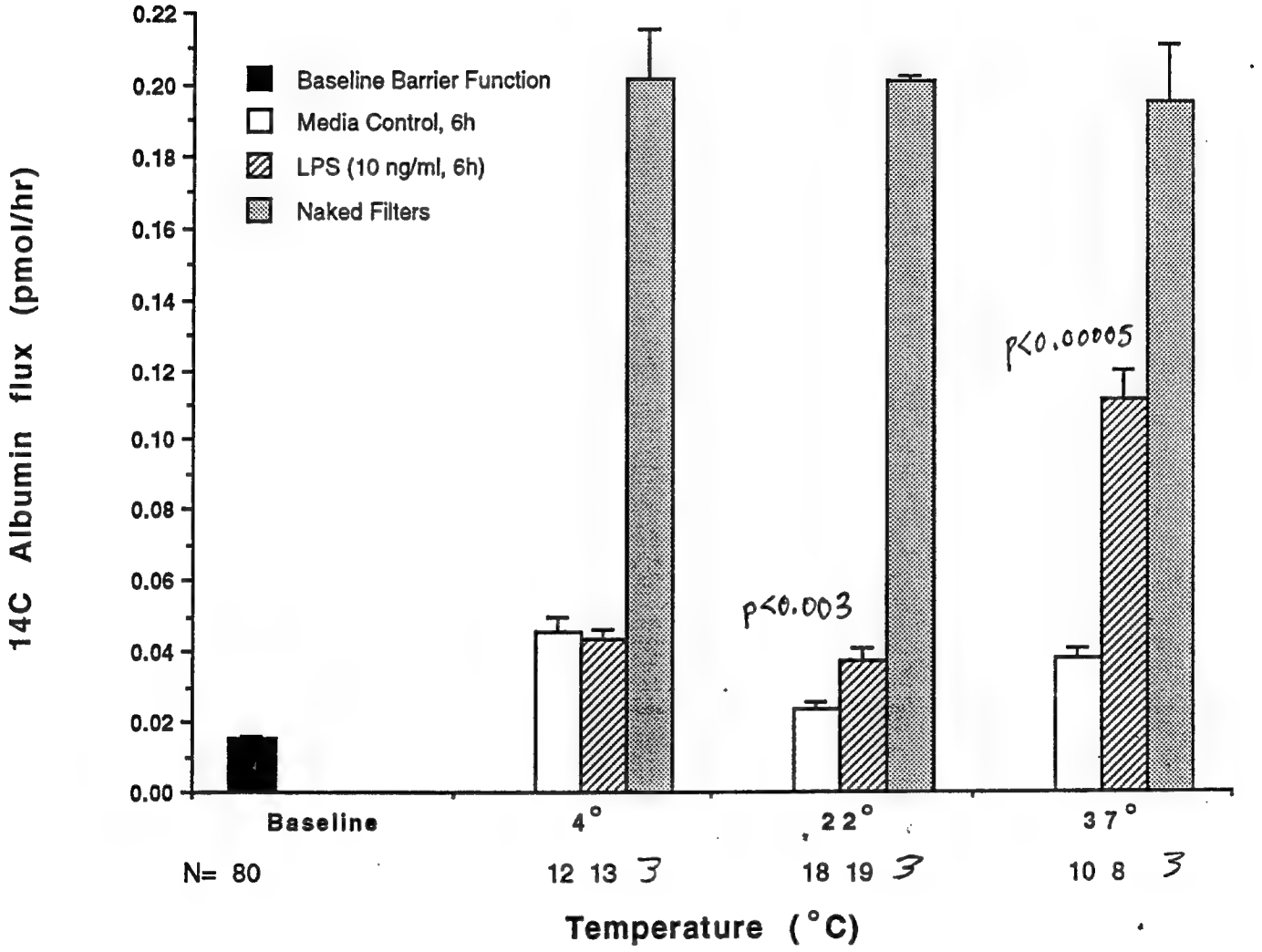
14C Albumin flux (pmol/hr)
0.22
0.20
0.18
0.16
0.14
0.12
0.10
0.08
0.06
0.04
0.02
0.00
Baseline Barrier Function
Media Control, 6h
LPS (10 ng/ml, 6h)
Naked Filters
p<0.003
p<0.00005
Baseline
4°
22°
37°
N= 80
12 13 3
18 19 3
10 8 3
Temperature (°C)

Figure 27

Figure 28

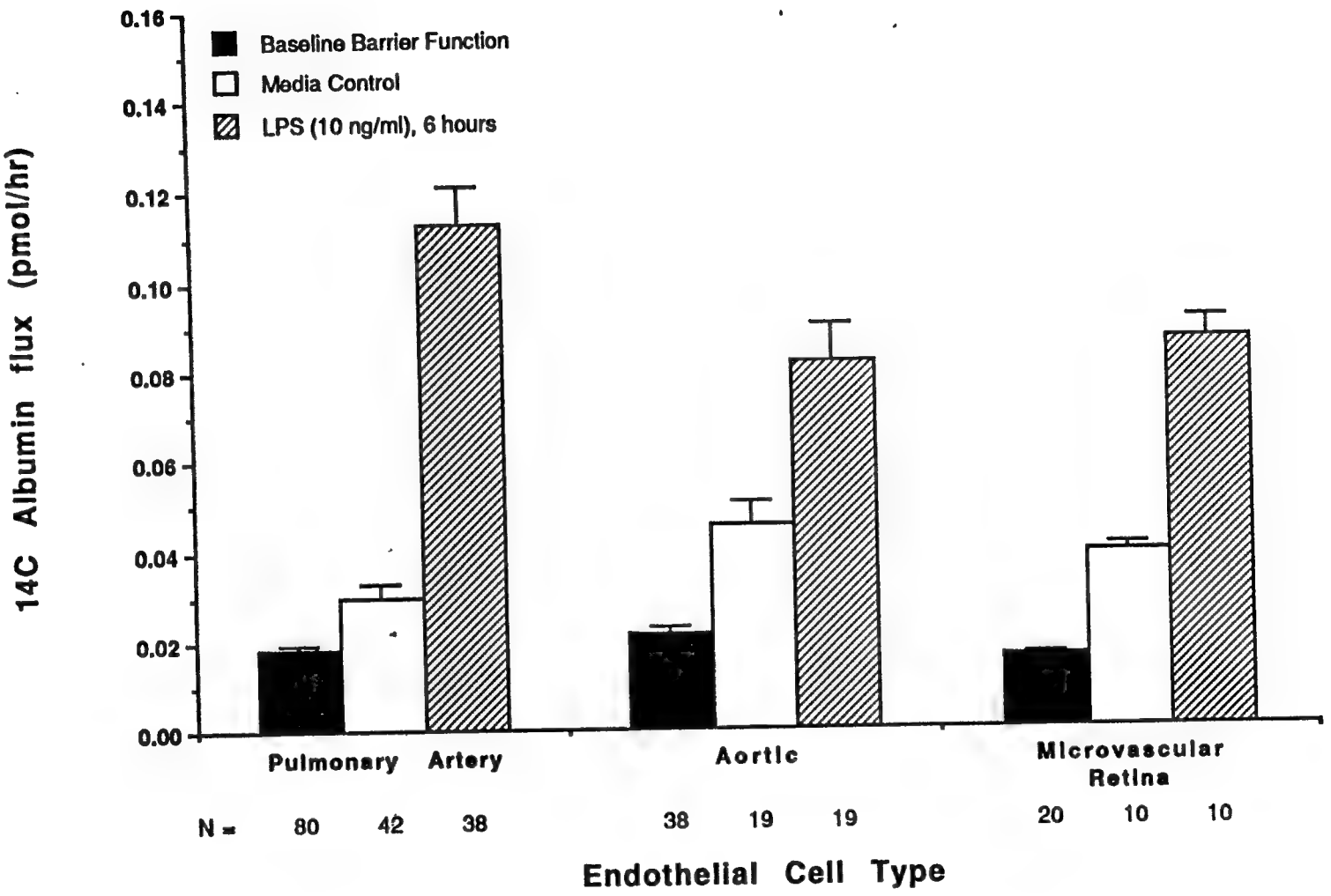
Baseline Barrier Function
Media Control
LPS (10 ng/ml), 6 hours
14C Albumin flux (pmol/hr)
0.16
0.14
0.12
0.10
0.08
0.06
0.04
0.02
0.00
Pulmonary Artery
Aortic
Microvascular Retina
N = 80 42 38 38 19 19 20 10 10
Endothelial Cell Type

Figure 29

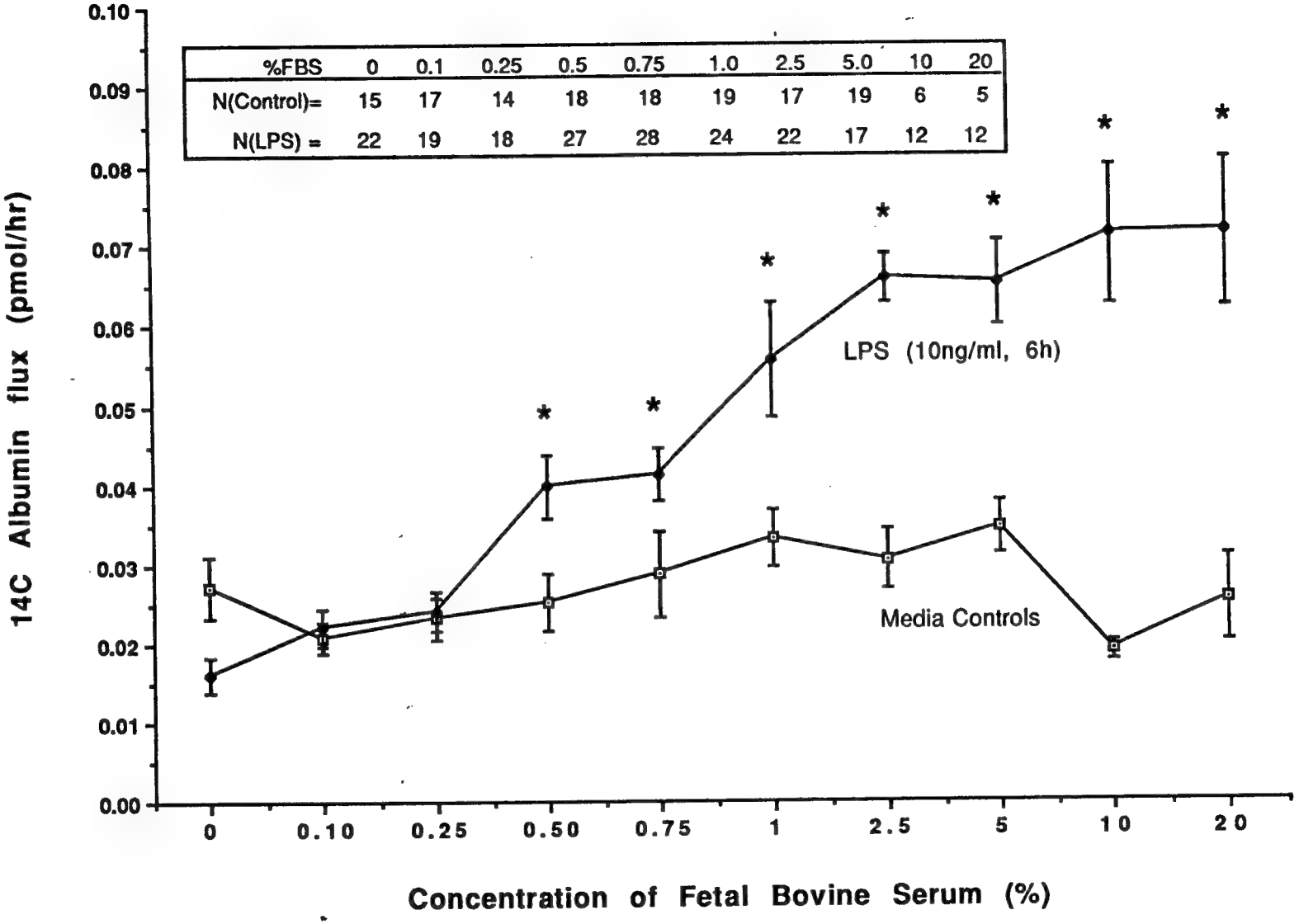
%FBS 0 0.1 0.25 0.5 0.75 1.0 2.5 5.0 10 20
N(Control)= 15 17 14 18 18 19 17 19 6 5
N(LPS) = 22 19 18 27 28 24 22 17 12 12
LPS (10ng/ml, 6h)
Media Controls
14C Albumin flux (pmol/hr)
0.10
0.09
0.08
0.07
0.06
0.05
0.04
0.03
0.02
0.01
0.00
0
0.10
0.25
0.50
0.75
1
2.5
5
10
20
Concentration of Fetal Bovine Serum (%)

Figure 30

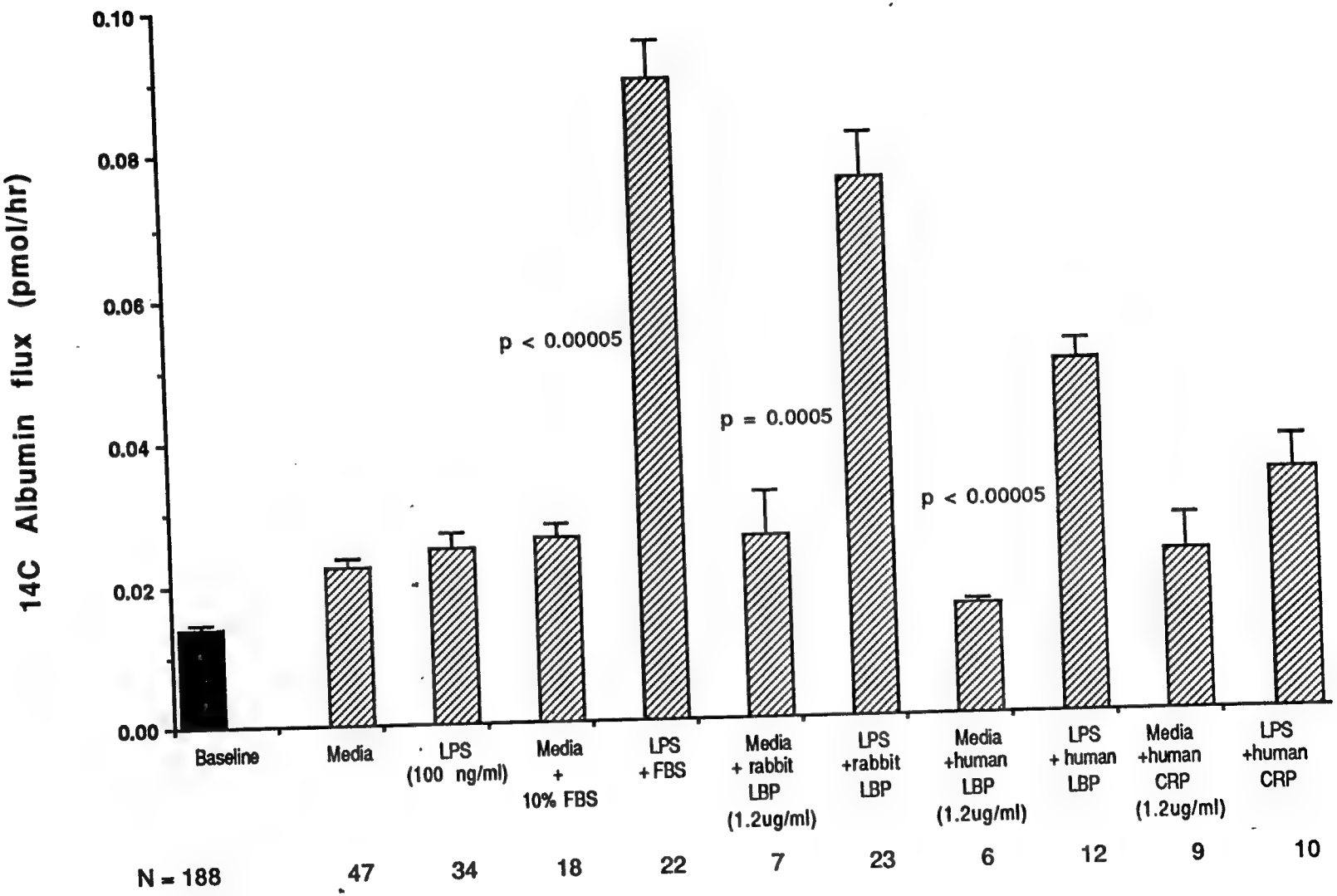
14C Albumin flux (pmol/hr)
0.10
0.08
0.06
0.04
0.02
0.00
p < 0.00005
p = 0.0005
p < 0.00005
Baseline
Media
LPS (100 ng/ml)
Media + 10% FBS
LPS + FBS
Media + rabbit LBP (1.2ug/ml)
LPS +rabbit LBP
Media +human LBP (1.2ug/ml)
LPS + human LBP
Media +human CRP (1.2ug/ml)
LPS +human CRP
N = 188
47
34
18
22
7
23
6
12
9
10

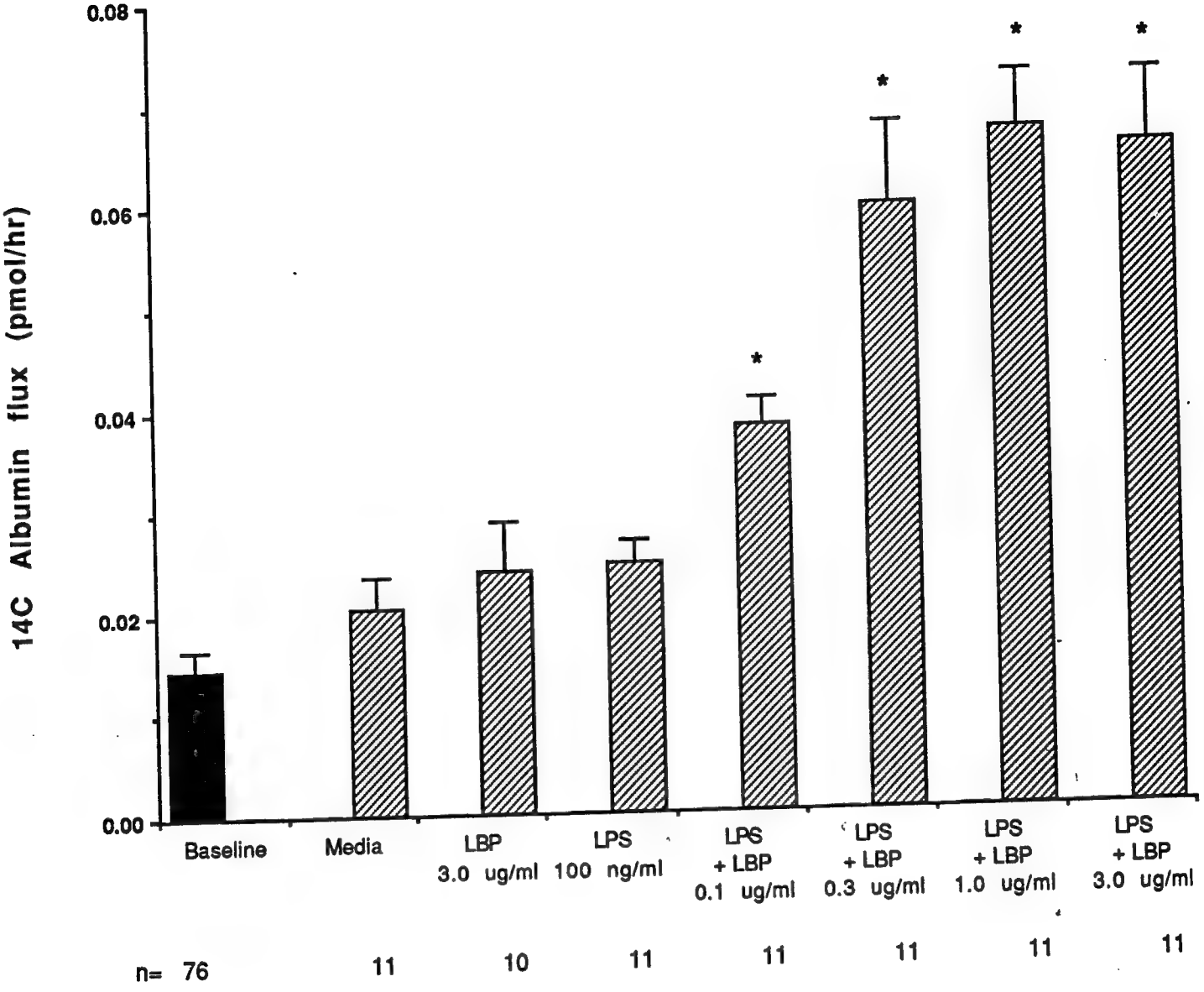
14C Albumin flux (pmol/hr)
0.08
0.06
0.04
0.02
0.00
*
*
*
*
Baseline
Media
LBP 3.0 ug/ml
LPS 100 ng/ml
LPS + LBP 0.1 ug/ml
LPS + LBP 0.3 ug/ml
LPS + LBP 1.0 ug/ml
LPS + LBP 3.0 ug/ml
n= 76
11
10
11
11
11
11
11

Figure 31

Figure 32

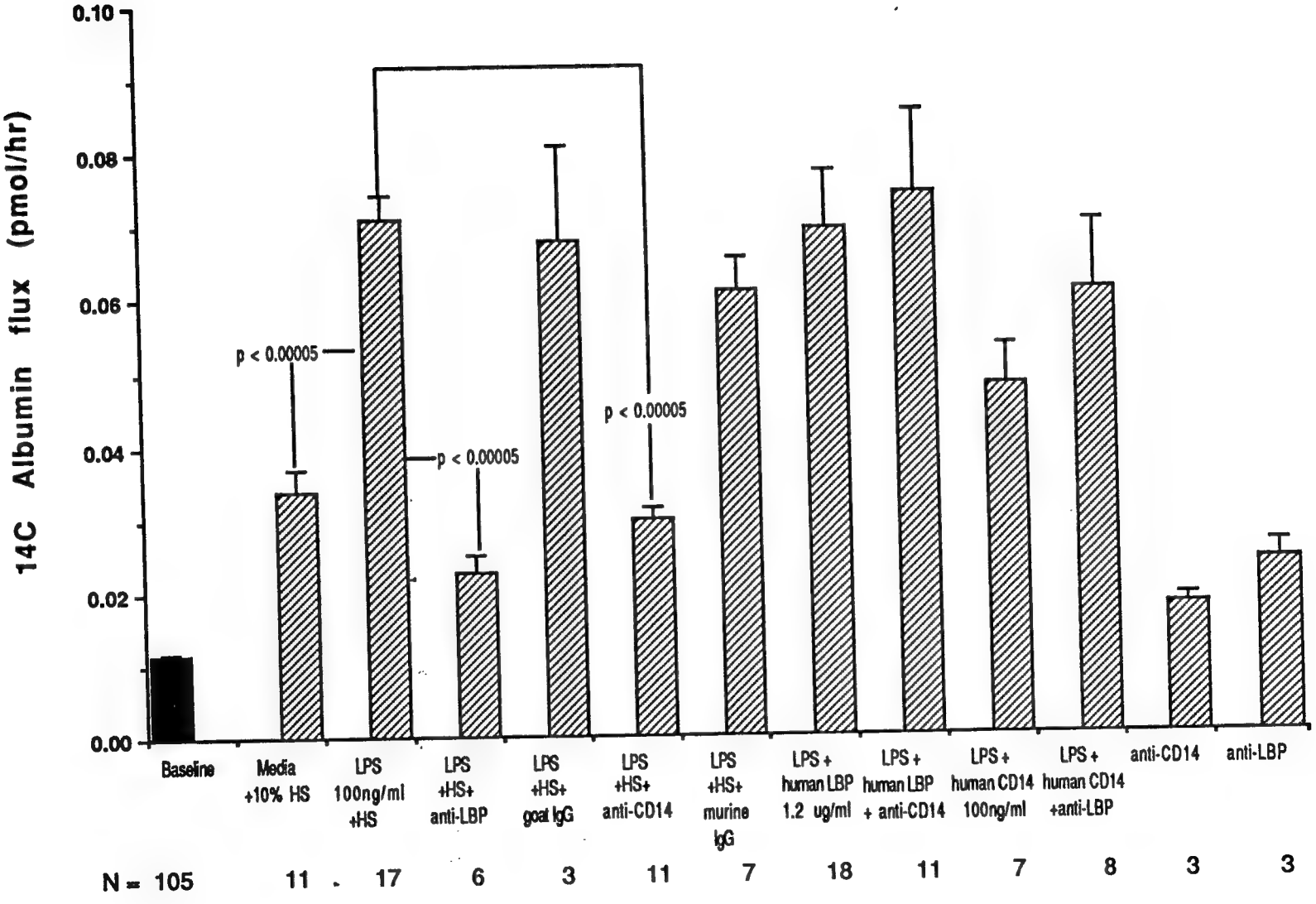
14C Albumin flux (pmol/hr)
0.10
0.08
0.06
0.04
0.02
0.00
p < 0.00005
p < 0.00005
p < 0.00005
Baseline
Media +10% HS
LPS 100ng/ml +HS
LPS +HS+ anti-LBP
LPS +HS+ goat IgG
LPS +HS+ anti-CD14
LPS +HS+ murine IgG
LPS + human LBP 1.2 ug/ml
LPS + human LBP + anti-CD14
LPS + human CD14 100ng/ml
LPS + human CD14 +anti-LBP
anti-CD14
anti-LBP
N = 105
11
17
6
3
11
7
18
11
7
8
3
3

Figure 33

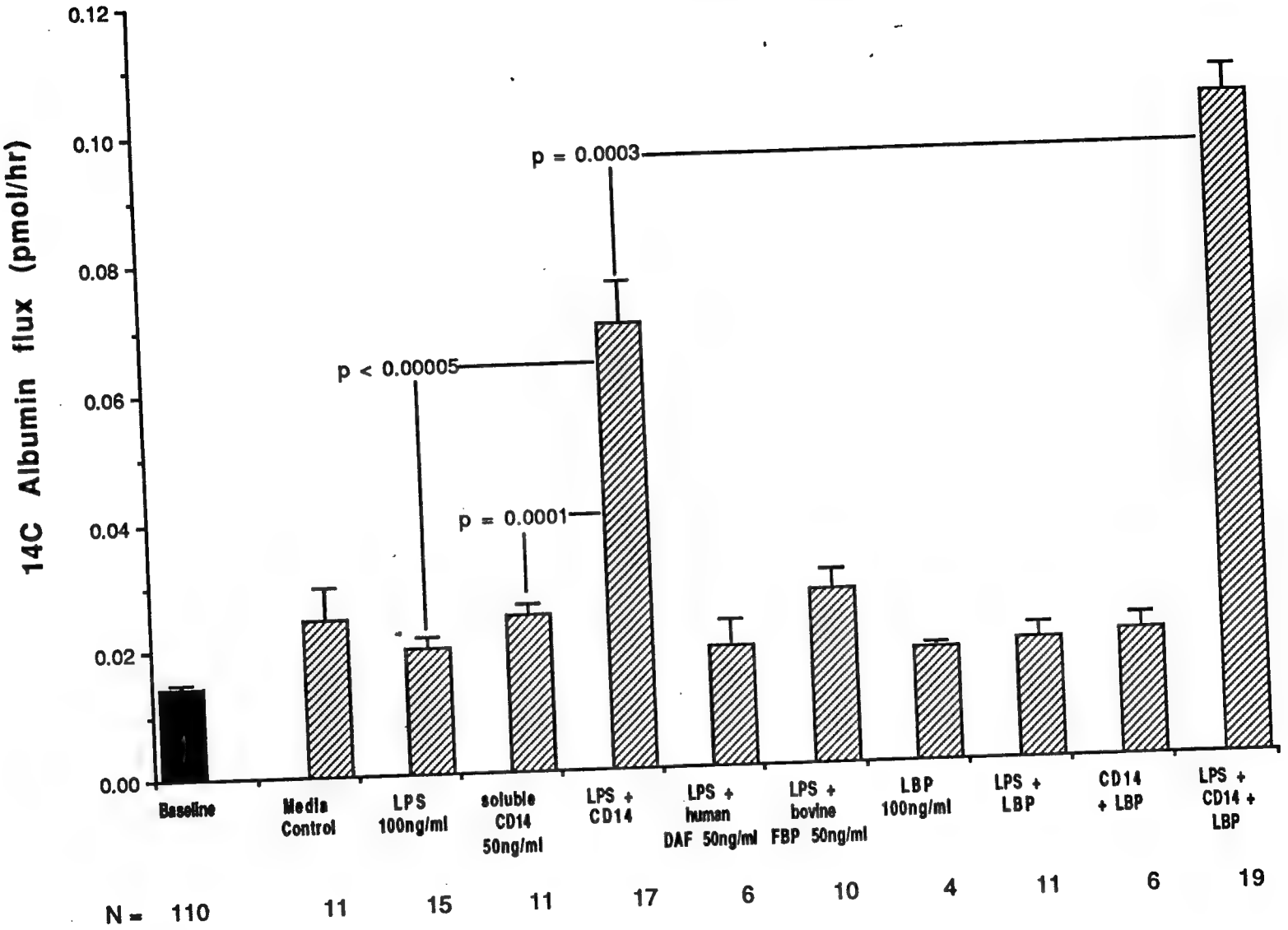
14C Albumin flux (pmol/hr)
0.12
0.10
0.08
0.06
0.04
0.02
0.00
p = 0.0003
p < 0.00005
p = 0.0001
Baseline
Media Control
LPS 100ng/ml
soluble CD14 50ng/ml
LPS + CD14
LPS + human DAF 50ng/ml
LPS + bovine FBP 50ng/ml
LBP 100ng/ml
LPS + LBP
CD14 + LBP
LPS + CD14 + LBP
N = 110 11 15 11 17 6 10 4 11 6 19

Figure 34

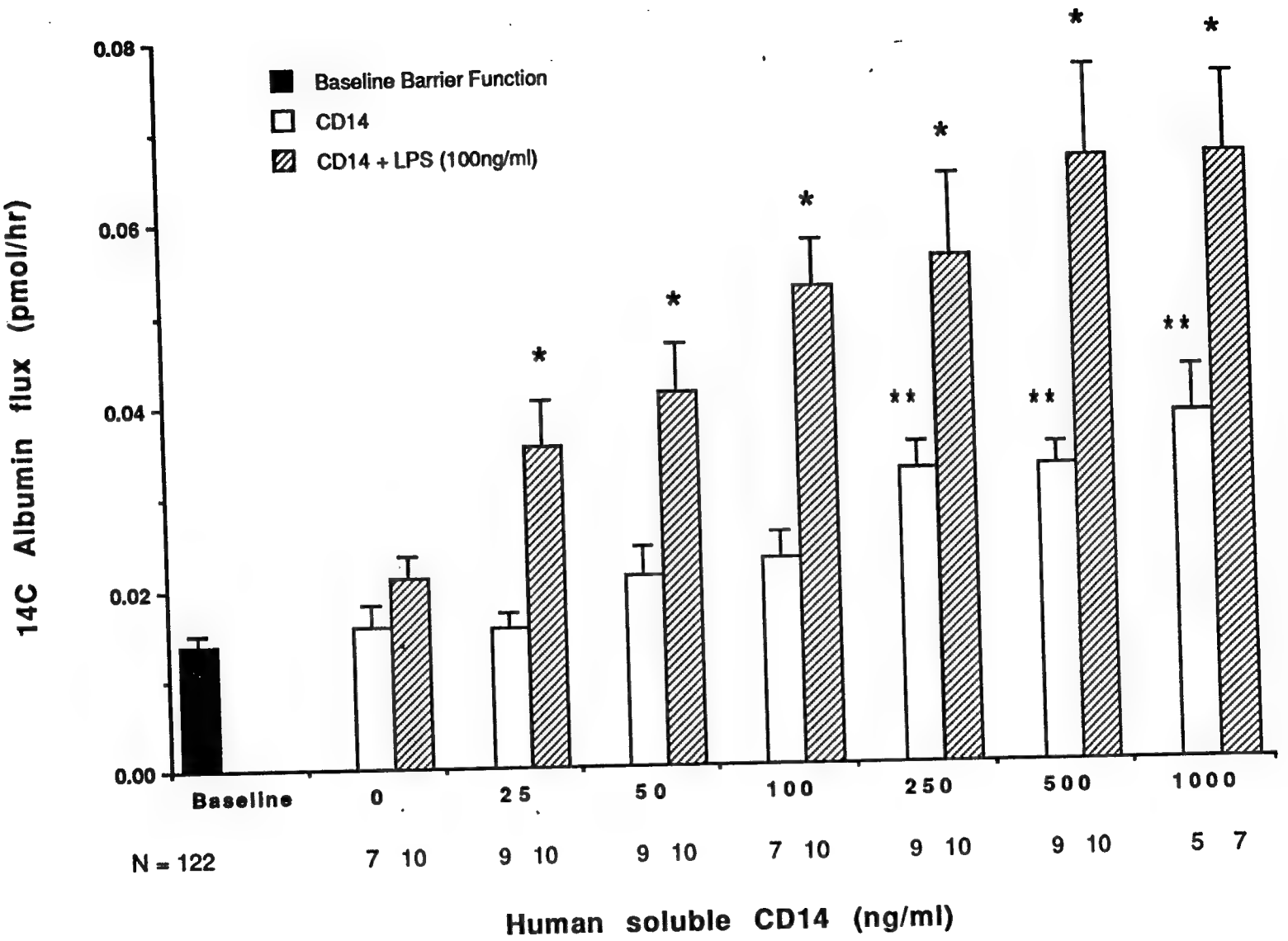
Baseline Barrier Function
CD14
CD14 + LPS (100ng/ml)
14C Albumin flux (pmol/hr)
0.08
0.06
0.04
0.02
0.00
Baseline
0
25
50
100
250
500
1000
N = 122
7 10
9 10
9 10
7 10
9 10
9 10
5 7
Human soluble CD14 (ng/ml)

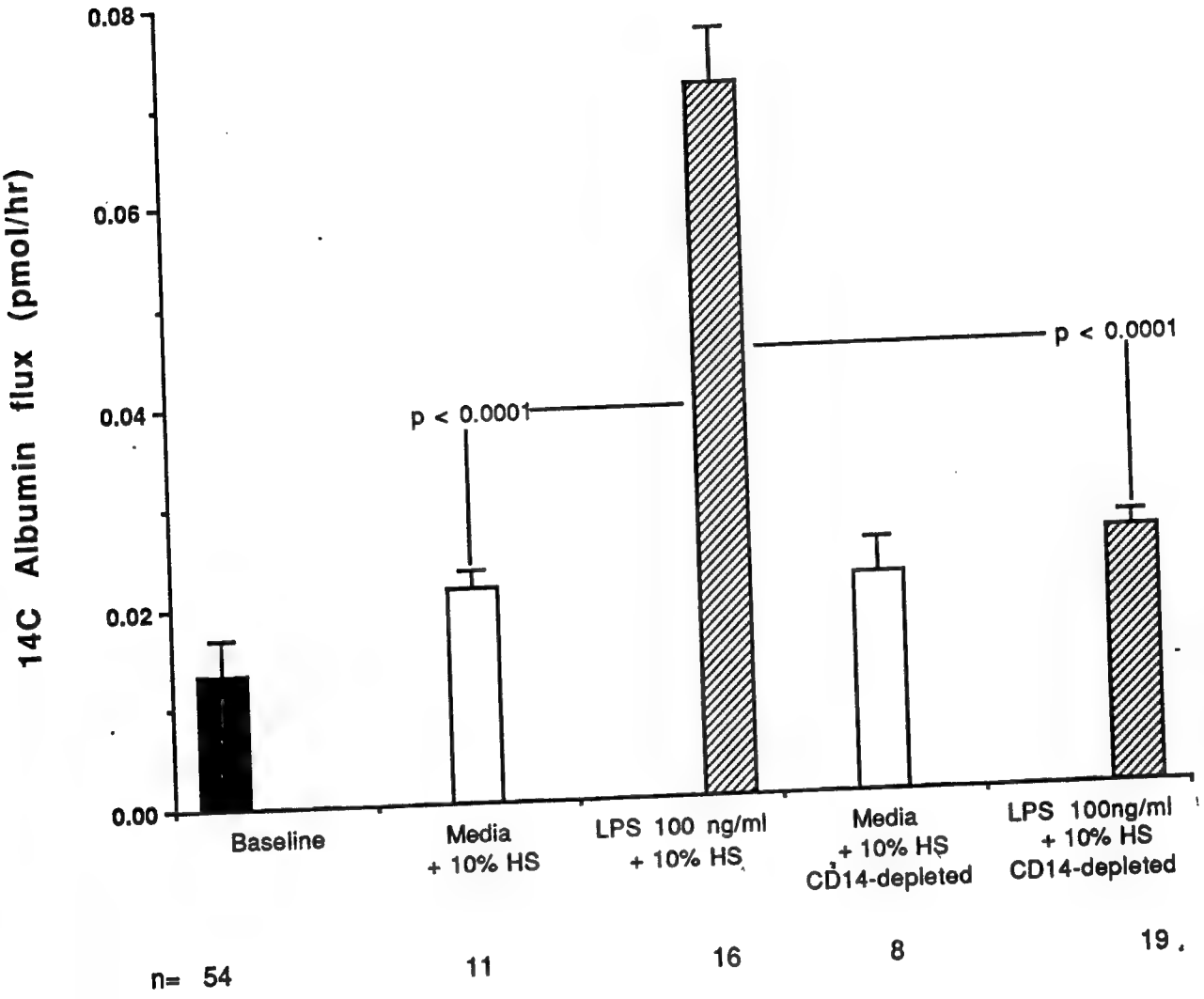
14C Albumin flux (pmol/hr)
0.08
0.06
0.04
0.02
0.00
p < 0.0001
p < 0.0001
Baseline
Media + 10% HS
LPS 100 ng/ml + 10% HS
Media + 10% HS CD14-depleted
LPS 100ng/ml + 10% HS CD14-depleted
n= 54
11
16
8
19

Figure 35

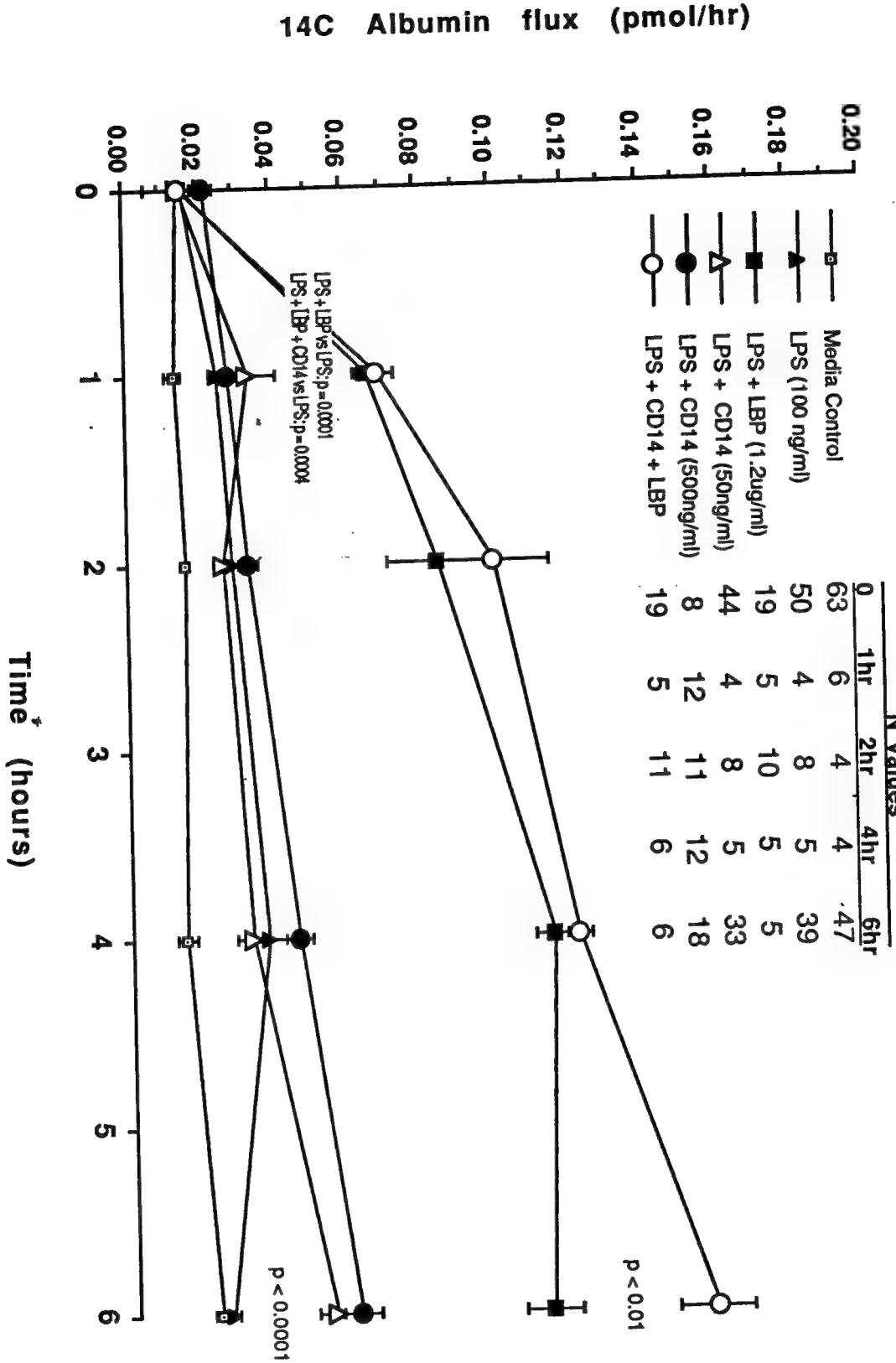
14C Albumin flux (pmol/hr)
0.20
0.18
0.16
0.14
0.12
0.10
0.08
0.06
0.04
0.02
0.00
0
1
2
3
4
5
6
Time (hours)
Media Control
LPS (100 ng/ml)
LPS + LBP (1.2ug/ml)
LPS + CD14 (50ng/ml)
LPS + CD14 (500ng/ml)
LPS + CD14 + LBP
N Values
0 1hr 2hr 4hr 6hr
63 6 4 4 47
50 4 8 5 39
19 5 10 5 5
44 4 8 5 33
8 12 11 12 18
19 5 11 6 6
LPS+LBP vs LPS;p=0.0001
LPS+LBP+CD14 vs LPS;p=0.0004
p < 0.01
p < 0.0001

Figure 36

Figure 37

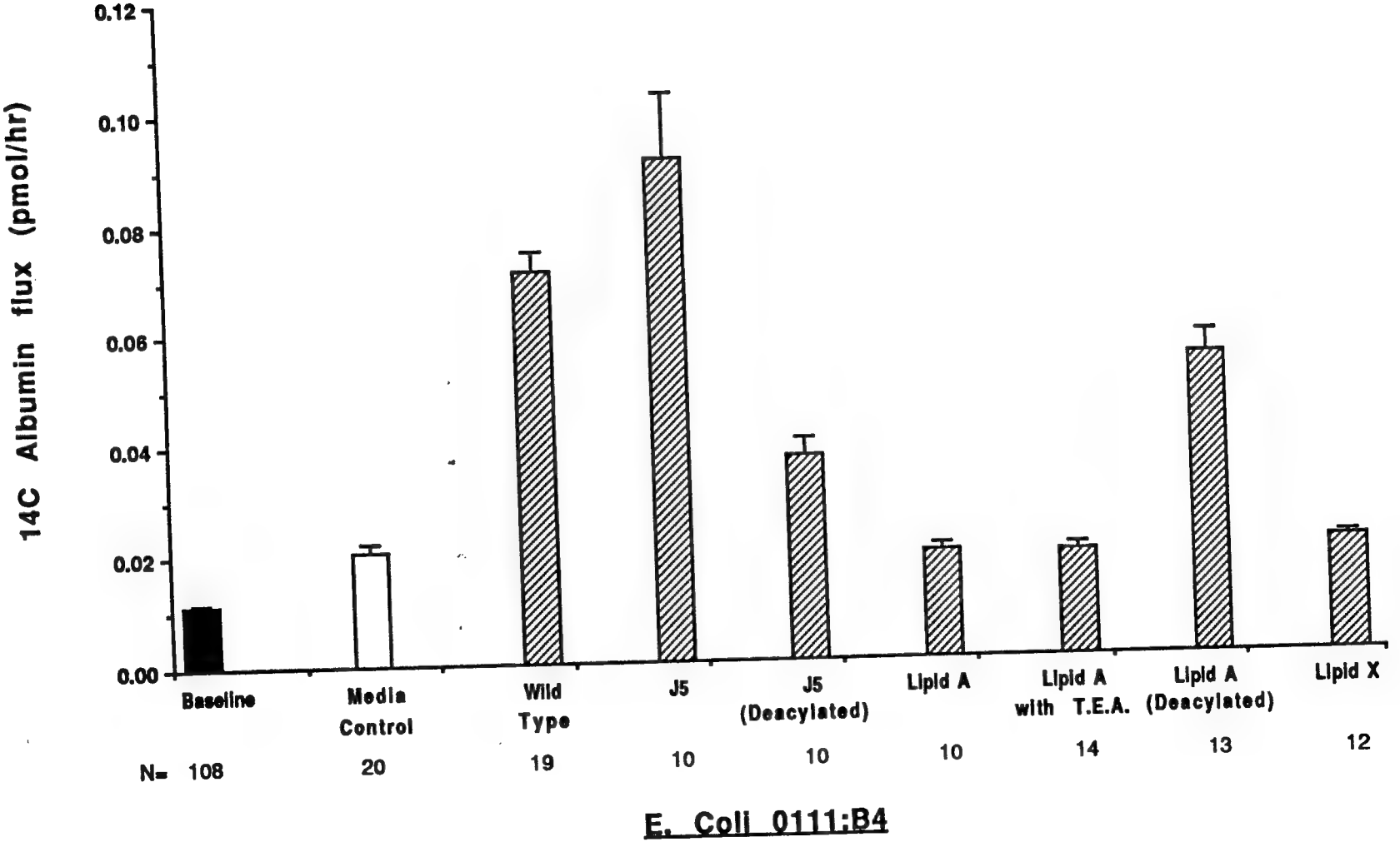
14C Albumin flux (pmol/hr)
0.12
0.10
0.08
0.06
0.04
0.02
0.00
Baseline
Media Control
Wild Type
J5
J5 (Deacylated)
Lipid A
Lipid A with T.E.A.
Lipid A (Deacylated)
Lipid X
N= 108
20
19
10
10
10
14
13
12
E. Coli 0111:B4

Figure 38

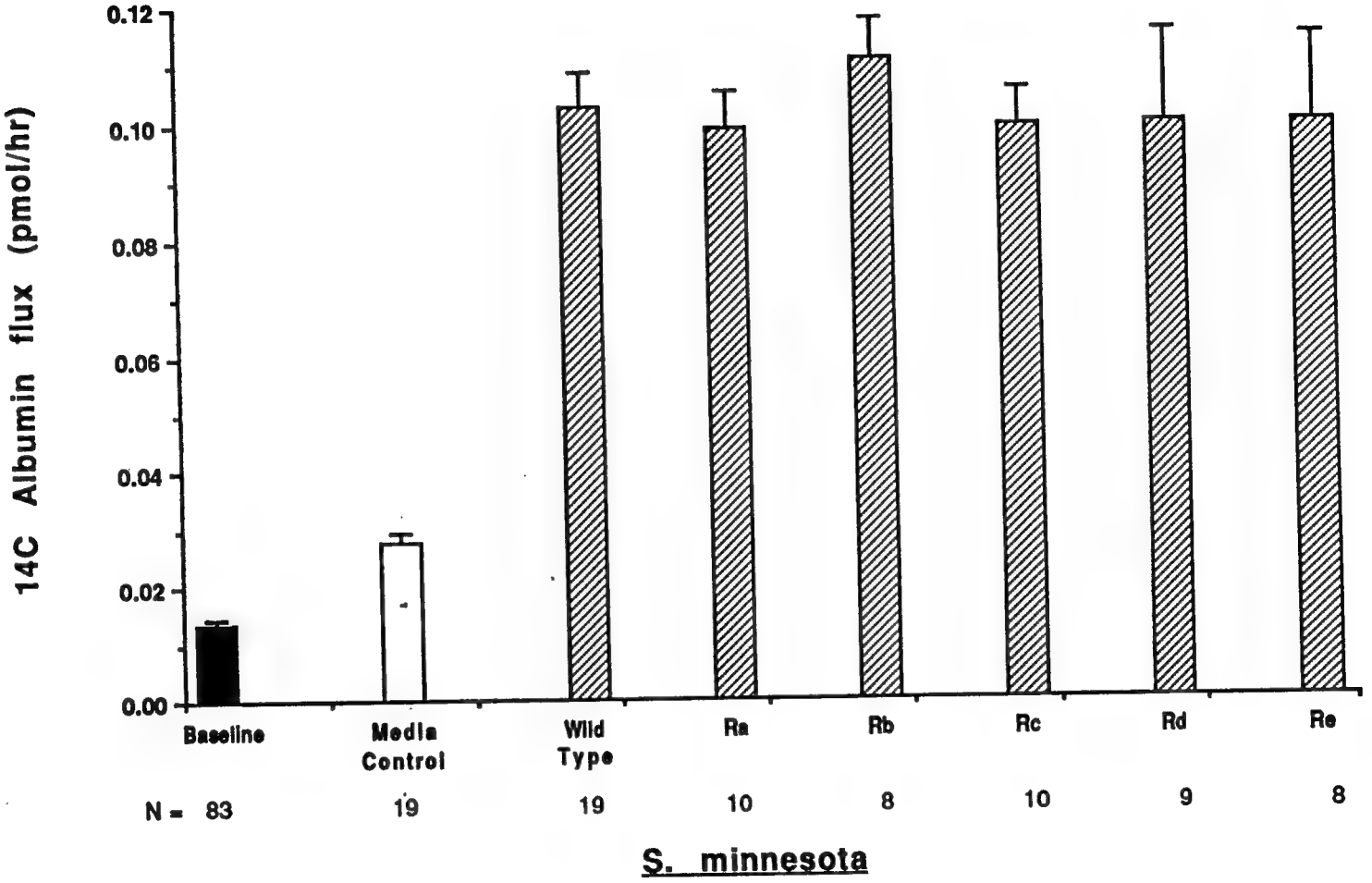
14C Albumin flux (pmol/hr)
0.12
0.10
0.08
0.06
0.04
0.02
0.00
Baseline
Media Control
Wild Type
Ra
Rb
Rc
Rd
Re
N = 83
19
19
10
8
10
9
8
S. minnesota

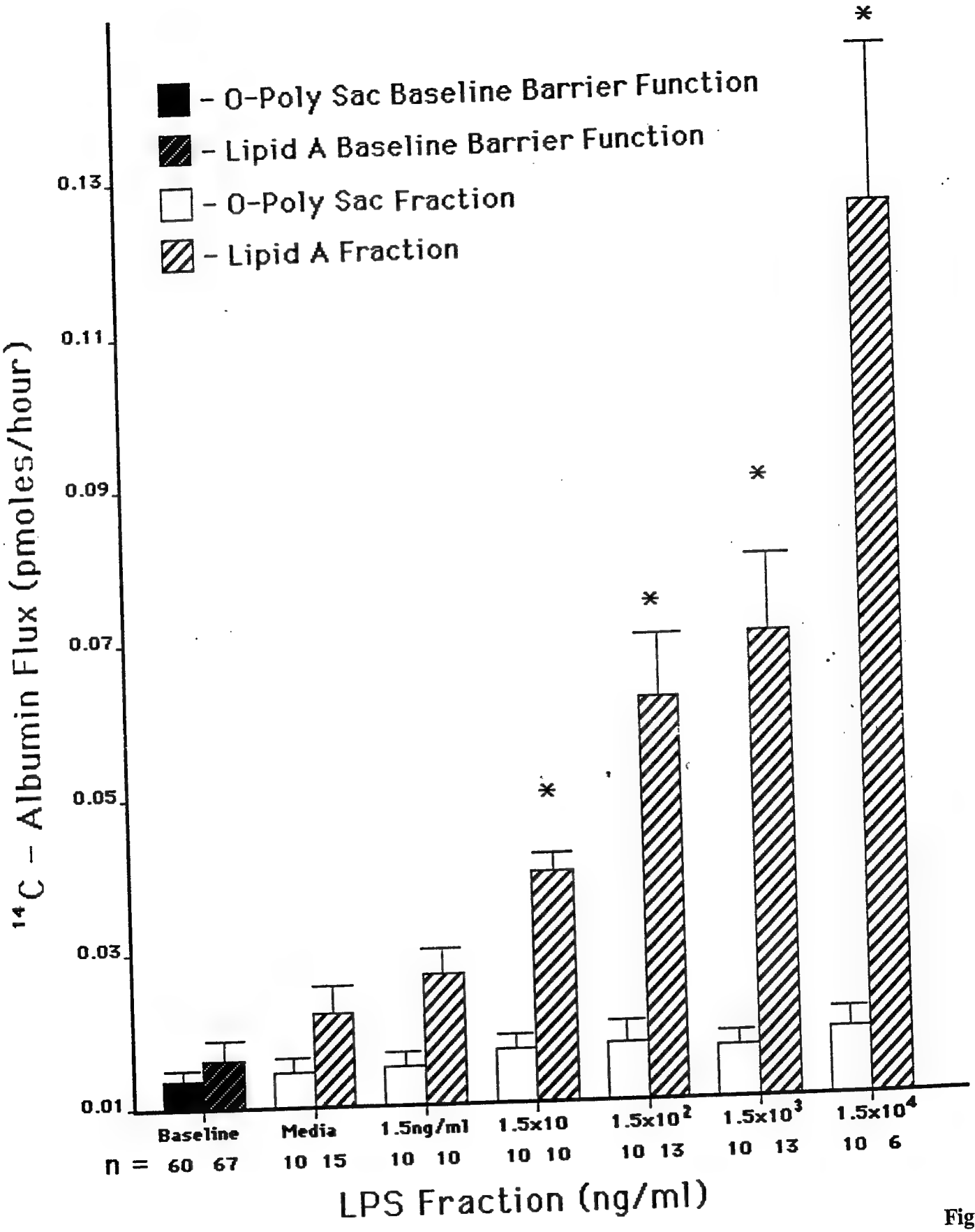
- O-Poly Sac Baseline Barrier Function
- Lipid A Baseline Barrier Function
- O-Poly Sac Fraction
- Lipid A Fraction
^{14}C - Albumin Flux (pmoles/hour)
0.13
0.11
0.09
0.07
0.05
0.03
0.01
*
Baseline
Media
1.5ng/ml
1.5x10
1.5x10^2
1.5x10^3
1.5x10^4
n = 60 67 10 15 10 10 10 10 10 13 10 13 10 6
LPS Fraction (ng/ml)

Figure 39

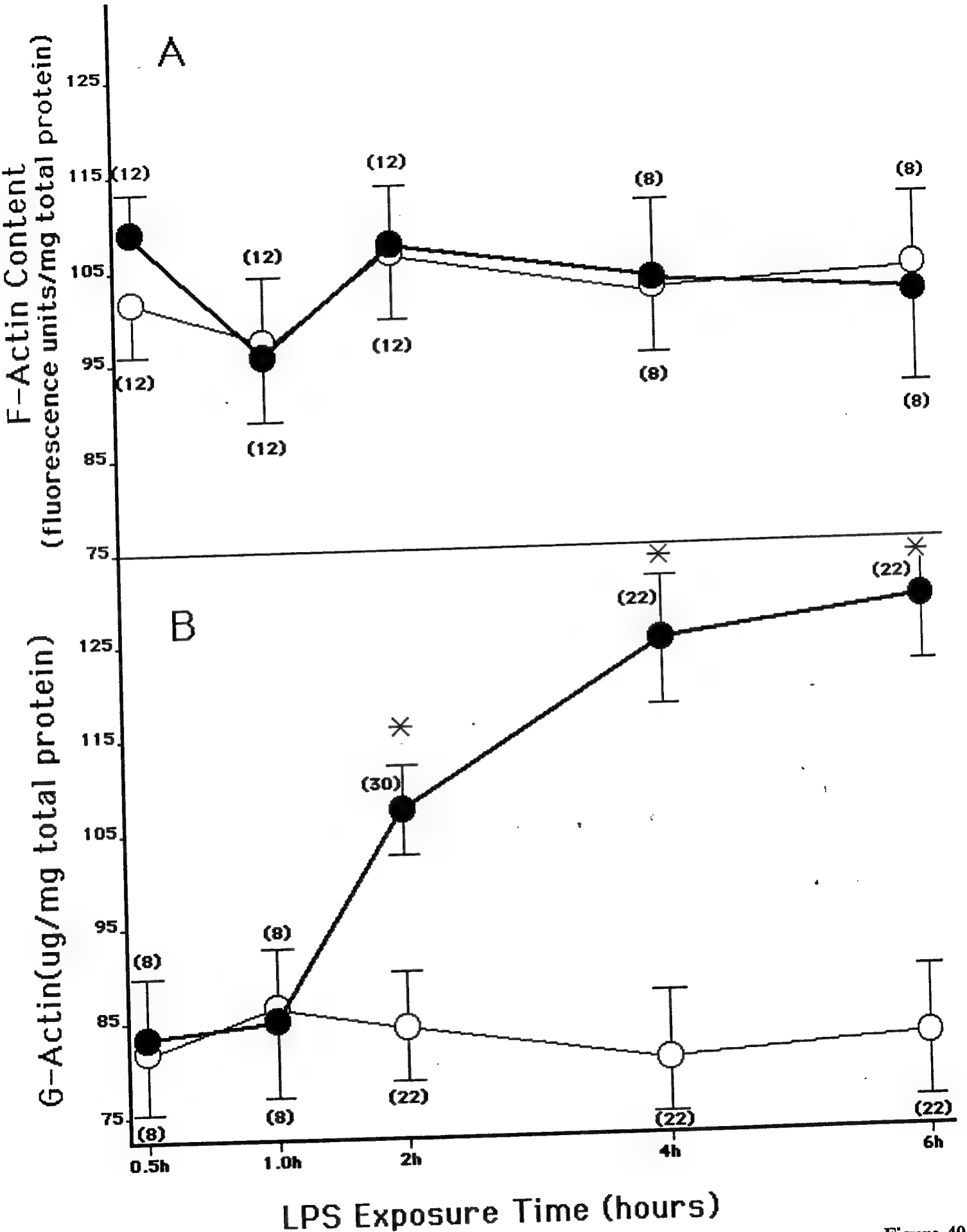
A
F-Actin Content
(fluorescence units/mg total protein)
125
115
105
95
85
75
(12)
(12)
(12)
(12)
(12)
(12)
(8)
(8)
(8)
B
G-Actin(ug/mg total protein)
125
115
105
95
85
75
(8)
(8)
(8)
(30)
(22)
(22)
(22)
(22)
(22)
0.5h
1.0h
2h
4h
6h
LPS Exposure Time (hours)

Figure 40

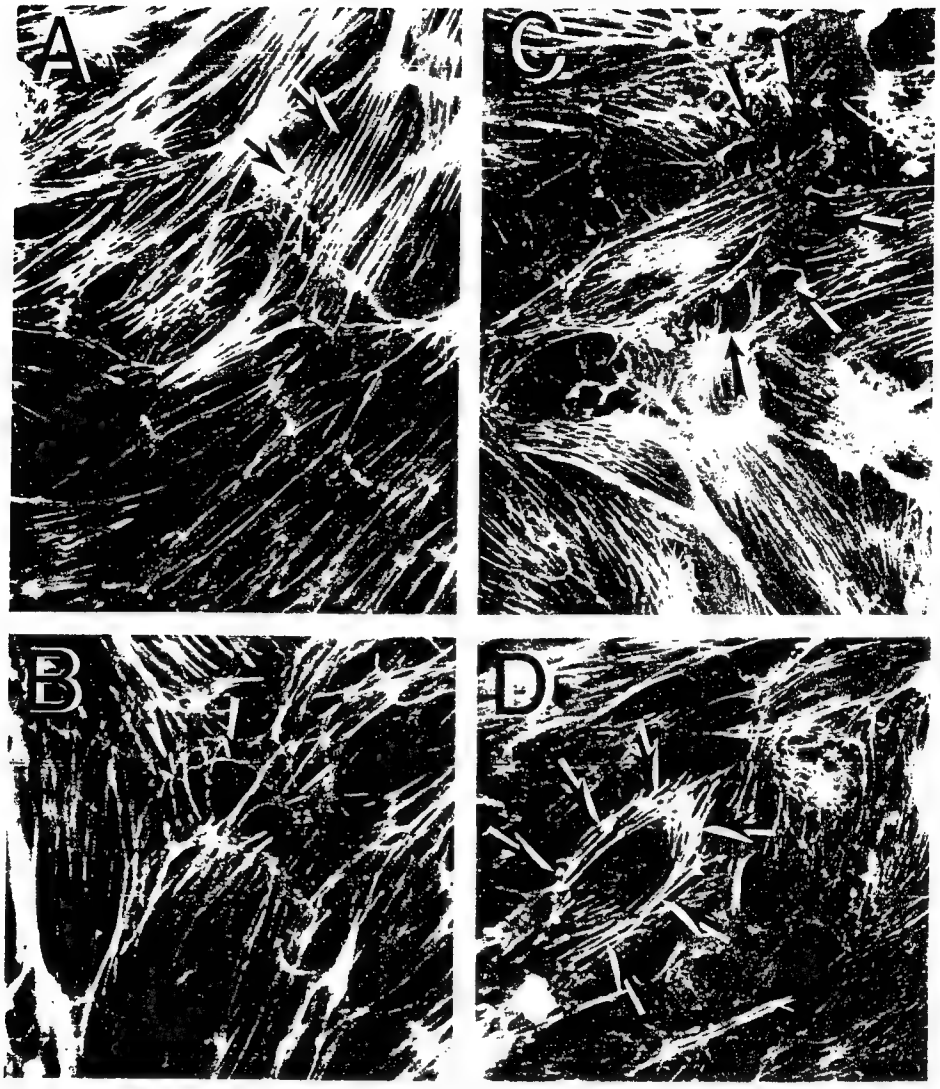

Fig. 2. Fluorescein-phalloidin staining of LPS-exposed endothelial monolayers. Endothelial monolayers grown on filters were exposed to media or LPS (10 ng ml) for increasing exposure times. The monolayers were fixed, permeabilized, stained with fluorescein-phalloidin, and examined by epifluorescence microscopy. **A:** Medium control; **B:** LPS, 2 h; **C, D:** LPS, 6 h. Arrows in A point to cycloplasmic actin filaments, arrows in B and C point to intercellular gaps, and arrows in D point to peripheral actin bands. ×400.

Figure 41

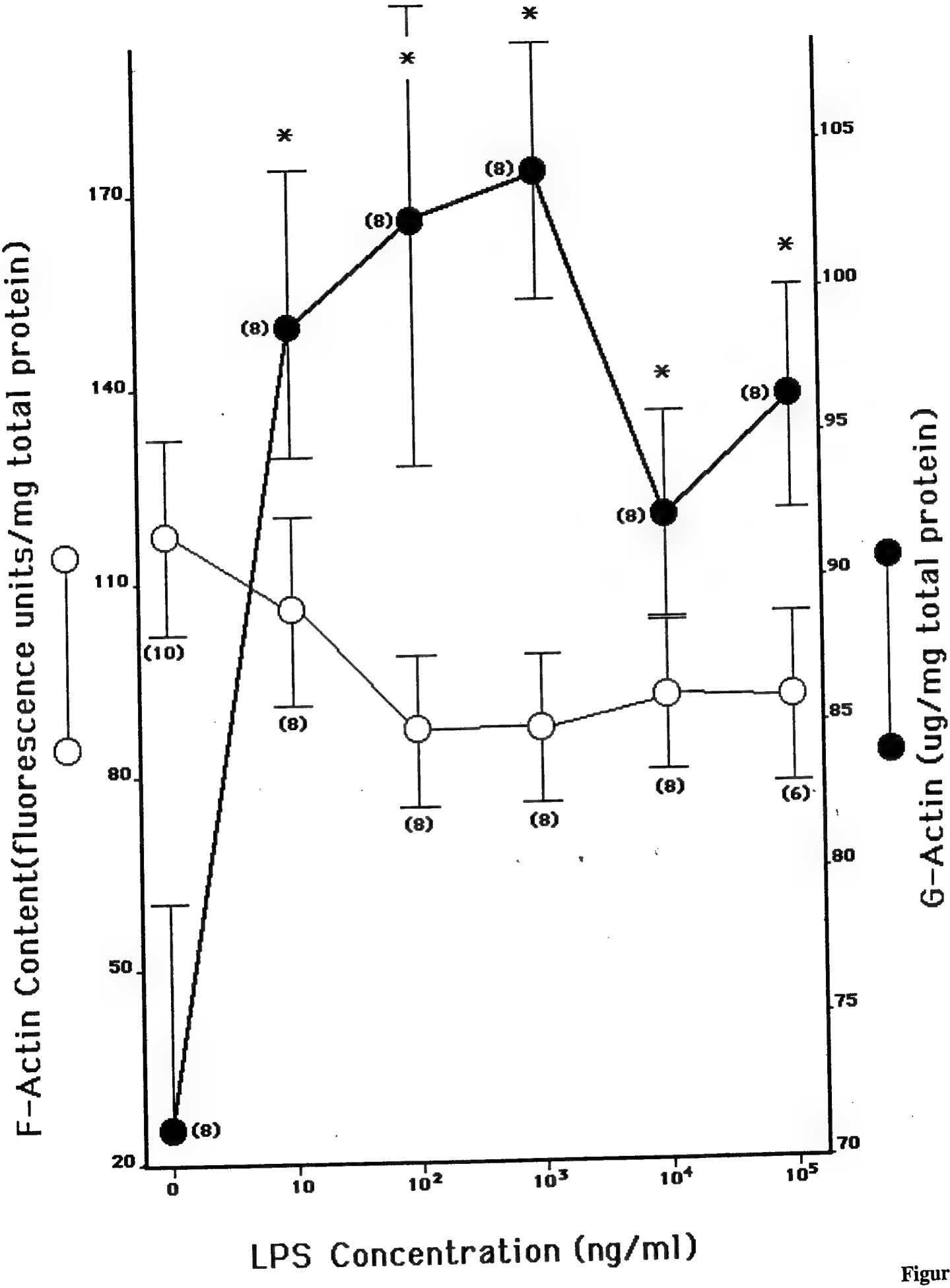
F-Actin Content(fluorescence units/mg total protein)
G-Actin (ug/mg total protein)
LPS Concentration (ng/ml)
170
140
110
80
50
20
105
100
95
90
85
80
75
70
0
10
10²
10³
10⁴
10⁵
(8)
(10)
(6)
*

Figure 42

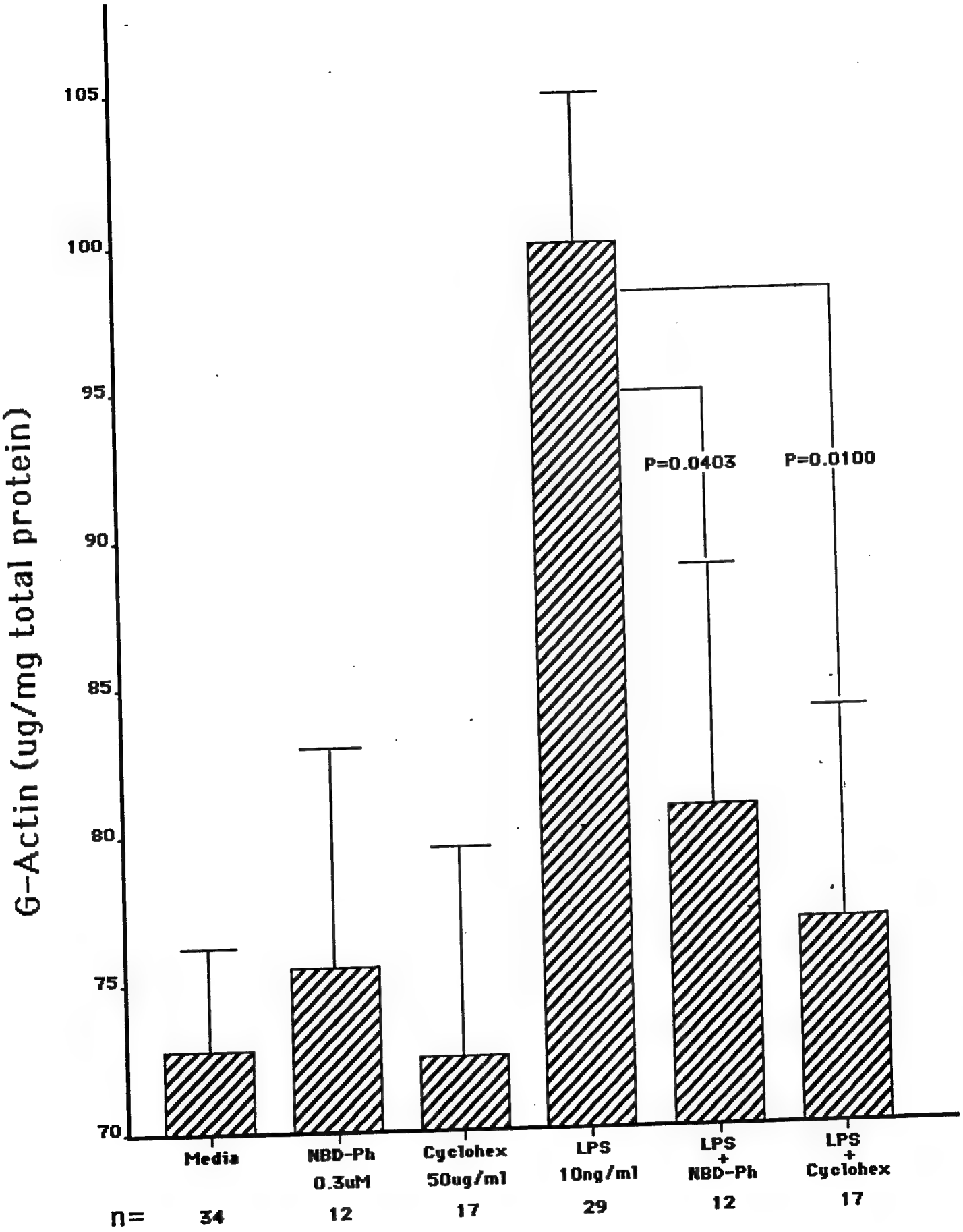
G-Actin (ug/mg total protein)
105
100
95
90
85
80
75
70
P=0.0403
P=0.0100
Media
NBD-Ph 0.3uM
Cyclohex 50ug/ml
LPS 10ng/ml
LPS + NBD-Ph
LPS + Cyclohex
n=
34
12
17
29
12
17

Figure 43

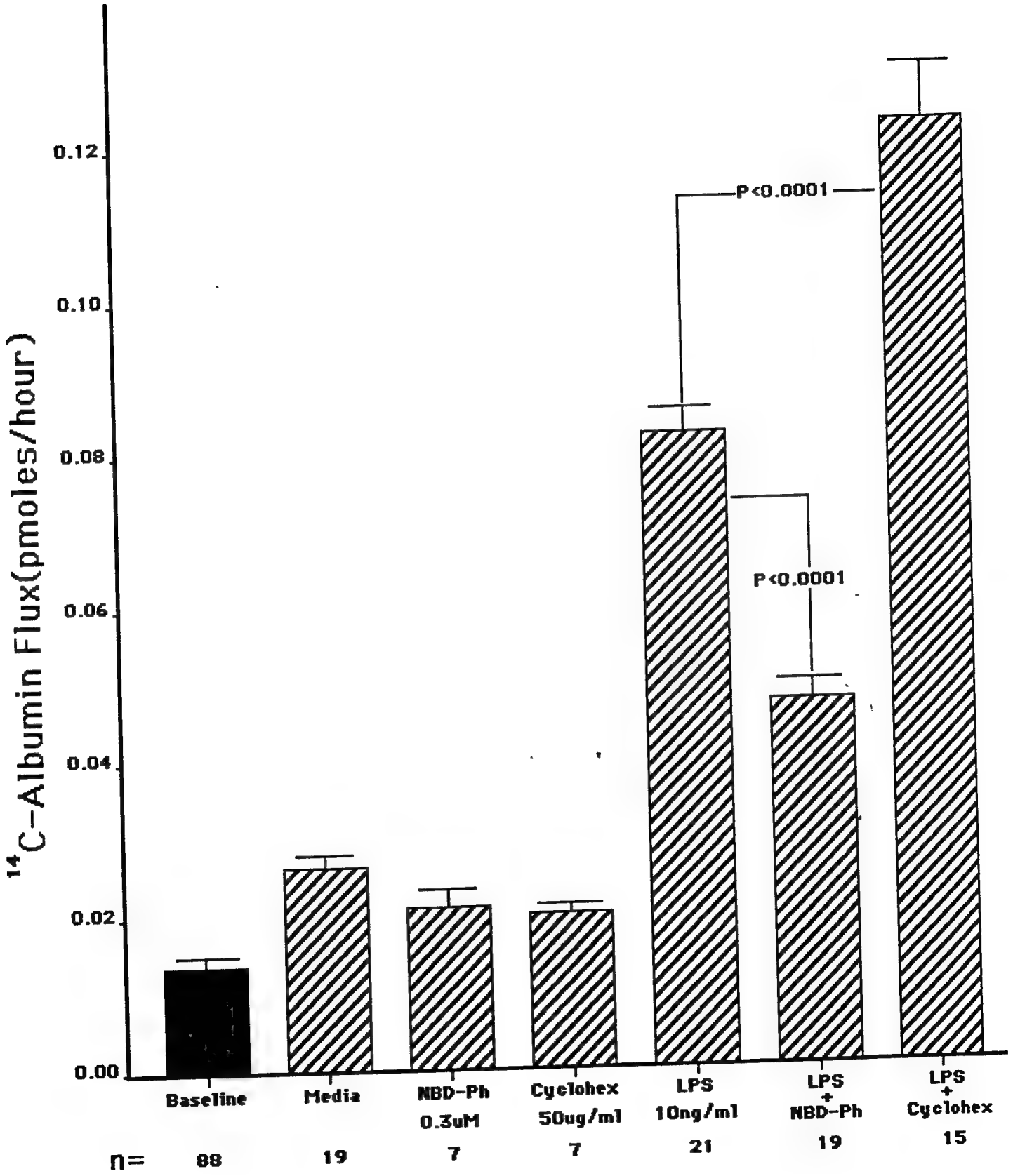
^{14}C-Albumin Flux(pmoles/hour)
0.12
0.10
0.08
0.06
0.04
0.02
0.00
P<0.0001
P<0.0001
Baseline
Media
NBD-Ph 0.3uM
Cyclohex 50ug/ml
LPS 10ng/ml
LPS + NBD-Ph
LPS + Cyclohex
n= 88 19 7 7 21 19 15

Figure 44

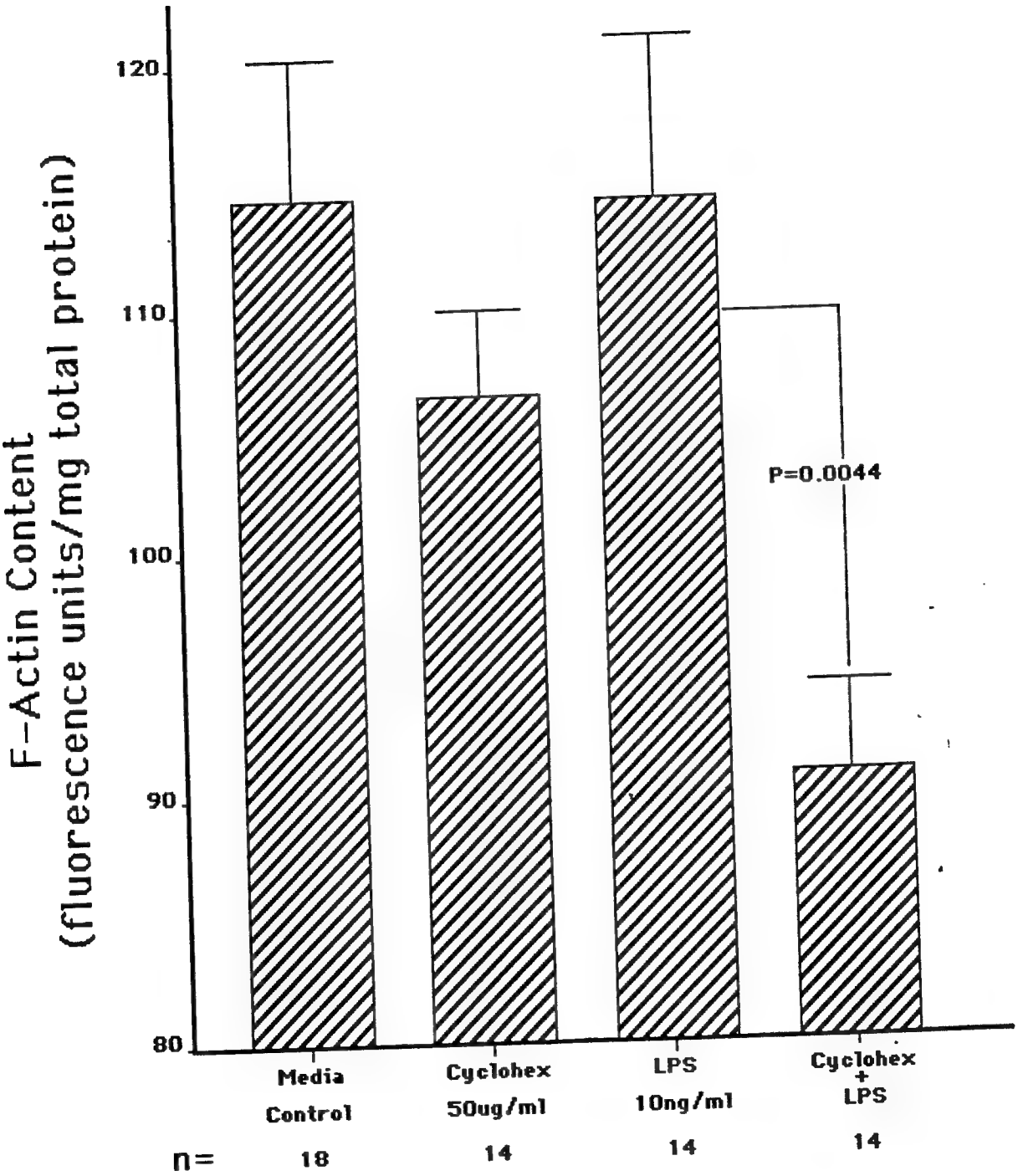
F-Actin Content
(fluorescence units/mg total protein)
120
110
100
90
80
P=0.0044
Media
Control
Cyclohex
50ug/ml
LPS
10ng/ml
Cyclohex
+
LPS
n=
18
14
14
14

Figure 45

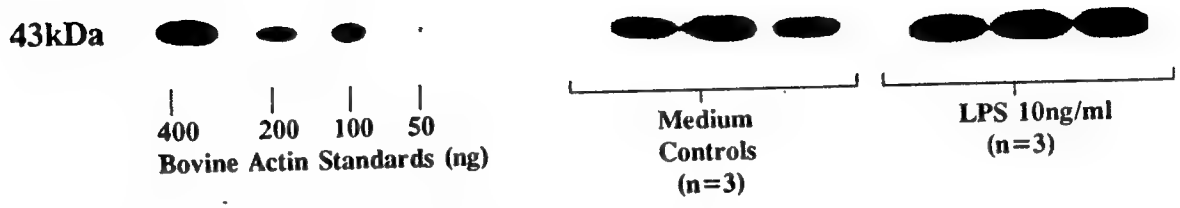

Fig. 7. Quantitative immunoblotting for total endothelial cell actin. Endothelial extracts obtained from LPS-exposed and medium control monolayers were electrophoresed on SDS polyacrylamide gels, transferred onto nitrocellulose, incubated with murine anti-avian actin IgG_1 followed by protein G-HRP conjugate with enhanced chemiluminescence substrates, and exposed to film. A simultaneous standard curve with known concentrations of bovine skeletal muscle actin were run on each gel. Autoradiographs were scanned by laser densitometry and actin quantified by interpolation from the actin standard curve.

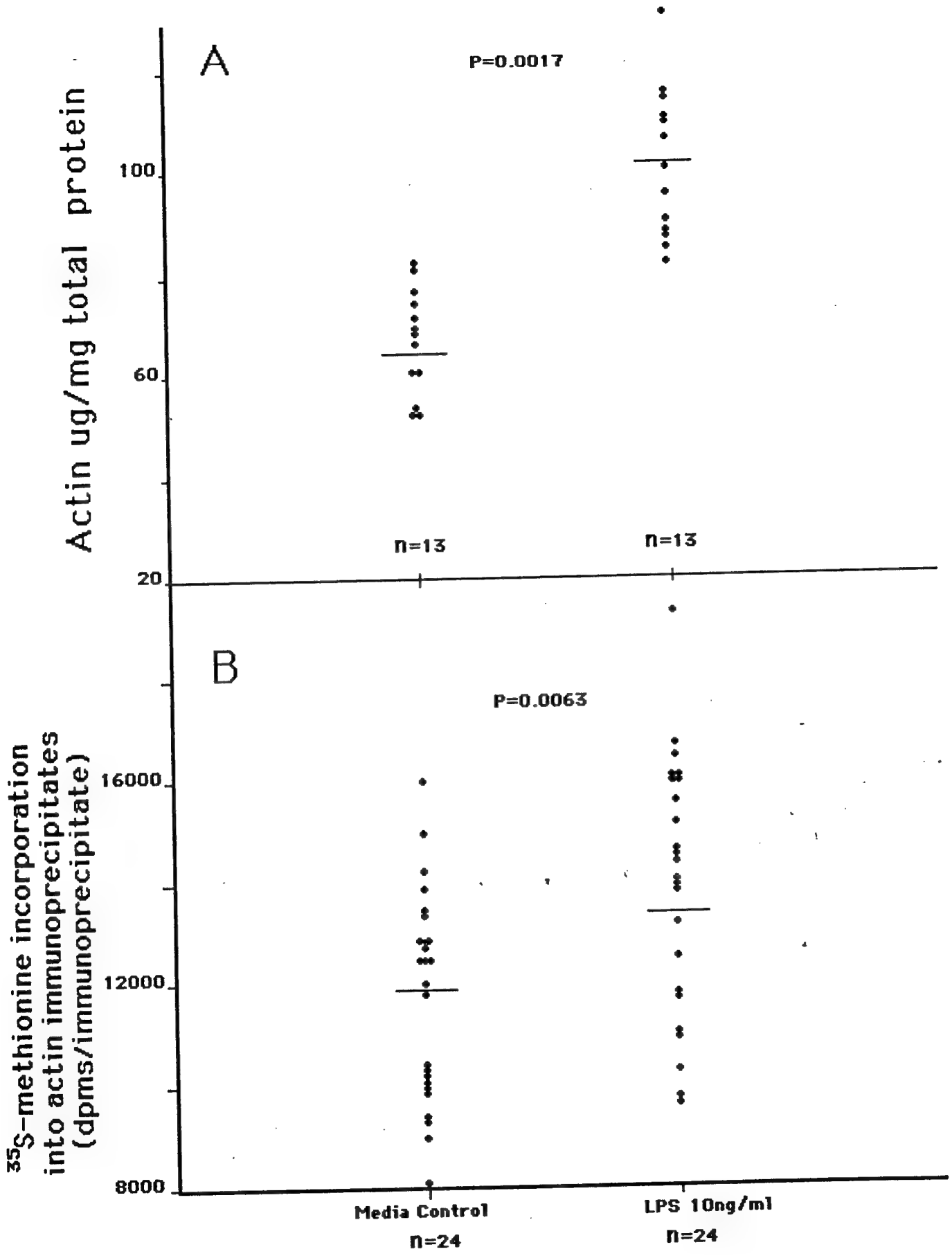
A
P=0.0017
Actin ug/mg total protein
100
60
20
n=13
n=13
B
P=0.0063
^{35}S-methionine incorporation into actin immunoprecipitates (dpms/immunoprecipitate)
16000
12000
8000
Media Control
n=24
LPS 10ng/ml
n=24

Figure 47

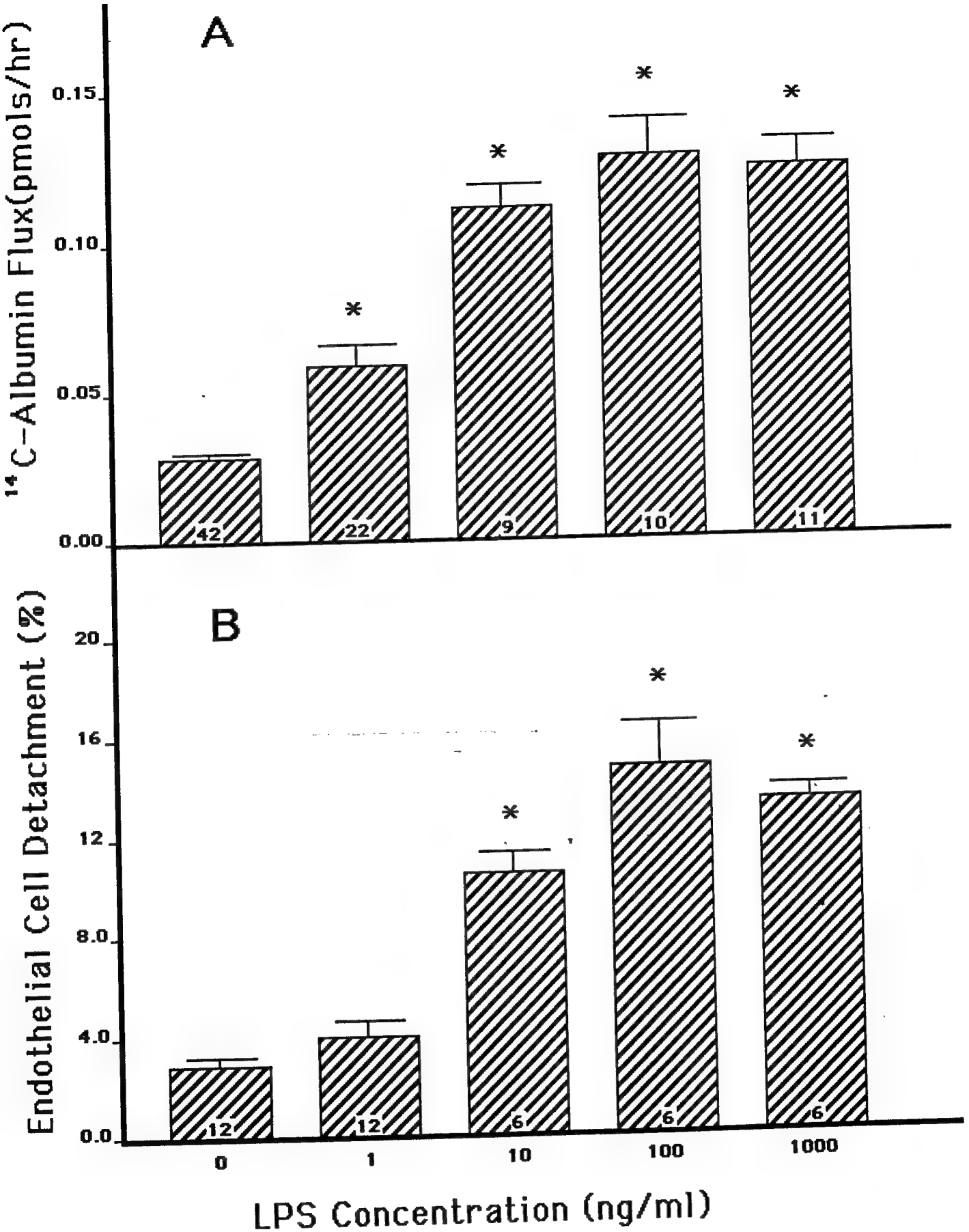
A
^{14}C-Albumin Flux(pmols/hr)
0.15
0.10
0.05
0.00
42
22
9
10
11
B
Endothelial Cell Detachment (%)
20
16
12
8.0
4.0
0.0
12
12
6
6
6
0
1
10
100
1000
LPS Concentration (ng/ml)

Figure 48

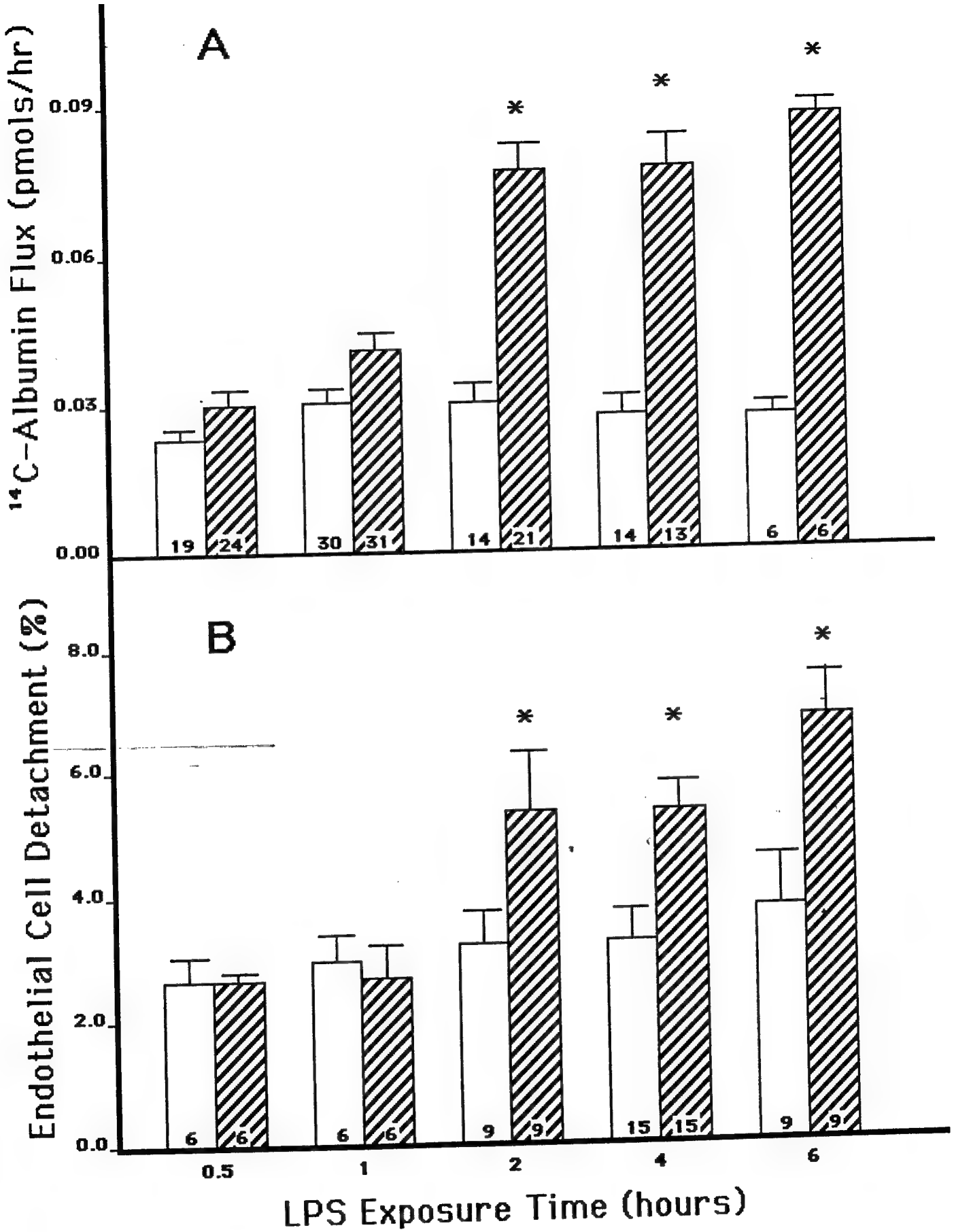
A
B
^{14}C-Albumin Flux (pmols/hr)
0.09
0.06
0.03
0.00
19
24
30
31
14
21
14
13
6
6
*
Endothelial Cell Detachment (%)
8.0
6.0
4.0
2.0
0.0
6
6
6
6
9
9
15
15
9
9
0.5
1
2
4
6
LPS Exposure Time (hours)

Figure 49

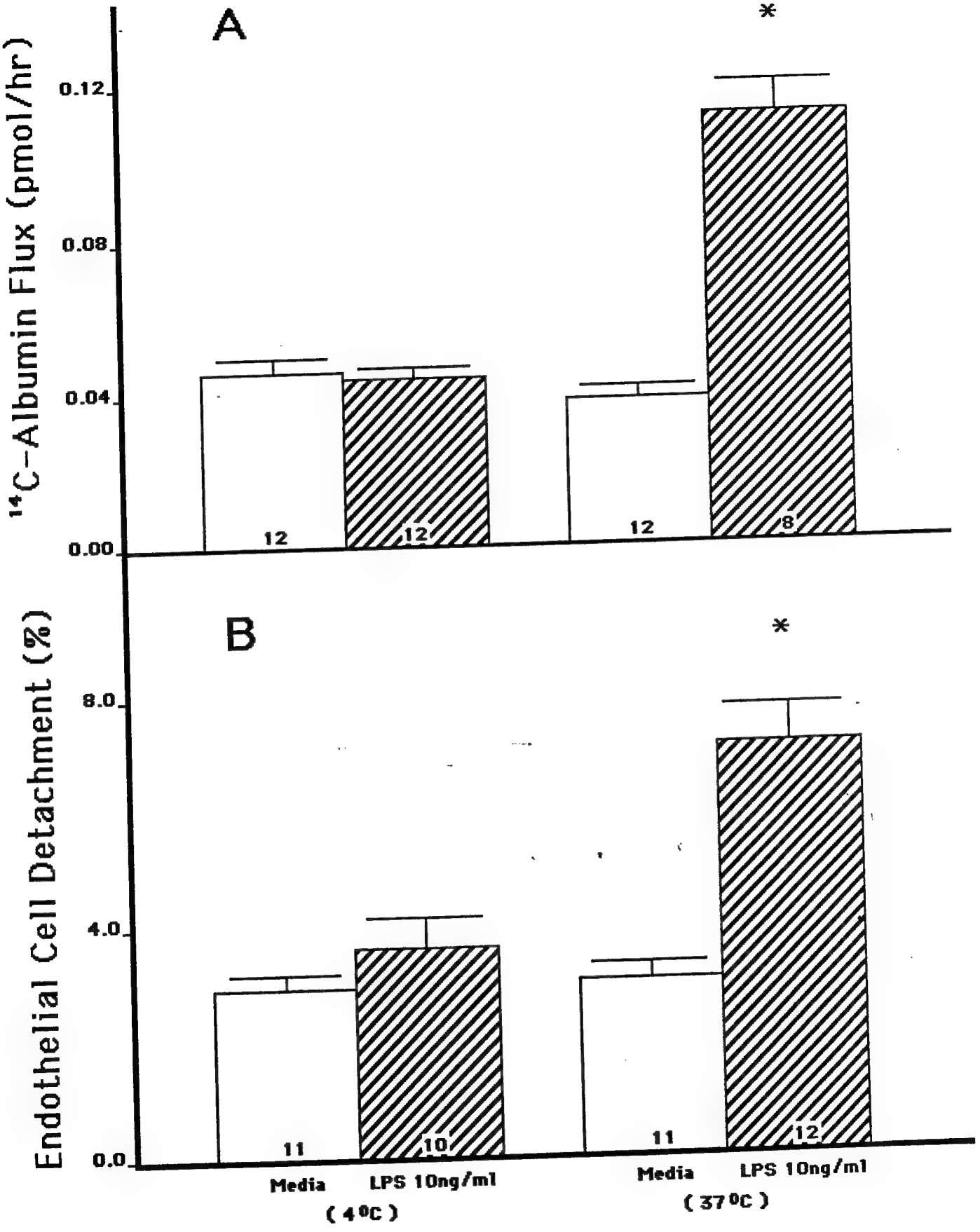
A
*
^{14}C-Albumin Flux (pmol/hr)
0.12
0.08
0.04
0.00
12
12
12
8
B
*
Endothelial Cell Detachment (%)
8.0
4.0
0.0
11
10
11
12
Media
LPS 10ng/ml
Media
LPS 10ng/ml
(4 °C)
(37 °C)

Figure 50

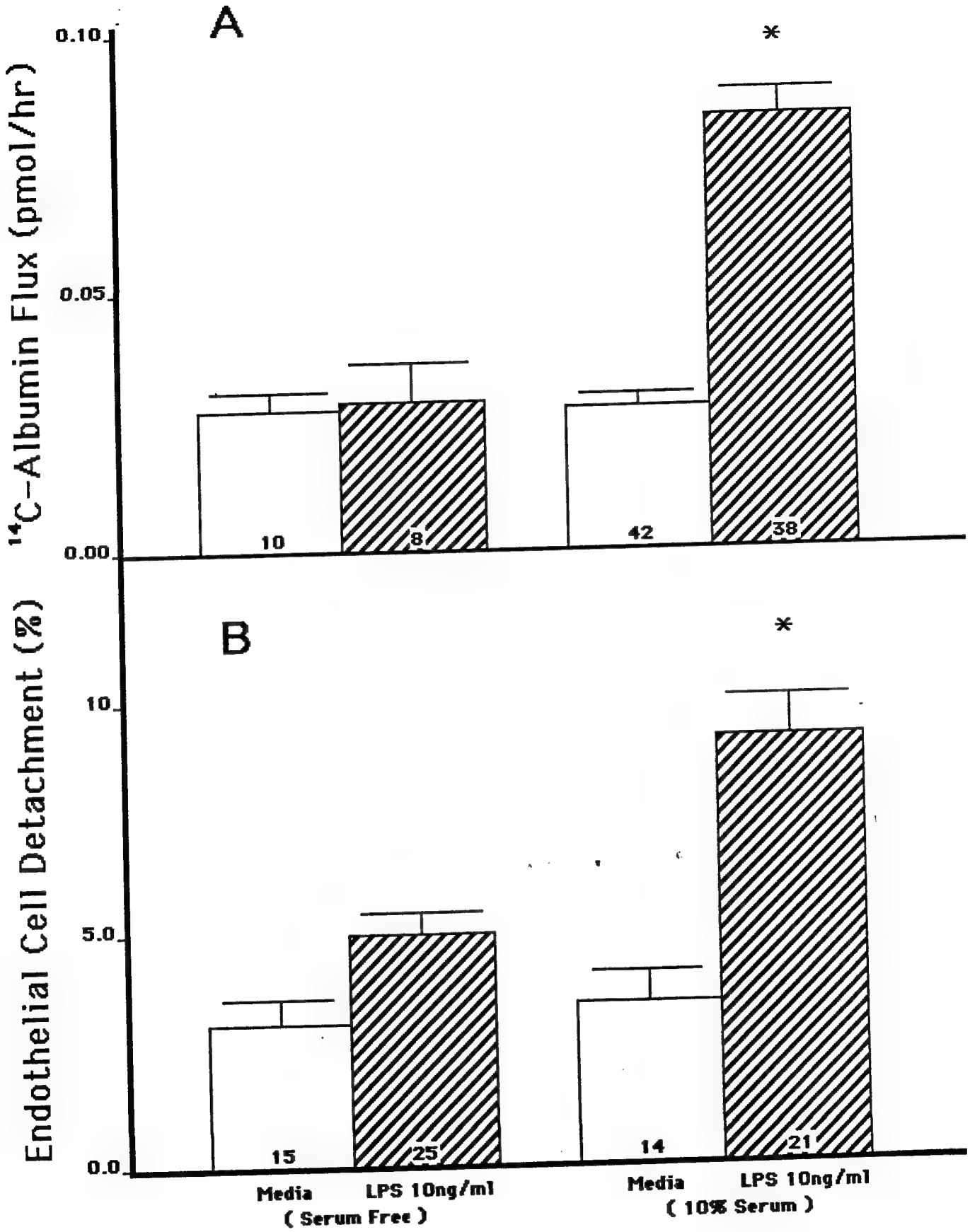
A
B
*
*
^{14}C-Albumin Flux (pmol/hr)
Endothelial Cell Detachment (%)
0.10
0.05
0.00
10
5.0
0.0
10
8
42
38
15
25
14
21
Media
LPS 10ng/ml
(Serum Free)
Media
LPS 10ng/ml
(10% Serum)

Figure 51

Figure 52

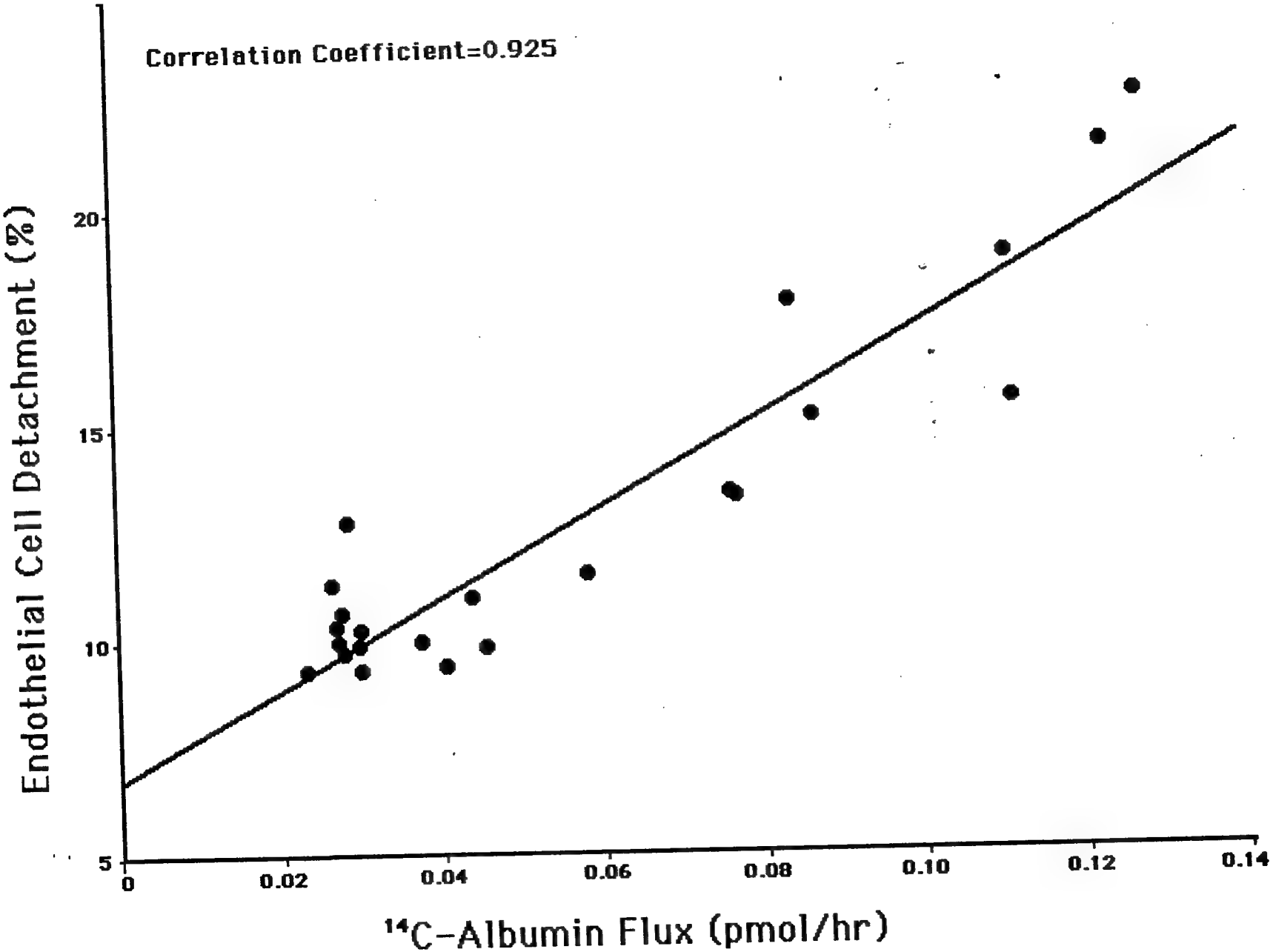
Correlation Coefficient=0.925
Endothelial Cell Detachment (%)
20
15
10
5
0
0.02
0.04
0.06
0.08
0.10
0.12
0.14
14C-Albumin Flux (pmol/hr)

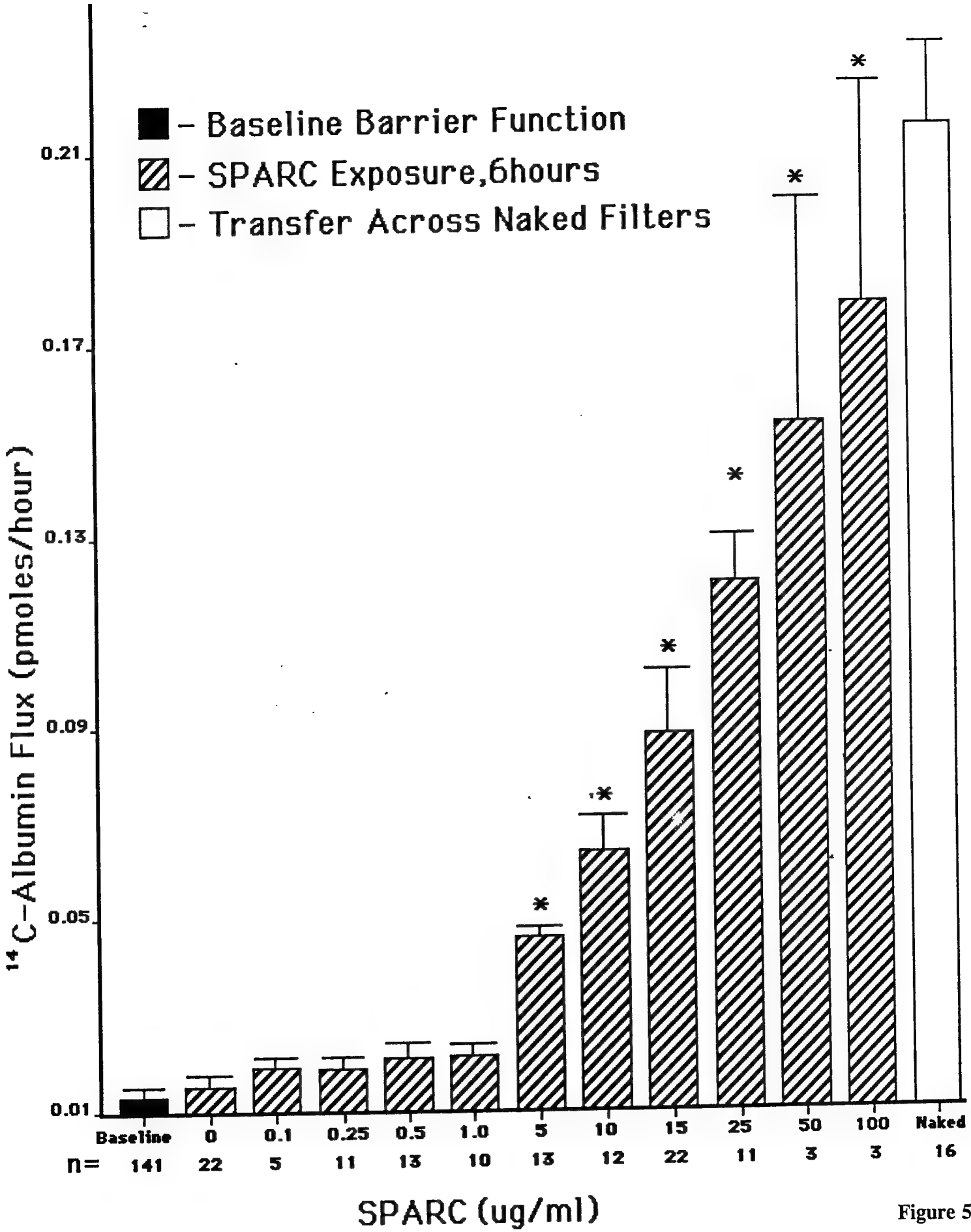
■ – Baseline Barrier Function
▨ – SPARC Exposure,6hours
□ – Transfer Across Naked Filters
^{14}C-Albumin Flux (pmoles/hour)
0.21
0.17
0.13
0.09
0.05
0.01
*
Baseline 0 0.1 0.25 0.5 1.0 5 10 15 25 50 100 Naked
n= 141 22 5 11 13 10 13 12 22 11 3 3 16
SPARC (ug/ml)

Figure 53

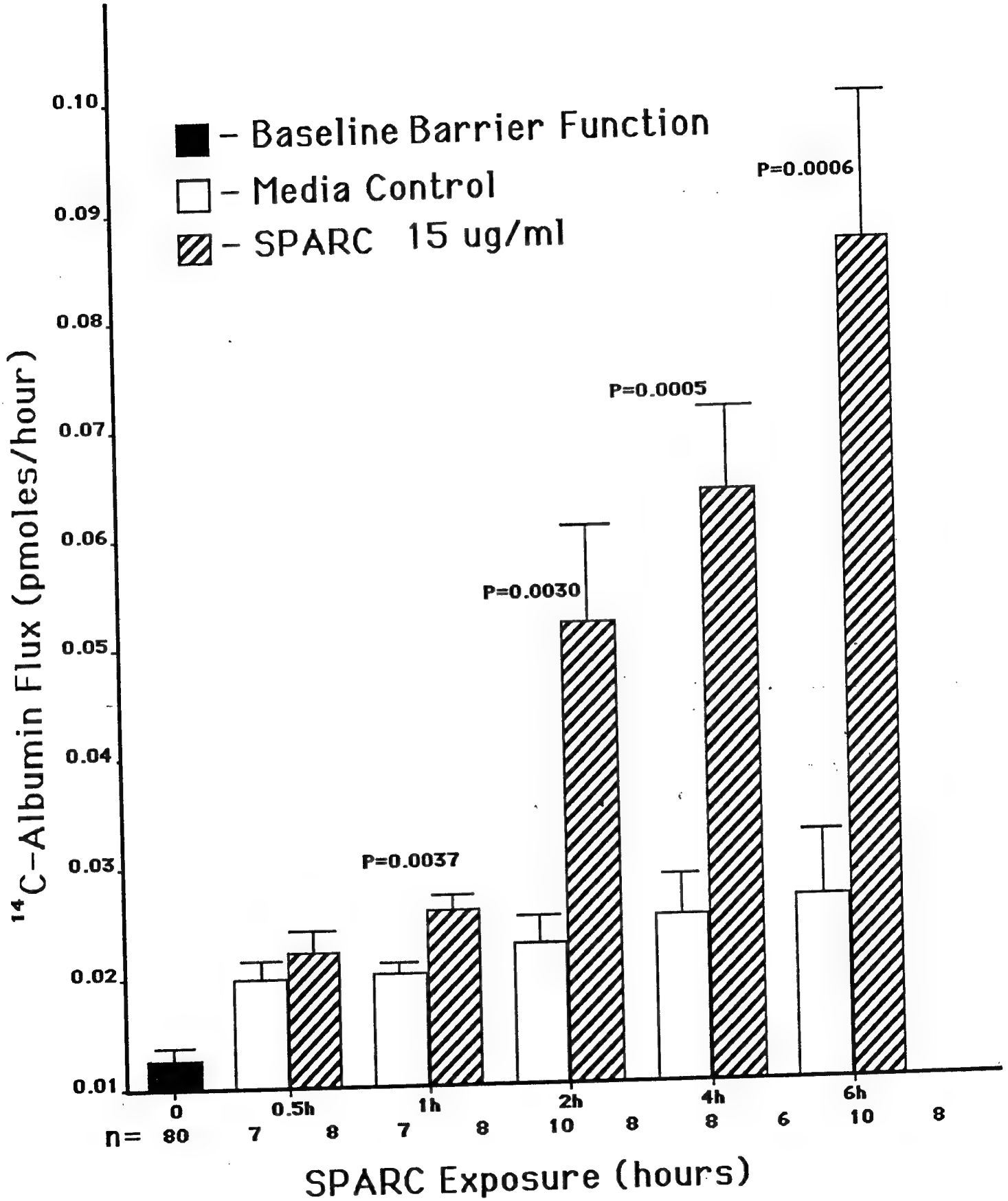
■ – Baseline Barrier Function
□ – Media Control
▨ – SPARC 15 ug/ml
P=0.0037
P=0.0030
P=0.0005
P=0.0006
^{14}C–Albumin Flux (pmoles/hour)
0.10
0.09
0.08
0.07
0.06
0.05
0.04
0.03
0.02
0.01
0 0.5h 1h 2h 4h 6h
n= 80 7 8 7 8 10 8 8 6 10 8
SPARC Exposure (hours)

Figure 54

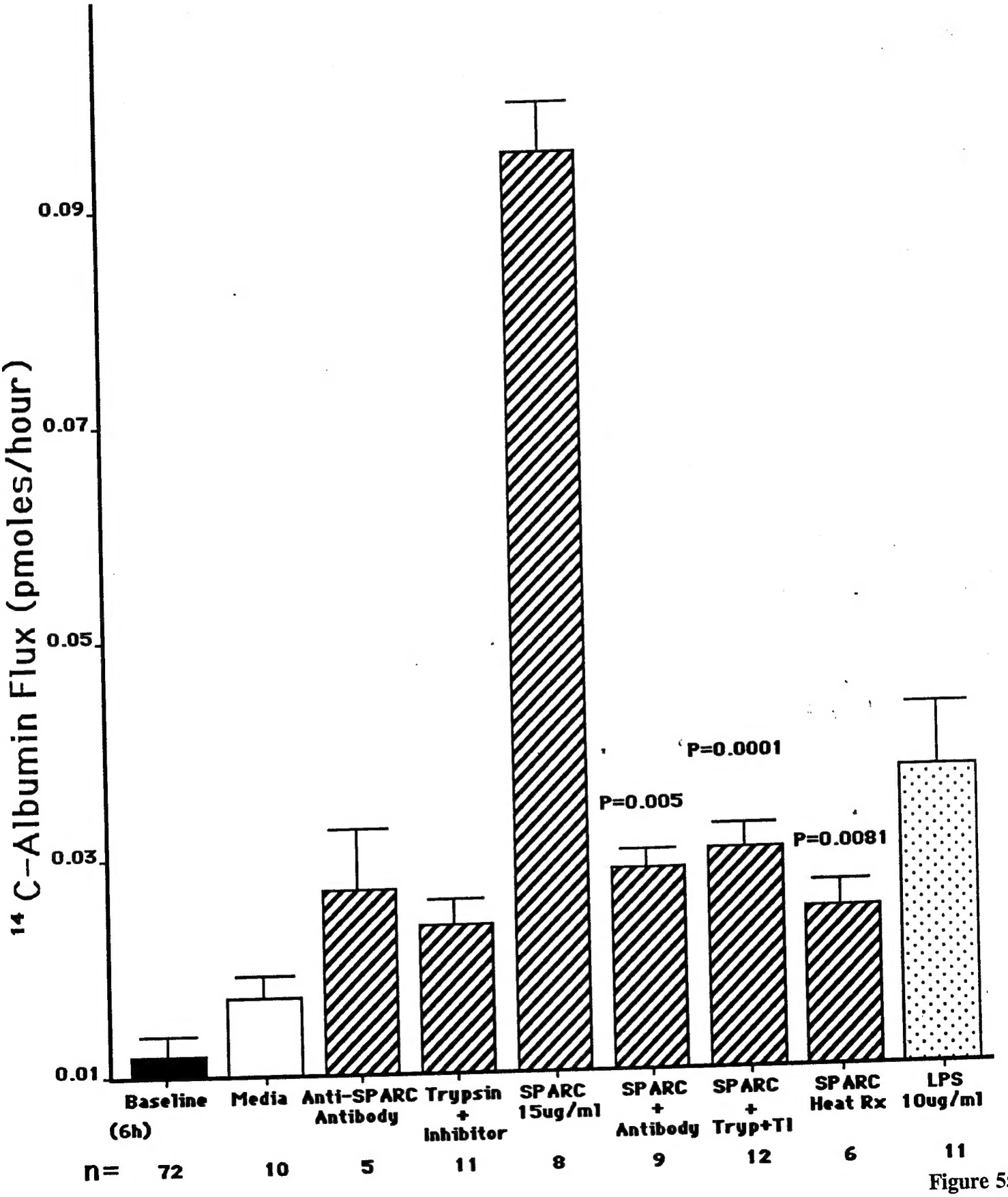
^{14}C-Albumin Flux (pmoles/hour)
0.09
0.07
0.05
0.03
0.01
P=0.005
P=0.0001
P=0.0081
Baseline (6h)
Media
Anti-SPARC Antibody
Trypsin + Inhibitor
SPARC 15ug/ml
SPARC + Antibody
SPARC + Tryp+TI
SPARC Heat Rx
LPS 10ug/ml
n= 72 10 5 11 8 9 12 6 11

Figure 55

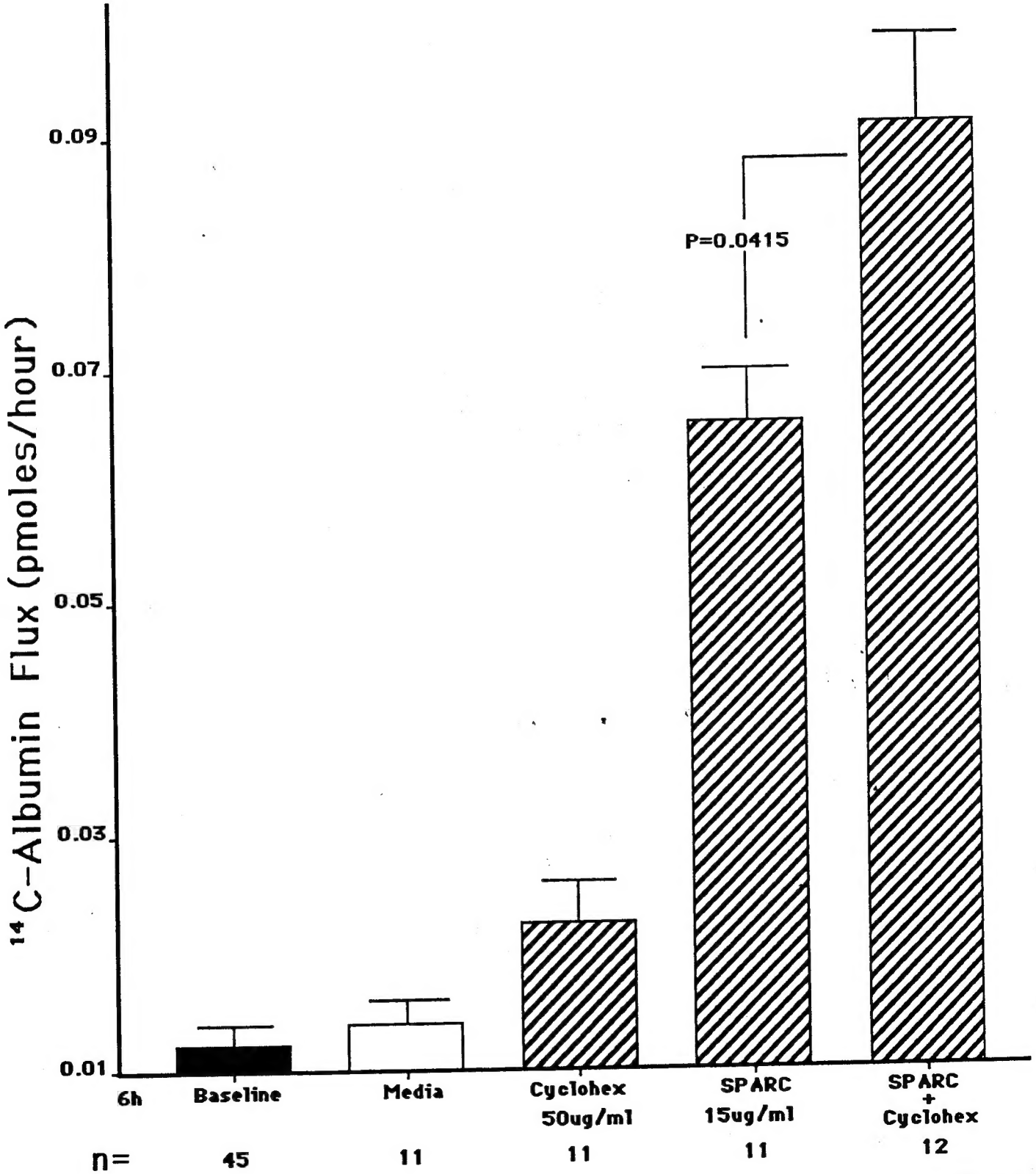
0.09
0.07
0.05
0.03
0.01
^{14}C-Albumin Flux (pmoles/hour)
P=0.0415
6h
Baseline
Media
Cyclohex 50ug/ml
SPARC 15ug/ml
SPARC + Cyclohex
n=
45
11
11
11
12

Figure 56

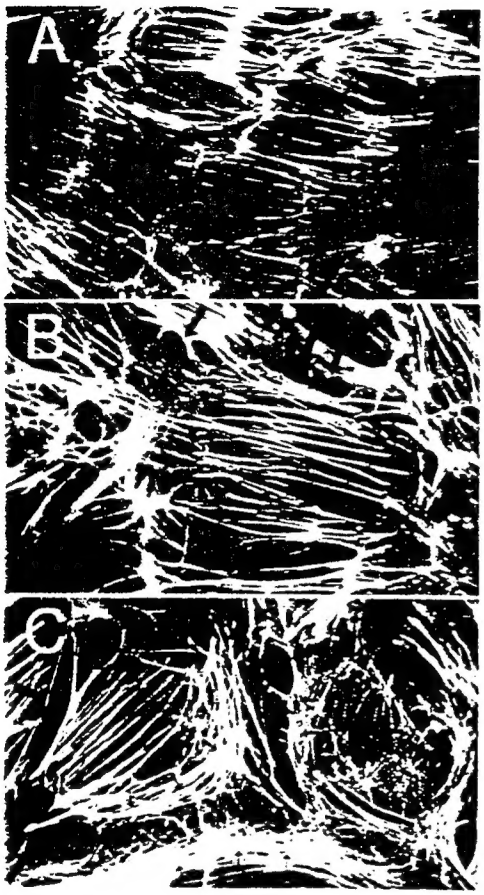
A
B
C

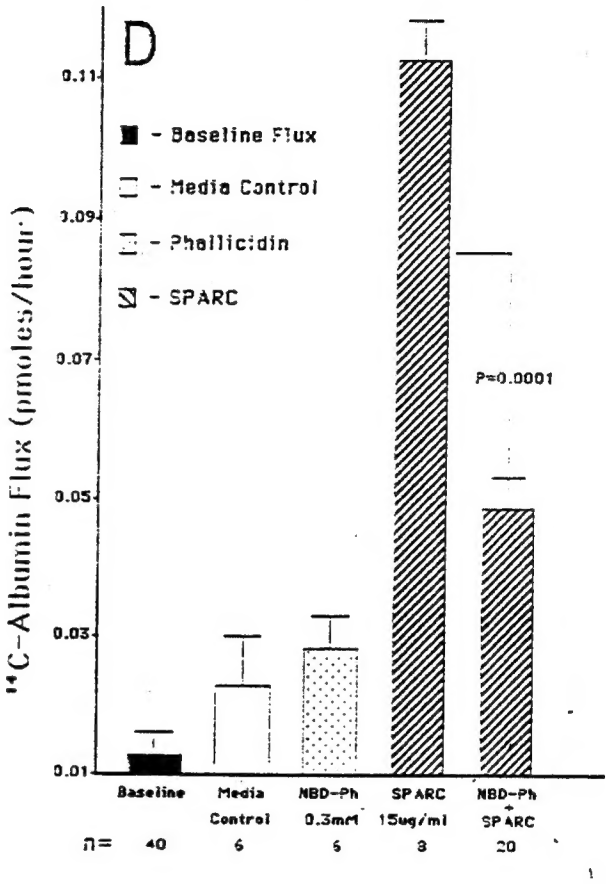
D
- Baseline Flux
- Media Control
- Phallicidin
- SPARC
P=0.0001
^{14}C-Albumin Flux (pmoles/hour)
0.11
0.09
0.07
0.05
0.03
0.01
Baseline
Media Control
NBD-Ph 0.3mM
SPARC 15ug/ml
NBD-Ph + SPARC
n= 40 6 6 8 20

Figure 57

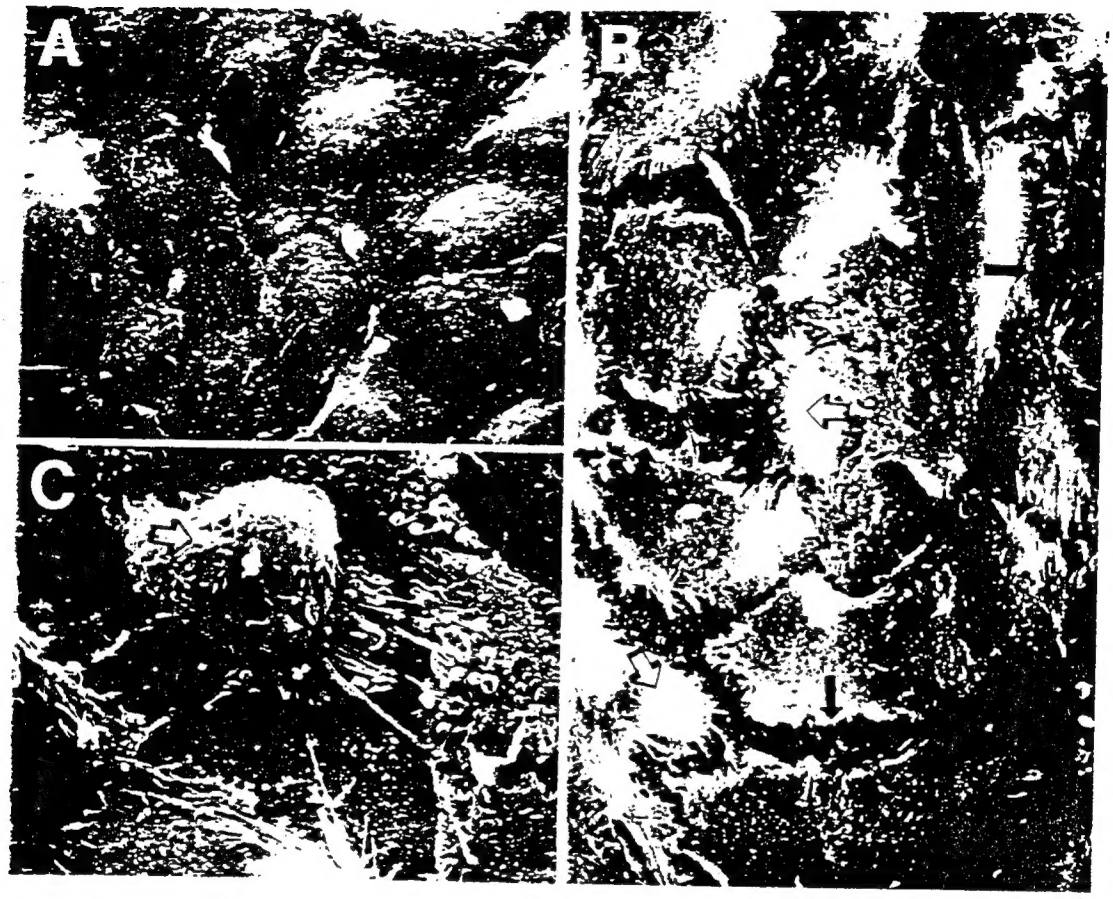

Figure 58